B—1944

INTERACTION OF ELECTROMAGNETIC FIELDS WITH HETEROGENEOUS BIOLOGICAL SYSTEMS

by

Sutus Rukspollmuang

A DISSERTATION

Submitted to
Michigan State University
in partial fulfillment of the requirements
for the degree of

DOCTOR OF PHILOSOPHY

Department of Electrical Engineering and Systems Science

1979

ABSTRACT

INTERACTION OF ELECTROMAGNETIC FIELDS
WITH HETEROGENEOUS BIOLOGICAL SYSTEMS

by

Sutus Rukspollmuang

This thesis presents the theoretical and experimental results of the induced electric field inside a biological system when it is irradiated by a non-ionized electromagnetic radiation. This study was conducted because of the need of quantifying the induced EM field in a biological body in the study of potential EM radiation hazards and in the biomedical applications involving EM radiation.

A numerical method based on a tensor integral equation is briefly outlined. The accuracy of this numerical method is verified by the exact solution of Mie theory for the induced EM heating inside the homogeneous spherical models of human and animal heads. The numerical method is also used to determine the induced EM heating in a realistic model of human or animal head that consists of a brain of realistic shape and eyes surrounded by a bony structure.

The induced electric fields in irradiated, electrically small cubes filled with phantom material were measured by an electric field probe. The measured results were in good agreement with theoretical results obtained from the tensor integral equation

method. An implantable electric field probe with an interference-free wire system was constructed at a nominal cost for the purpose of measuring the induced electric fields in a phantom model when it is irradiated by EM waves of various frequencies. A phantom model of man which was constructed with thin plexiglass filled with phantom material, was irradiated by 500 to 3000 MHz EM waves in a microwave anechoic chamber. The distribution of the measured electric field was compared with the distribution of theoretical results obtained numerically from the tensor integral equation method. A quanlitative agreement was obtained between experiment and theory.

A study has been conducted to investigate effective methods of inducing hyperthermia in the tumors embedded in animal and human bodies by ultilizing EM fields. The distributions of SARs in biological bodies with embedded tumors induced by various EM fields are theoretically quantified to assess the effectiveness of various local EM heating schemes.

The tensor integral equation method is combined with an iteration process to provide a scheme that extends the tensor integral equation method to handle a body consisting of a very large number of cells, while sidestepping the problem of computer storage limitation. In some medical applications, a local part of a biological body is magnetized and irradiated by an EM field. To analyze such a body the existing tensor integral equation method is generalized to handle a body with an arbitrary permeability in addition to arbitrary conductivity and permittivity. In addition, three computer programs used in this study are described along with their instructions and the program listings.

DEDICATION

"To my parents, Dr. Natee and Suparb Rukspollmuang,

my wife Chanita, and my son Dawin."

ACKNOWLEDGEMENTS

I wish to express my appreciation to my major professor, Dr. K.M. Chen, for his guidance, encouragement and invaluable advice throughout the course of this work. I also wish to thank the other members of my guidance committee, Dr. D.P. Nyquist, Dr. J. Asmussen, Dr. B. Ho and Dr. J. Shapiro, for their time and assistance.

This research was supported by the National Science Foundation under Grant ENG 74-12603, and in part, by U.S. Army Research Office under Grant DAAG 29-76-G-0201.

I would like to express my deep appreciation to my parents and to my wife, Chanita, for their support, understanding and encouragement during my graduate study. I sincerely thank Joanna Gruber who has done a great job typing this thesis.

TABLE OF CONTENTS

LIST OF TABLES

CHAPTER 1

INTRODUCTION

In recent years, many researchers have studied the induced electromagnetic heating inside biological systems because of the controversy of potential health hazards due to non-ionizing EM radiation and the applications of EM radiation in biomedical area. Electromagnetic waves in the frequency range of HF to UHF may cause adverse effects in biological systems. Some of these effects can be harmful at high intensities, causing cancer, burns, cataracts, etc. However, if it is under the controlled condition at lower intensities, electromagnetic radiation can be used for therapeutic purpose and to make useful diagnostic measurements. In order to predict the effects of EM radiation on biological systems, and for the applications of EM radiation, induced EM heating inside biological body needs to be determined. The determination of the induced EM fields inside biological system can be approached from both the theoretical and experimental viewpoints.

Theoretically, biological systems have been approximated by simple mathematical models such as plane slabs, spheres or cylinders. These simple models, however, can provide only very approximate results. In reality, a biological system is usually a heterogeneous finite body with an irregular shape, and it is necessary to use a realistic model for the biological system if accurate results on

the induced EM fields inside the system are needed.

To handle such an irregular geometry, the only potent method is the numerical method with the help of a high-speed computer. This research deals with the theoretical and experimental studies of the induced EM fields inside biological systems irradiated by various types of EM radiation. The numerical technique called the tensor integral equation method has been used in this research, and this method is outlined in Chapter 2.

The accuracy of tensor integral equation method is verified by the exact solution of Mie theory and the experimental results in Chapter 3 and 4, respectively. In Chapter 3, we compare the numerical results with the exact solutions of Mie theory for the induced EM heatings inside homogeneous spherical models of human and animal heads at 918 and 2450 MHz. The induced EM heatings inside realistic models of human and animal heads are also included. Chapter 4 contains numerical and experimental results for the induced electric fields inside the cubical phantom models with different sizes.

Chapter 5 is devoted to the theoretical and experimental studies on the induced electric field inside human body irradiated by EM waves of various frequencies. A phantom model of man was constructed with thin plexiglass filled with phantom material. The model was irradiated by 500 to 3000 MHz EM wave in a microwave anechoic chamber. Induced electric fields were probed over 28 locations in one side of the model. The distribution of the measured electric fields was compared with the distribution of theoretical results obtained from the tensor integral equation method.

Chapter 6 is devoted to the theoretical study on local EM heating of tumors in biological bodies. One of the therapies for cancer is that of hyperthermia in combination with chemotherapy. When the temperature of a tumor is raised a few degrees above that of surrounding tissue, accompanying chemotherapy has been found to be effective in treating the tumor. The purpose of this study is to find a noninvasive method by which to heat the tumor without overheating other parts of the body. In order to find such a method, we have theoretically studied the heating pattern induced inside the body with tumor when it is irradiated by various EM fields with certain schemes.

The combination of the tensor integral equation method (TIEM) with an iteration technique is discussed in Chapter 7. When the TIEM is applied to quantify the induced EM field in an electrically large body, it is necessary to divide the body into a large number of cells to obtain accurate results. This will lead to a large number of unknowns in the numerical calculation and overloading the computer storage. This method of combining an iteration technique with TIEM is designed to overcome these problems.

In some biological applications it may be feasible to introduce nontoxic magnetic powder into a local region so that the absorbed power at the local region is enhanced when it is irradiated by an EM field. The generalized TIEM which is designed to handle the body with arbitrary permeability in addition to arbitrary conductivity and permittivity is discussed in Chapter 8.

Chapter 9 includes a description and listing of the computer programs used in this study. Part 1, program FIELDS is used to quantify

the induced electric field inside an arbitrarily shaped biological body. Part 2, program ITERATE, is the extension of program FIELDS with an addition of iteration process. This program is useful for a large body with a large number of cells. Part 3, program EMFIELD, is used to quantify the induced electric and magnetic fields inside an arbitrarily shaped biological body with arbitrary permeability, permittivity and conductivity. Definitions of input variables, the construction of data files and the useage instruction are given in each part.

CHAPTER 2

REVIEW OF TENSOR INTEGRAL EQUATION METHOD

In this chapter the tensor integral equation method is briefly outlined. Induced electric field inside the irradiated, arbitrary-shape biological body or system was obtained by this tensor integral equation method which surved as our theory in this study. The accuracy of our theory (numerical result) has been checked by comparing with the exact solution of Mie theory in Chapter 3 and comparing with the experimental result in Chapter 4.

2.1 Description of problem

The theoretical method used in this study is based on a tensor integral equation developed by Livesay and Chen (1). When a biological system is illuminated by an electromagnetic wave, an electromagnetic field is induced inside the body and an electromagnetic wave is scattered by the body in the region exterior to the body. In general the biological system is an irregularly shaped heterogeneous conducting medium and its electrical parameters are dependent on frequency of incident electromagnetic wave and locations within the body. Conventionally they are assumed to be

$$\sigma = \sigma\ (\omega,\vec{r})$$

$$\varepsilon = \varepsilon\ (\omega,\vec{r})$$

$$\mu = \mu_o$$

The induced electromagnetic field inside the body, in general, depends on the body's physiological parameters and geometry, as well as

the frequency and polarization of the incident wave.

Based on Maxwell's equations, we can obtain a tensor integral equation which relates unknown induced electric field inside the system to the incident electric field. After using a pulse-function expansion of the unknown induced electric field and point-matching, we employ the method of moments to solve the integral equation numerically.

2.2 Tensor Integral Equation for the Induced Electric Field

Consider a finite biological body of arbitrary shape with permittivity $\varepsilon(\vec{r})$, conductivity of $\sigma(\vec{r})$ and permeability μ_o, illuminated in free space by an incident electromagnetic wave with an electric field $\vec{E}^i(\vec{r})$ and magnetic field $\vec{H}^i(\vec{r})$. We can write Maxwell's equations for this incident EM field in free space as

$$\nabla \times \vec{E}^i(\vec{r}) = -j\omega\mu_o \vec{H}^i(\vec{r}) \tag{2.1}$$

$$\nabla \times \vec{H}^i(\vec{r}) = j\omega\varepsilon_o \vec{E}^i(\vec{r}) \tag{2.2}$$

$$\nabla \cdot \vec{E}^i(\vec{r}) = 0 \tag{2.3}$$

$$\nabla \cdot \vec{H}^i(\vec{r}) = 0 \tag{2.4}$$

where μ_o and ε_o are the permeability and permittivity of free space. When a biological body is illuminated by the incident electromagnetic field, it creates a distribution of induced charges and currents throughout the body. These charges and currents produce a scattered field. Thus, the total electromagnetic field inside the body is the sum of the incident field and the scattered field:

$$\vec{E}(\vec{r}) = \vec{E}^{i}(\vec{r}) + \vec{E}^{s}(\vec{r}) \tag{2.5}$$

$$\vec{H}(\vec{r}) = \vec{H}^{i}(\vec{r}) + \vec{H}^{s}(\vec{r}) \tag{2.6}$$

Combining eq. (2.1), (2.2), (2.3), (2.4) with eq. (2.5), (2.6) and Maxwell's equations for the total electromagnetic field we obtain Maxwell's equations for the scattered field as

$$\nabla \times \vec{E}^{s}(\vec{r}) = - j \omega \mu_o \vec{H}^{s}(\vec{r}) \tag{2.7}$$

$$\nabla \times \vec{H}^{s}(\vec{r}) = \{\sigma(\vec{r}) + j\omega [\varepsilon(\vec{r}) - \varepsilon_o]\} \vec{E}(\vec{r}) + j\omega\varepsilon_o \vec{E}^{s}(\vec{r}) \tag{2.8}$$

Defining an equivalent volume current density $\vec{J}_{eq}(\vec{r})$ as

$$\vec{J}_{eq}(\vec{r}) = \tau(\vec{r})\, \vec{E}(\vec{r}) \tag{2.9}$$

where $\tau(\vec{r}) = \sigma(\vec{r}) + j\omega [\varepsilon(\vec{r}) - \varepsilon_o]$ is the equivalent complex conductivity. Eq. (2.8) can be rewritten as

$$\nabla \times \vec{H}^{s}(\vec{r}) = \vec{J}_{eq}(\vec{r}) + j\omega\varepsilon_o \vec{E}^{s}(\vec{r}) \tag{2.10}$$

The equation of continuity for $\vec{J}_{eq}(\vec{r})$ defines an equivalent volume charge density $\rho_{eq}(\vec{r})$ as

$$\nabla \cdot \vec{J}_{eq}(\vec{r}) + j\omega\rho_{eq}(\vec{r}) = 0 \tag{2.11}$$

or

$$\rho_{eq}(\vec{r}) = \frac{j}{\omega} \nabla \cdot \vec{J}_{eq}(\vec{r}) \tag{2.12}$$

Taking the divergence of eq. (2.10) and using eq. (2.12) gives

$$\nabla \cdot \vec{E}^{s}(\vec{r}) = \frac{\rho_{eq}(\vec{r})}{\varepsilon_o} \tag{2.13}$$

Finally, Maxwell's equations for $\vec{E}^s(\vec{r})$ and $\vec{H}^s(\vec{r})$ can be written as

$$\nabla \times \vec{E}^s(\vec{r}) = - j \omega \mu_o \vec{H}^s(\vec{r}) \tag{2.14}$$

$$\nabla \times \vec{H}^s(\vec{r}) = \vec{J}_{eq}(\vec{r}) + j \omega \varepsilon_o \vec{E}^s(\vec{r}) \tag{2.15}$$

$$\nabla \cdot \vec{E}^s(\vec{r}) = \frac{1}{\varepsilon_o} \rho_{eq}(\vec{r}) \tag{2.16}$$

$$\nabla \cdot \vec{H}^s(\vec{r}) = 0 \tag{2.17}$$

The scattered electric field $\vec{E}^s(\vec{r})$ within the body can be determined from the following equation (2,3):

$$\vec{E}^s(\vec{r}) = \text{P.V.} \int_V \vec{J}_{eq}(\vec{r}') \cdot \overleftrightarrow{G}(\vec{r},\vec{r}') \, dv' - \frac{\vec{J}_{eq}(\vec{r})}{3j\omega\varepsilon_o} \tag{2.18}$$

where

$$\overleftrightarrow{G}(\vec{r},\vec{r}') = -j\omega\varepsilon_o \left[\overleftrightarrow{I} + \frac{\nabla\nabla}{k_o^2}\right] \Psi(\vec{r},\vec{r}')$$

$$\Psi(\vec{r},\vec{r}') = \frac{e^{-jk_o|\vec{r}-\vec{r}'|}}{4\pi|r-r'|}$$

$$\overleftrightarrow{I} = \hat{x}\hat{x} + \hat{y}\hat{y} + \hat{z}\hat{z}$$

$$k_o = \omega\sqrt{\mu_o\varepsilon_o}$$

P.V. symbol means the principle value of the integral, and $\overleftrightarrow{G}(\vec{r},\vec{r}')$ is the free space tensor green's function.

By substituding eq. (2.18) in eq. (2.5), rearranging terms, and recalling that $\vec{J}_{eq}(\vec{r}) = \tau(\vec{r})\,\vec{E}(\vec{r})$, we can obtain a tensor integral equation as

$$\left[1 + \frac{\tau(\vec{r})}{3j\omega\varepsilon_o}\right]\vec{E}(\vec{r}) - \text{P.V.}\int_V \tau(\vec{r}')\vec{E}(\vec{r}')\cdot\overleftrightarrow{G}(\vec{r},\vec{r}')dv' = \vec{E}^i(\vec{r}) \qquad (2.19)$$

$\vec{E}^i(\vec{r})$ and $\tau(\vec{r}')$ are known quantities and $\vec{E}(\vec{r})$ is the total induced field inside the body.

2.3 Moment Solution of Tensor Integral Equation

It is very difficult to solve the tensor integral equation by performing integral which involved unknown $\vec{E}(\vec{r})$ inside the integral. One simple possibility is to solve the tensor integral equation numerically by using the method of moments.

If the body is partitioned into N subvolumes or cells and $\vec{E}(\vec{r})$ and $\tau(\vec{r})$ are assumed to be constant within each cell, tensor integral equation (eq. 2.19) can be transformed into 3N simultaneous equations for E_x, E_y, and E_z at the center of N cells by the point matching method. These simultaneous equations can be written into a matrix form as

$$\begin{bmatrix} G_{xx} & G_{xy} & G_{xz} \\ G_{yx} & G_{yy} & G_{yz} \\ G_{zx} & G_{zy} & G_{zz} \end{bmatrix}\begin{bmatrix} E_x \\ E_y \\ E_z \end{bmatrix} = \begin{bmatrix} E_x^i \\ E_y^i \\ E_z^i \end{bmatrix} \qquad (2.20)$$

The $[G]$ matrix is a 3N x 3N matrix, while $[E]$ and $[E^i]$ are 3N column matrices expressing the total electric field and the incident electric field at the centers of N cells. The elements of $[G]$ matrix have been evaluated in the next section. Therefore, with the known incident electric field $\vec{E}^i(\vec{r})$ the total induced electric field $\vec{E}(\vec{r})$ inside the body can be obtained from eq. (2.20) by inverting the $[G]$ matrix.

2.4 Calculation of Matrix Elements

The expressions for the elements of each NxN submatrix $[G_{x_p x_q}]$, p, q = 1,2,3 are given in this section.

Let

$$x_1 = x, \quad x_2 = y \quad \text{and} \quad x_3 = z$$

The $(m,n)^{th}$ off diagonal element of the $[G_{x_p x_q}]$ matrix is given (1) by

$$G^{mn}_{x_p x_q} = \frac{-j\omega\mu_o k_o \tau(r_n)\Delta v_n e^{-j\alpha_{mn}}}{4\pi\alpha^3_{mn}} \left[(\alpha^2_{mn} - 1 - j\alpha_{mn})\,\delta_{pq} + \cos\theta^{mn}_{x_p} \cos\theta^{mn}_{x_q} (3 - \alpha^2_{mn} + 3j\alpha_{mn})\right], \quad m \neq n \tag{2.21}$$

where

$$\alpha_{mn} = k_o R_{mn}; \quad R_{mn} = |\vec{r}_m - \vec{r}_n|$$

$$\cos\theta^{mn}_{x_p} = \frac{x^m_p - x^n_p}{R_{mn}}; \quad \cos\theta^{mn}_{x_q} = \frac{x^m_q - x^n_q}{R_{mn}}$$

$$\vec{r}_m = (x_1^m , x_2^m , x_3^m); \quad \vec{r}_n = (x_1^n , x_2^n , x_3^n)$$

$$\Delta v_n = \int_{v_n} dv'$$

The $(n,n)^{th}$ diagonal element of the $\left[G_{x_p x_q}\right]$ matrix is given by (1)

$$G_{x_p x_q}^{nn} = -\delta_{pq}\left\{\frac{2j\omega\mu_o\tau(\vec{r}_n)}{3k_o^2}\left[e^{-jk_o a_n}(1 + jk_o a_n) - 1\right] + \left[1 + \frac{\tau(r_n)}{3j\omega\varepsilon_o}\right]\right\} \tag{2.22}$$

where

$$a_n = \left[\frac{3\Delta v_n}{4\pi}\right]^{1/3}$$

After all the elements of $\left[G\right]$ matrix are determined, the total induced electric field $\vec{E}(\vec{r})$ inside the body can be obtained by inverting the $\left[G\right]$ matrix as

$$\begin{bmatrix} E_x \\ E_y \\ E_z \end{bmatrix} = \begin{bmatrix} G_{xx} & G_{xy} & G_{xz} \\ G_{yx} & G_{yy} & G_{yz} \\ G_{zx} & G_{zy} & G_{zz} \end{bmatrix}^{-1} \begin{bmatrix} E_x^i \\ E_y^i \\ E_z^i \end{bmatrix}$$

After $\vec{E}(\vec{r})$ field is determined, the absorbed power density is determined from $P = \sigma/2 \ |\vec{E}|^2$. To verify the accuracy of the tensor integral equation method, the numerical results generated by this method were compared with the existing exact solution and experimental results in the following chapters.

CHAPTER 3

INDUCED EM FIELDS IN SPHERICAL BODIES...
HUMAN AND ANIMAL HEADS

In this chapter the accuracy of the tensor integral equation method which serves as our theoretical tool is checked. The induced heating patterns inside a homogeneous spherical brain obtained by the tensor integral equation method are compared with the corresponding results obtained from the exact solution of Mie theory (4,5). After the theory was verified it was used to predict the induced heating patterns inside human and animal heads.

3.1 The Mie Theory (4,5)

Consider a sphere of radius a which is illuminated by a plane wave, whose electric field is linearly polarized in the x-direction and propagates in the + z direction. The expression of this incident field in terms of vector spherical wave functions is:

$$\vec{E}^i = E_o e^{-jwt} \sum_{n=1}^{\infty} \frac{2n+1}{n(n+1)} (\vec{M}_{o1n} - j\vec{N}_{o1n}) \qquad (3.1)$$

where E_o is the amplitude of the incident electric field.

When EM wave is incident upon a sphere, it will give rise to a forced oscillation of free and bound charges synchronous with the applied field. This oscillation of charges will set up a secondary field both inside and outside the sphere.

According to Mie theory, the electric field $\vec{E}$ induced inside a conducting sphere by a plane EM wave with an incident electric field $\vec{E}^i$ can be calculated from the general vector spherical wave solution of the wave equation as

$$\vec{E} = \vec{E}^i \sum_{n=1}^{\infty} (j)^n \frac{2n+1}{n(n+1)} \left(a_n \vec{M}_{o1n} - j\, b_n \vec{N}_{o1m}\right) \qquad (3.2)$$

where the vector functions $\vec{M}_{o1n}$ and $\vec{N}_{o1m}$ are defined, and the coefficients a_n and b_n are obtained in Stratton (5). Numerical results computed from eq. (3.2) were considered to be the exact solution to the problem.

3.2 Formulation of the problem

To check the accuracy of the tensor integral equation method (outlined in Chapter 2), the method was employed to determine the distributions of the absorbed power density or the EM heating induced by plane EM waves of 918 MHz and 2450 MHz in the spherical models of animal and human brains having radii of 3 cm and 7 cm, respectively. Numerical results obtained from this method were then compared with the exact solution of Mie theory.

In order to apply the numerical method, a sphere is first approximated by a "cubic sphere" which is constructed with a number of small cubic cells. Figure 3.1 shows an example that one eighth of a sphere is approximated by one eighth of a "cubic sphere" which is constructed with 73 small cubic cells. It is evident that a better approximation can be achieved by a larger number of smaller cubic cells. However, to economize the computing time, the number of cubic cells or subdivisions should be compromised.

In the present study, we subdivide one eighth of the sphere either into 40 or 73 cubic cells.

A plane EM wave propagating in the + z direction is assumed to be incident upon the sphere with a vertically polarized electric field $\vec{E}^i$ in the x-direction and the associated magnetic field in the y-direction. The $\vec{E}^i$ field can be expressed as

$$\vec{E}^i = \hat{x} E_o e^{-jk_o z} \quad v/m \tag{3.3}$$

where E_o is the amplitude of the incident electric field and is equal to

$$E_o = \sqrt{2\zeta_o P_i} \quad v/m \tag{3.4}$$

In eq. (3.4), P_i is the incident power density in W/m^2 and ζ_o is the impedance of free space having a value of 377 ohms. In the following examples, we used P_i = 1 mW/cm^2 and E_o = 66.83 V/m. K_o in eq. (3.3) is the propagation constant of the EM wave in free space.

With eq. (3.3), $\vec{E}^i$ at the center of each cubic cell of the "cubic sphere" can be specified. With this information on $\vec{E}^i$, electrical properties of cubic cells and given geometry of the "cubic sphere", the induced electric field $\vec{E}$ in each cubic cell is numerically computed based on the tensor integral equation method. After $\vec{E}$ is determined, the absorbed power density or the specific absorption rate (SAR) of the EM energy is obtained from $P = \sigma/2|\vec{E}|^2$. The average heating is obtained by averaging out P inside the sphere.

The maximum heating is identified by the maximum value of P at a certain location inside the sphere. The curve showing the relative

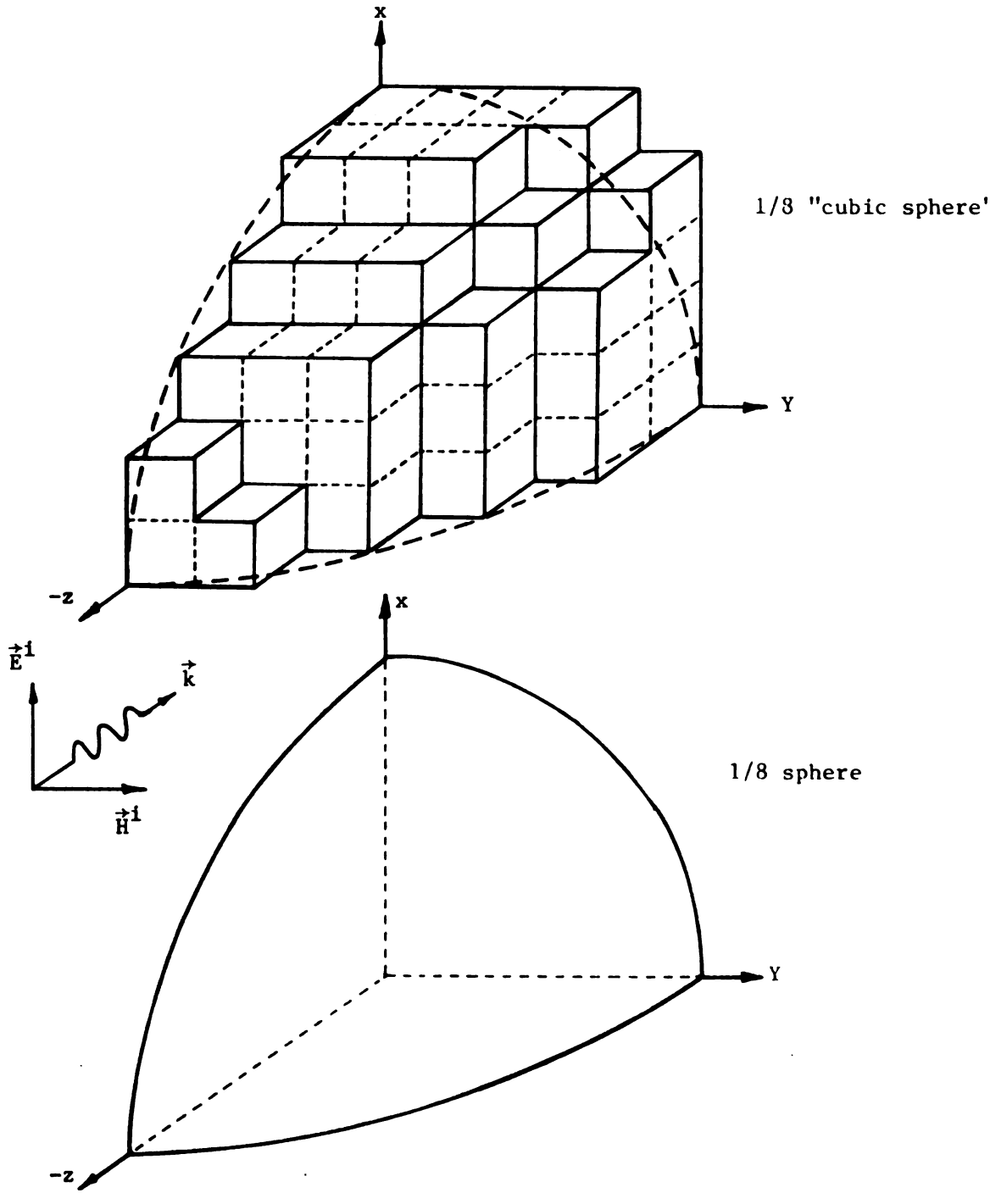

Figure 3.1 One eighth of a sphere is approximated by one eighth of a "cubic sphere" which is constructed with 73 small cubic cells.

heating as a function of location is obtained by normalizing the distribution of P with respect to the maximum heating. The dielectric constant ε_r and conductivity σ of the brain at 918 MHz and 2450 MHz are obtained from values reported by Schwan (6).

3.3 Induced EM Field in Homogeneous Spheres

As the first example, we consider the case of a spherical model of animal brain of 3 cm radius exposed to a plane EM wave of 918 MHz propagating in the + z direction and with a power density of 1 mW/cm^2. At this frequency, the dielectric constant ε_r of the sphere (brain) is assumed to be 35 and the conductivity σ=0.7 s/m. The brain is approximated by a "cubic sphere" and one eighth of it is constructed by 40 cubic cells. The numerical results are shown in Figure 3.2a where relative heatings along the x, y and z axes inside the "cubic sphere" are plotted, and the average and maximum heatings are indicated. The three curves marked X, Y and Z show the distributions of the relative heatings or the relative SARs along the X, Y and Z axes, respectively. These curves show strong standing wave patterns with a peak heating located somewhere in the front half of the brain. The average and maximum heatings are found to be 0.3202 mW/cm^3 and 0.885 mW/cm^3, respectively.

To check the accuracy of the numerical results presented in Figure 3.2a, the induced EM heating was computed in a spherical brain of the same radius based on the exact solution of Mie theory. The corresponding results are shown in Figure 3.2b. The relative heating curves along the X, Y and Z axes based on the exact solution resemble closely with that shown in Figure 3.2a. It is noted that the curves

(40 Subdivisions)

Brain (3 cm radius) Pi = 1 mW/cm^2

Freq. = 918 MHz Ave. heating = 0.3202 mW/cm^3

ε_r = 35, σ = 0.7 S/m Max. heating = 0.885 mW/cm^3

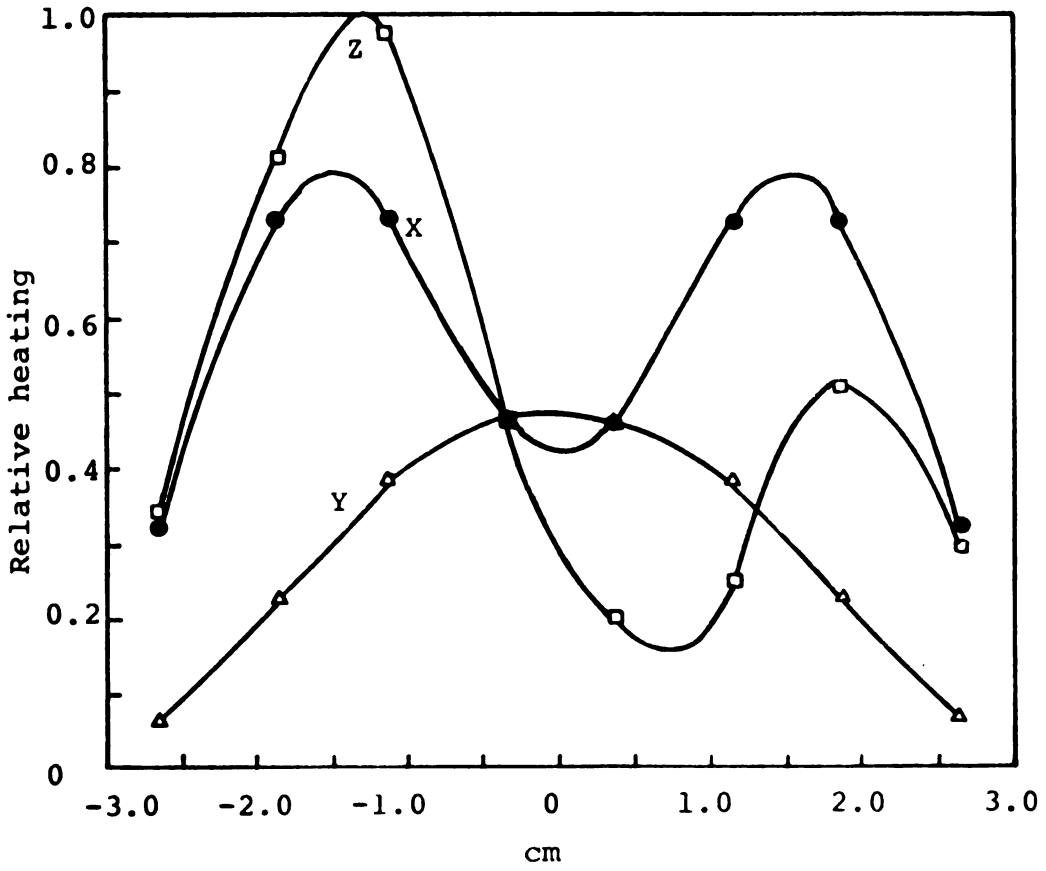

Figure 3.2a. Distributions of heating along the x, y and z axes of a "cubic spherical" brain of 3 cm radius induced by a plane EM wave of 918 MHZ propagating in the +z direction with a power density of 1 mW/cm^2. Electrical properties of the brain, the average and maximum heatings are shown. One eighth of the "cubic sphere" is constructed with 40 cubic cells.

(Exact Solution)

Brain (3 cm radius) Pi = 1 mW/cm^2

Freq. = 918 MHz Ave. heating = 0.295 mW/cm^3

ε_r = 35, σ = 0.7 S/m Max. heating = 0.814 mW/cm^3

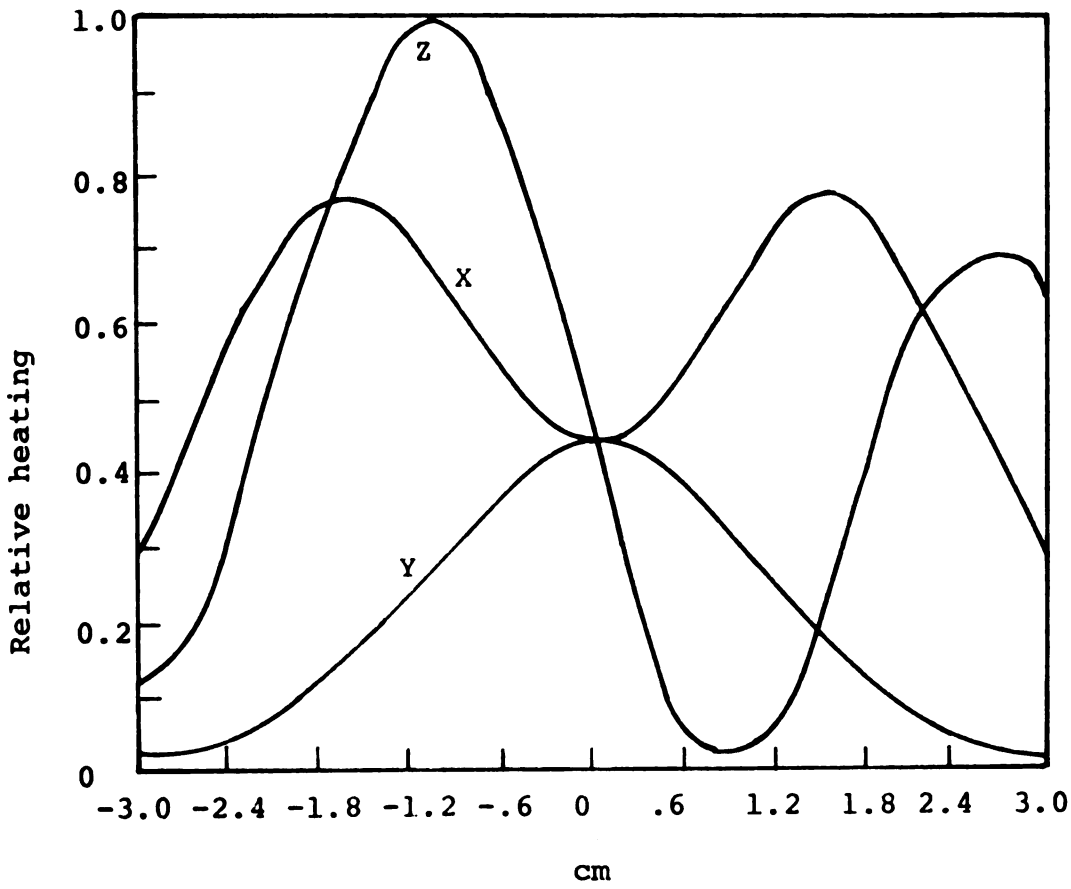

Figure 3.2b. Distributions of heating along the x, y and z axes of a spherical brain of 3 cm radius induced by a plane EM wave of 918 MHz propagating in the +z direction with a power density of 1 mW/cm^2. Electrical properties of the brain, the average and maximum heatings are shown. Numerical results are obtained from the exact solution of Mie theory.

shown in Figure 3.2b are the distributions of SARs along the X, Y and Z axes while those curves shown in Figure 3.2a are, strickly speaking, the distributions of SARs along the centers of cubic cells which line adjacent to the X, Y and Z axes. Therefore, a perfect agreement between those two sets of curves is not expected. The average and maximum heatings based on the exact solution are found to be 0.295 mW/cm^3 and 0.814 mW/cm^3, respectively. These values are in agreement with the corresponding numerical results shown in Figure 3.2a with a deviation of less than 9%. The comparison of Figure 3.2a and 3.2b confirms the accuracy of our numerical method.

In the second example, we consider the same spherical model of animal brain of the first example exposed to a plane EM wave of 2450 MHz propagating in the + z-direction with a power density of 1 mW/cm^2. At this frequency, ε_r and σ of the brain are assumed to be 30.9 and 1.1 S/m, respectively. Figure 3.3a shows the numerical results on the distributions of relative heating, the average and maximum heating in the spherical brain that is approximated by a "cubic sphere" with one eighth of it constructed with 40 cubic cells. The distributions of heating along the X, Y and Z axes show a strong resonant peak in the center of the brain. The maximum heating near the center of the brain is found to be 1.576 mW/cm^3 which is about twice the value for the case of 918 MHz. The average heating is found to be 0.235 mW/cm^3 which is about the same as the case of 918 MHz.

The corresponding results for this example based on the exact solution of Mie theory are given in Figure 3.3b. The distributions of relative heating along the X, Y and Z axes show similar but somewhat sharper resonant peaks than that shown in Figure 3.3a. The average

(40 Subdivisions)

Brain (3 cm radius) Pi = 1 mW/cm^2

Freq. = 2450 MHz Ave. heating = 0.235 mW/cm^3

ε_r = 30.9, σ = 1.1 S/m Max. heating = 1.571 mW/cm^3

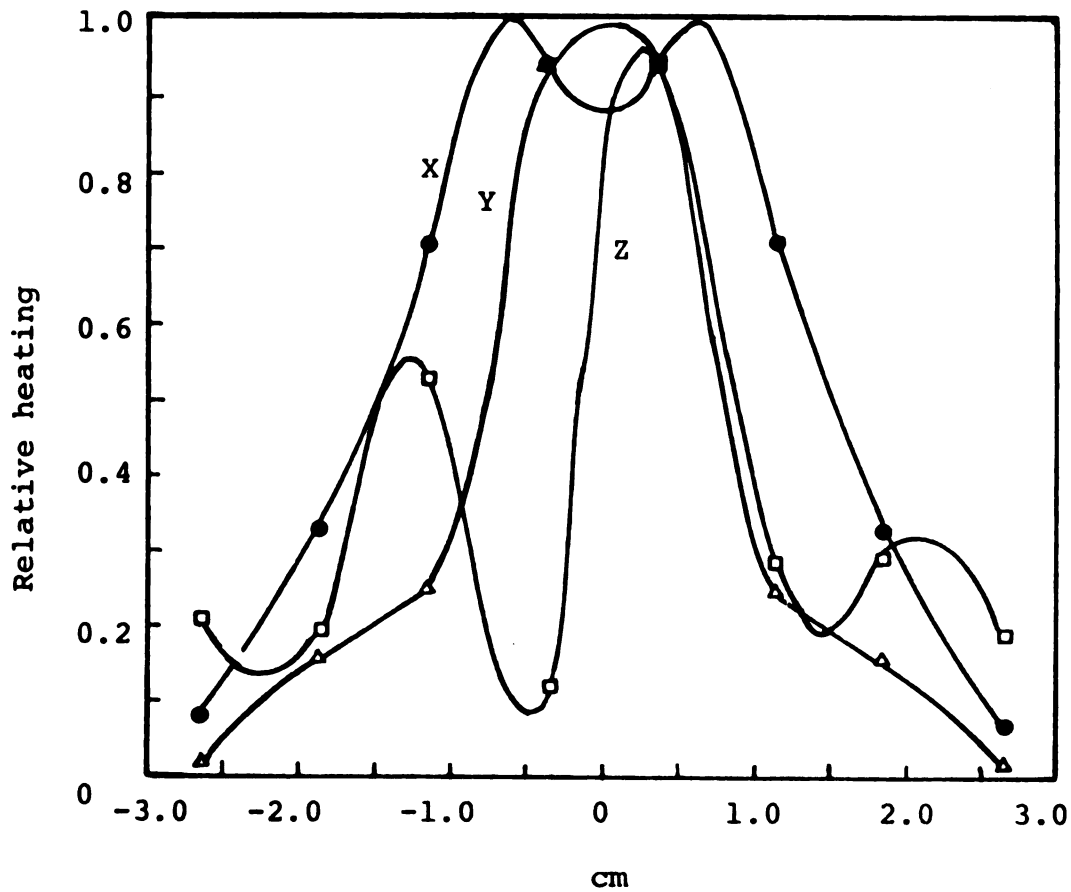

Figure 3.3a. Distributions of heating along the x, y and z axes of a "cubic spherical" brain of 3 cm radius induced by a plane EM wave of 2450 MHz propagating in the +z direction with a power density of 1 mW/cm^2. Electrical properties of the brain, the average and maximum heatings are shown. One eighth of the "cubic sphere" is constructed with 40 cubic cells.

and maximum heatings are 0.278 mW/cm^3 and 1.698 mW/cm^3, respectively. These values based on the exact solution are quite close to the numerical results given in Figure 3.3a.

In the third example, we consider a spherical model of human brain of 7 cm radius exposed to a plane EM wave of 918 MHz propagating in the + z direction with a power density of 1 mW/cm^2. At this frequency, ϵ_r and σ of the brain are assumed to be 35 and 0.7 s/m, respectively. Figure 3.4a shows the numerical results on the induced EM heatings calculated with the model of a "cubic sphere" of 7 cm radius, with one eighth of it constructed with 40 cubic cells. We observe that a resonance is induced in the brain and the peak heating occurs in the central part of the brain. The average and maximum heatings are found to be 0.1065 mW/cm^3 and 0.5937 mW/cm^3, respectively.

When one eighth of the same "cubic sphere" of 7 cm radius is constructed with 73 smaller cubic cells, numerical results on the induced EM heating are somewhat modified as shown in Figure 3.4b. The resonant peak of heating become sharper compared with that of Figure 3.4a and the average and maximum heating become 0.115 mW/cm^3 and 0.619 mW/cm^3, respectively.

The corresponding numerical results in a spherical brain of 7 cm radius based on the exact solution of Mie theory are shown in Figure 3.4c. The resonant peaks of heating in Figure 3.4c are somewhat sharper than that of Figure 3.4b, and the average and maximum heating are found to be 0.117 mW/cm^3 and 0.458 mW/cm^3, respectively.

If we compare the results of Figures 3.4a and 3.4b with that of Figure 3.4c, it is clear that numerical results of our numerical

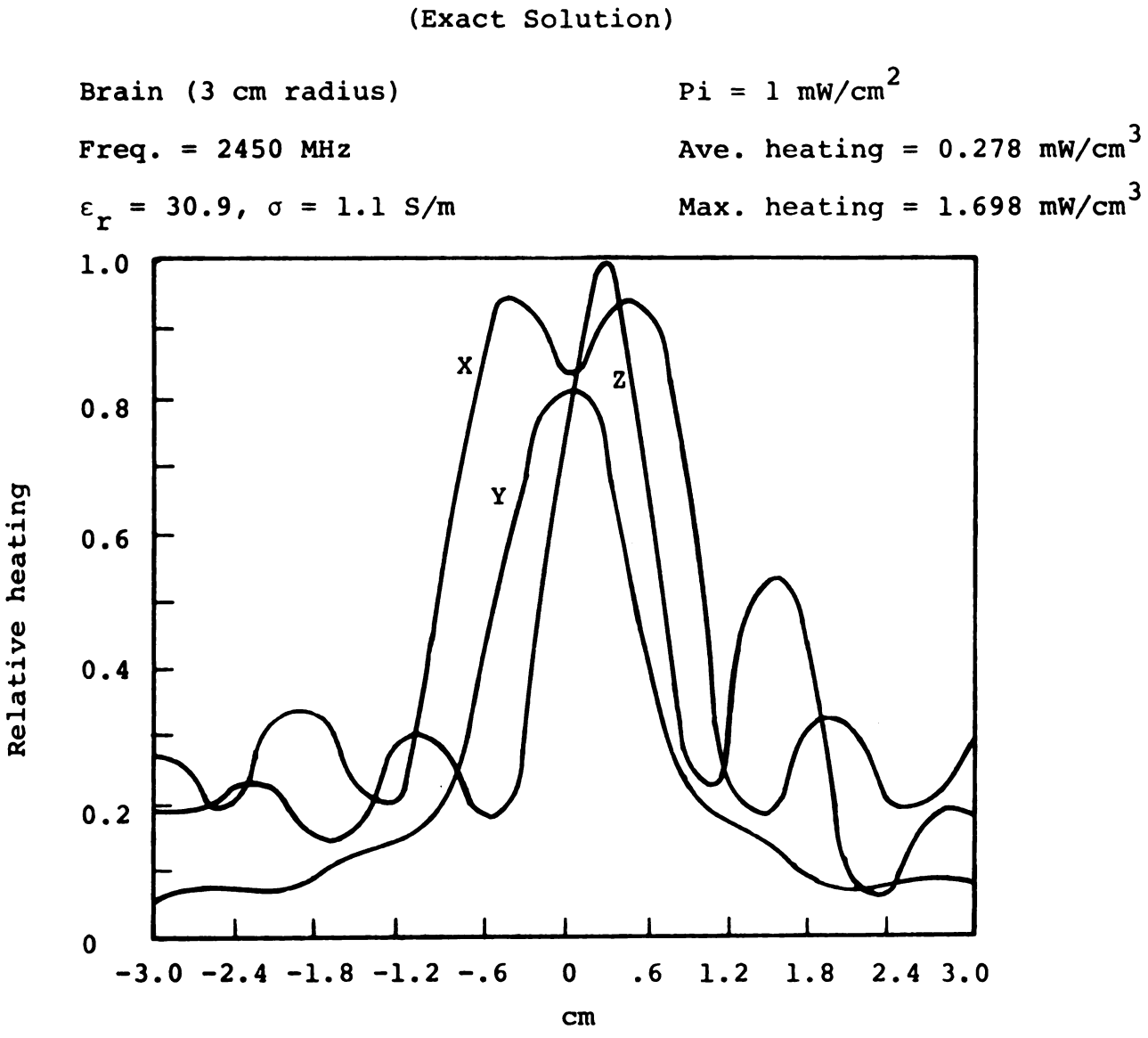

Fibure 3.3b. Distributions of heating along the x, y and z axes of a spherical brain of 3 cm radius induced by a plane EM wave of 2450 MHz propagating in the +z direction with a power density of 1 mW/cm^2. Electrical properties of the brain, the average and maximum heatings are shown. Numerical results are obtained from the exact solution of Mie theory.

(40 Subdivisions)

Brain (7 cm radius) Pi = 1 mW/cm^2

Freq. = 918 MHz Ave. heating = 0.1065 mW/cm^3

ε_r = 35, σ = 0.7 S/m Max. heating = 0.5937 mW/cm^3

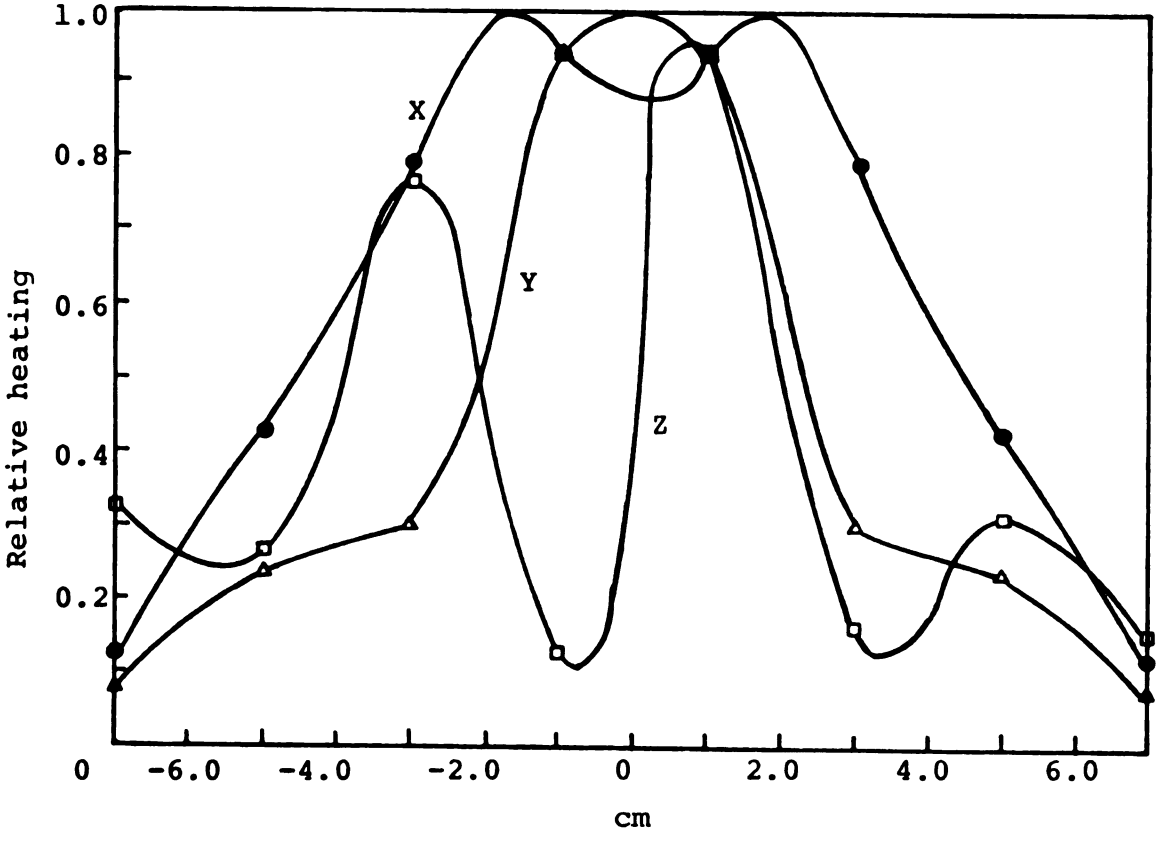

Figure 3.4a. Distributions of heating along the x, y and z axes of a "cubic spherical" brain of 7 cm radius induced by a plane EM wave of 918 MHz propagating in the +z direction with a power density of 1 mW/cm^2. Electrical properties of the brain, the average and maximum heatings are shown. One eighth of the "cubic sphere" is constructed with 40 cubic cells.

(73 Subdivisions)

Brain (7 cm radius) Pi = 1 mW/cm^2

Freq. = 918 MHz Ave. heating = 0.115 mW/cm^3

ε_r = 35, σ = 0.7 S/m Max. heating = 0.619 mW/cm^3

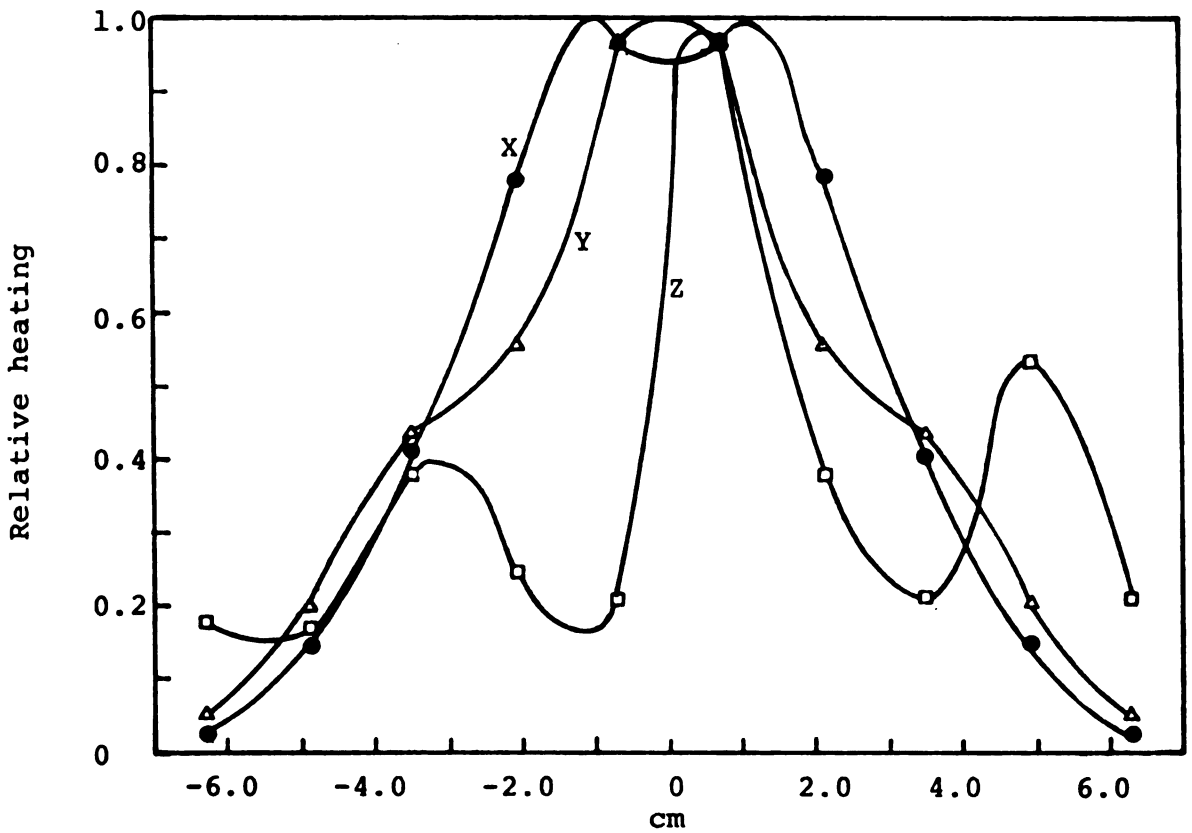

Figure 3.4b. Distributions of heating along the x, y and z axes of a "cubic spherical" brain of 7 cm radius induced by a plane EM wave of 918 MHz propagating in the +z direction with a power density of 1 mW/cm^2. Electrical properties of the brain, the average and maximum heatings are shown. One eighth of the "cubic sphere" is constructed with 73 cubic cells.

(Exact Solution)

Brain (7 cm radius)

Freq. = 918 MHz

ε_r = 35, σ = 0.7 S/m

Pi = 1 mW/cm^2

Ave. heating = 0.117 mW/cm^3

Max. heating = 0.458 mW/cm^3

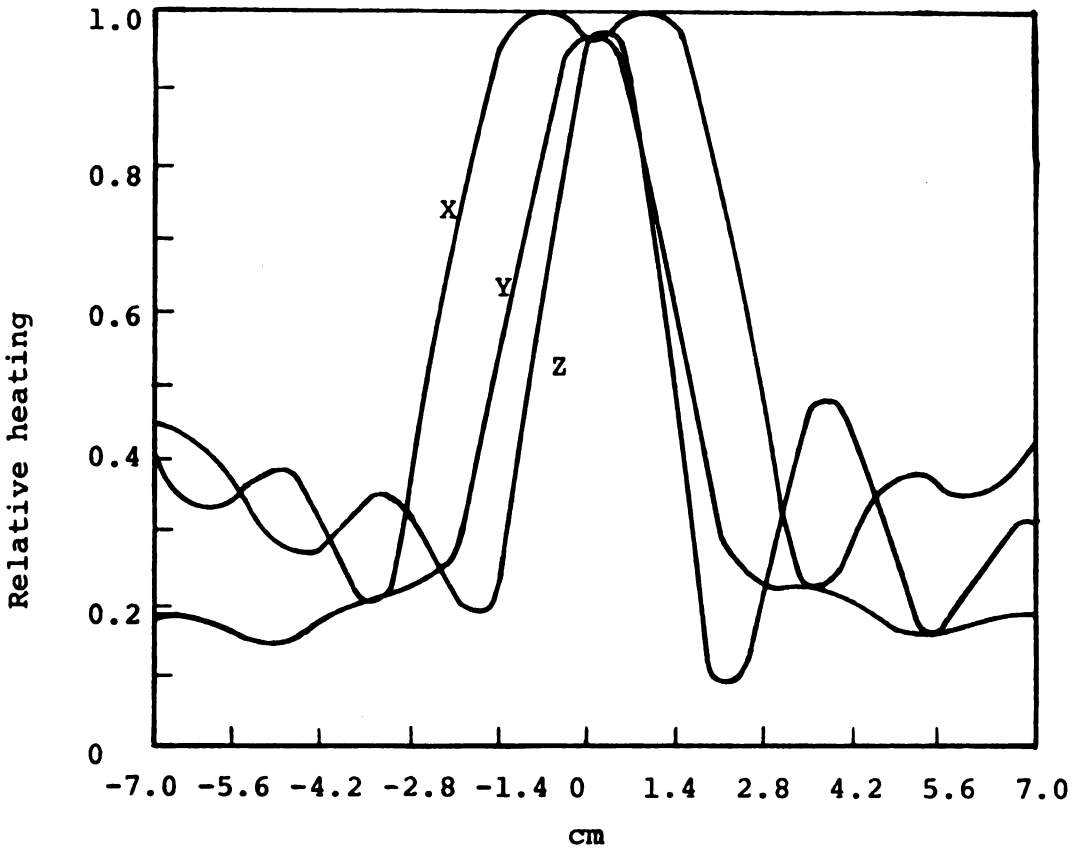

Figure 3.4c. Distributions of heating along the x, y and z axes of a spherical brain of 7 cm radius induced by a plane EM wave of 918 MHz propagating in the +z direction with a power density of 1 mW/cm^2. Electrical properties of the brain, the average and maximum heatings are shown. Numerical results are obtained from the exact solution of Mie theory.

method can be improved significantly by increasing the number of subdivision on the sphere. It appears that when one eighth of a spherical brain of 7 cm radius is subdivided into 73 cubic cells, our numerical method is capable of producing satisfactory results at 918 MHz.

The last example is for the case of the same spherical model of human brain exposed to a plane EM wave of 2450 MHz propagating in the + z direction with a power density of 1 mW/cm^2. ε_r and σ for the brain are assumed to be 30.9 and 1.1 s/m respectively. Numerical results on the induced EM heatings calculated in a "cubic spherical" brain of 7 cm radius, and with one eighth of it constructed with 40 cubic cells, are shown in Figure 3.5a. The corresponding numerical results calculated in the same "cubic spherical" brain but with one eighth of it constructed with 73 cubic cells are shown in Figure 3.5b. Numerical results for a spherical brain of 7 cm radius obtained from the exact solution of Mie theory are shown in Figure 3.5c. Comparing the results of Figures3.5a and 3.5b with that of Figure 3.5c, it is observed that when one eighth of the brain of 7 cm radius is subdivided into 40 cubic cells, our numerical method produced poor results at 2450 MHz. However, if the subdivision is increased from 40 to 73, much improved results are obtained. The main difficulty our numerical method encounted in this case was the failure in predicting the rapidly attenuating nature of the induced heating in the front surface of the brain. The reason for this difficulty is that the skin depth of a 2450 MHz EM wave is quite shallow in a spherical brain tissue of 7 cm radius, and the numerical

(40 Subdivisions)

Brain (7 cm radius) Pi = 1 mW/cm^2

Freq. = 2450 MHz Ave. heating = 0.068 mW/cm^3

ε_r = 30.9, σ = 1.1 S/m Max. heating = 0.141 mW/cm^3

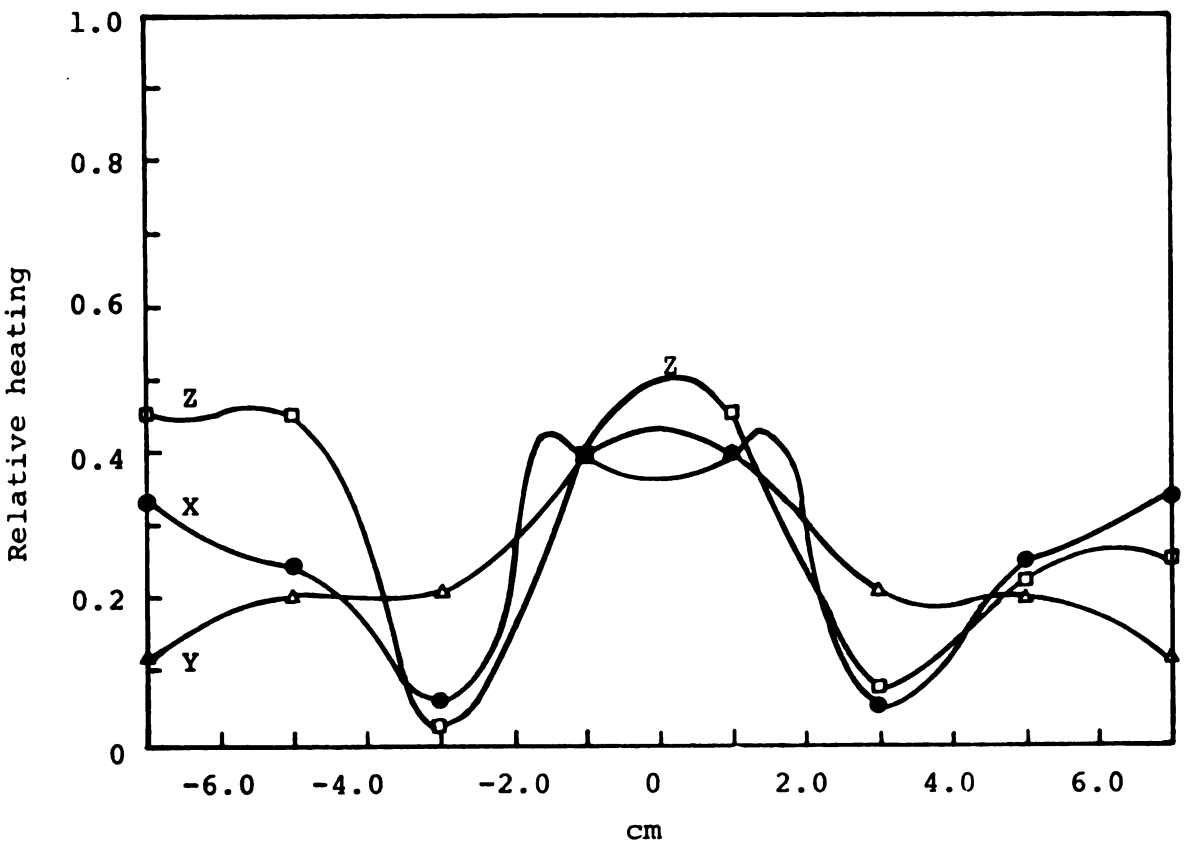

Figure 3.5a. Distributions of heating along the x, y and z axes of a "cubic spherical" brain of 7 cm radius induced by a plane EM wave of 2450 MHz propagating in the +z direction with a power density of 1 mW/cm^2. Electrical properties of the brain, the average and maximum heatings are shown. One eighth of the "cubic sphere" is constructed with 40 cubic cells.

(73 Subdivisions)

Brain (7 cm radius)

Freq. = 2450 MHz

ε_r = 30.9, σ = 1.1 S/m

Pi = 1 mW/cm^2

Ave. heating = 0.094 mW/cm^3

Max. heating = 1.1 mW/cm^3

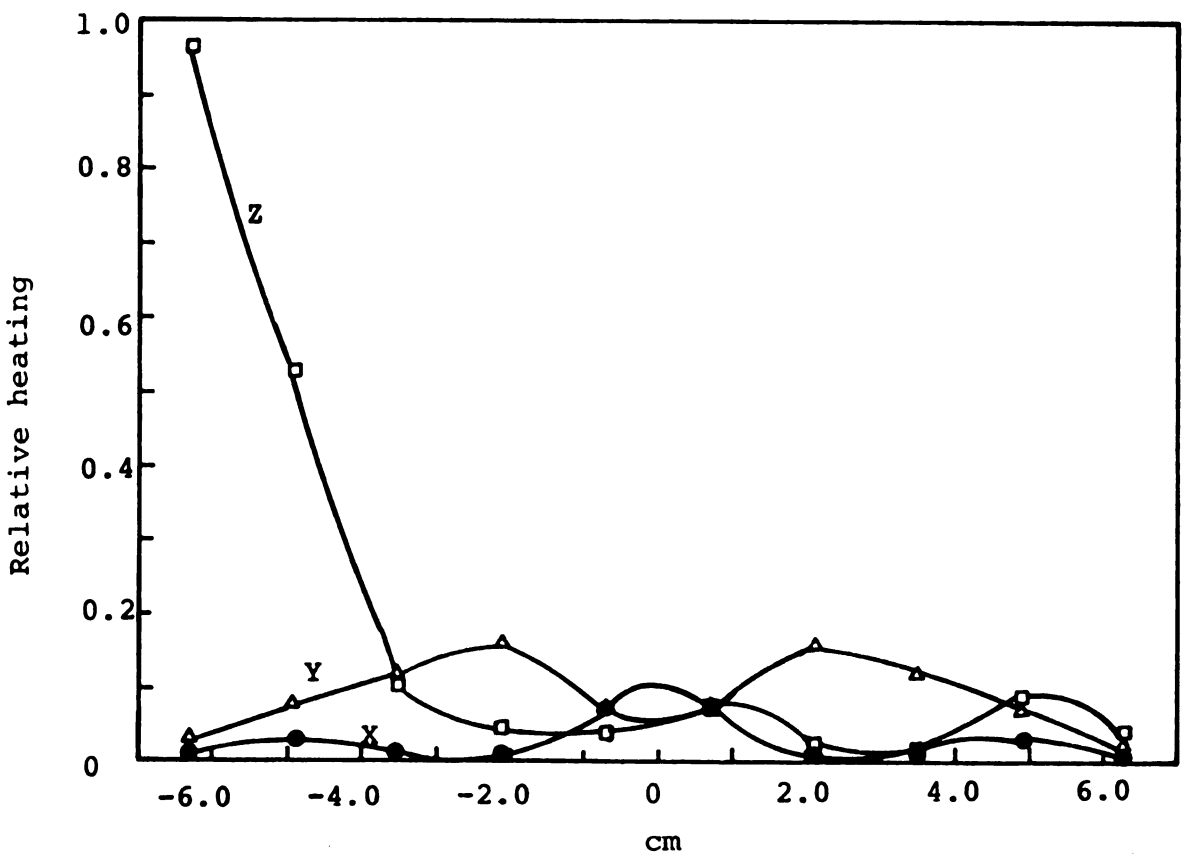

Figure 3.5b. Distributions of heating along the x, y and z axes of a "cubic spherical" brain of 7 cm radius induced by a plane EM wave of 2450 MHz propagating in the +z direction with a power density of 1 mW/cm2. Electrical properties of the brain, the average and maximum heatings are shown. One eighth of the "cubic sphere" is constructed with 73 cubic cells.

(Exact Solution)

Brain (7 cm radius) Pi = 1 mW/cm^2

Freq. = 2450 MHz Ave. heating = 0.092 mW/cm^3

ε_r = 30.9, σ = 1.1 S/m Max. heating = 0.396 mW/cm^3

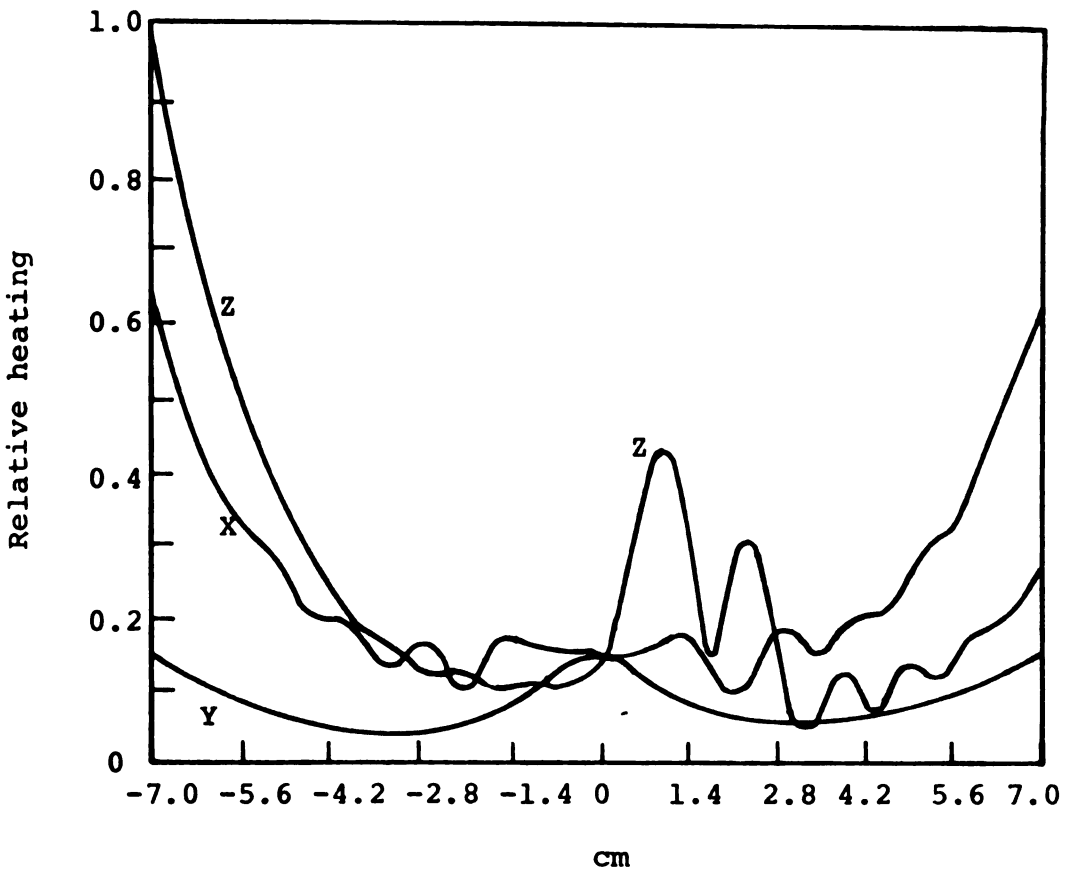

Figure 3.5c. Distributions of heating along the x, y and z axes of a spherical brain of 7 cm radius induced by a plane EM wave of 2450 MHz propagating in the +z direction with a power density of 1 mW/cm^2. Electrical properties of the brain, the average and maximum heatings are shown. Numerical results are obtained from the exact solution of Mie theory.

result on the induced EM heating in each cubic cell is the average heating within the cell, therefore unless the size of the cubic cell is small or comparable with the skin depth, the rapidly attenuating nature of the induced EM heating cannot be predicted by our numerical method. In Figure 3.5a, the rapidly attenuating nature of the induced EM heating in the front surface is missing because the cubic cell in this case is relatively large electrically. However, as the size of the cubic cell is reduced as in Figure 3.5b, the rapidly attenuating nature of the induced EM heating is recovered in the front surface of the spherical brain. The average heatings predicted by the numerical method are quite good, especially, for the case of 73 subdivision. For the maximum heating, numerical results at this frequency are poor.

From this example, it appears that to calculate the internal EM field induced by a 2450 MHz EM wave inside a typical spherical model of human brain with our numerical method, the subdivision of one eighth of the spherical brain into 73 cubic cells can only yield fair results. More accurate results will necessitate the subdivision of the spherical brain into a larger number of smaller cubic cells. Fortunately, the case of 2450 MHz is not as important as the case of 918 MHz, because the latter induces a strong resonance in a human brain. For the frequency of 918 MHz, our numerical method yields satisfactory results when one eighth of the sphere brain is subdivided into 73 cubic cells.

Table 3.1 shows comparisons of numerical results on the average and maximum heatings produced by our numerical method with that obtained from the exact solution of Mie theory. From this table, we can conclude that our numerical method predicts the average heating very well even

	Brain of 3 cm rad. at 918 MHz		Brain of 3 cm rad. at 2450 MHz		Brain of 7 cm rad. at 918 MHz			Brain of 7 cm rad. at 2450 MHz		
	numerical results 40 cells	exact solution	numerical results 40 cells	exact solution	numerical results 40 cells	numerical results 73 cells	exact solution	numerical results 40 cells	numerical results 73 cells	exact solution
Average heating ($\frac{mW}{cm^3}$)	0.3202	0.295	0.235	0.278	0.107	0.115	0.117	0.068	0.094	0.092
Maximum heating ($\frac{mW}{cm^3}$)	0.885	0.814	1.571	1.698	0.594	0.619	0.458	0.141	1.1	0.396

Table 3.1 Comparisons of numerical results on the average and maximum heatings calculated from the numerical method and that obtained from the exact solution of Mie theory. (incident power density = 1 mW/cm^2).

though the brain is subdivided into a relatively small number of cubic cells. For the maximum heating, our method can also produce satisfactory results if the dimension of cubic cell is kept to be electrically small, for example, one tenth of the free space wavelength or smaller.

3.4 Induced EM heating in Realistic Models of Human and Animal Heads.

The controversy of potential health hazards due to non-ionizing electromagnetic radiation has led to many studies on the induced EM heating in the brain and eyes of humans and animals. Existing theoretical studies by many researchers (4, 7-9) on the induced EM heating in the brain were either based on a homogeneous spherical model or a multilayer spherical model. It was reported in these studies that a UHF EM wave can excite an EM resonance and create a hot spot inside the human brain, and a microwave can cause a similar phenomenon inside an animal brain.

In reality, the brain is not spherical in shape and it is surrounded by other tissues of irregular geometries. Therefore, it seems important to quantify the induced EM heating inside a realistic model of a human head or an animal head that consists of a brain of realistic shape and eyes surrounded by a bony structure. To handle such an irregular geometry, the only potent method is the numerical method.

After the accuracy of the numerical method was verified in the case of spherical brains as explained in the preceeding section, the method was employed to quantify the induced EM heating in a realistic model of human or animal head that consists of a brain of realistic

shape and two eyes surrounded by a bony structure as shown in Figure 3.6a, where the brain and eyes are indicated by shaded regions. The head was subdivided into 180 cubic cells of various sizes in the numerical calculation. We have also calculated the EM heating induced in the bare brain without the surrounding bony structure. This case was considered for the purpose of assessing the effect of the surrounding bony structure on the induced EM heating in the brain.

Figure 3.6a shows the distribution of the EM heating or SARs in mW/m^3 inside a human head, with dimensions of 18x18x24 cm, induced by a plane EM wave of 918 MHz with a vertically polarized electric field of 1 V/m, incident upon the head from its front surface. The dielectric constant ε_r and conductivity σ for the brain and eyes are assumed to be 51.0 and 1.6 S/m, respectively, at this frequency. ε_r and σ for the surrounding bony structure are assumed to be 5.6 and 0.101 S/m, respectively. Since the human head is in near resonance at the frequency of 918 MHz, strong induced SARs inside the head are expected. The distribution of SARs in Figure 3.6a shows that the induced SARs are generally strong inside the head, with the maximum SAR located at the central part of the head. The SARs in the brain and eyes are relatively low compared with that in the surrounding bony structure. However, the maximum SAR in the brain can reach a value of 21.5 mW/m^3. The total power dissipated in the brain is 3.202×10^{-6} W and that in the whole head is 4.522×10^{-5} W. It is noted that if the incident EM wave has a power density of 1 mW/cm^2, the induced SARs in Figure 3.6a should be multiplied by a factor of 4.466×10^3. Thus, the maximum heating inside the brain is estimated to be 0.096 mW/cm^3. This value

is about one fifth of the value predicted with the model of a spherical brain as shown in Figures 3.4a, 3.4b and 3.4c.

Figure 3.6b shows the distribution of SARs inside a bare human brain, without the surrounding bony structure, induced by a plane EM wave of 918 MHz with a vertically polarized electric field of 1 V/m. ε_r and σ of the brain and eyes are assumed to be 51.0 and 1.6 S/m, respectively. The induced SARs in the central part of the bare brain are found to be considerably higher than the SARs induced inside the brain surrounded by the bony structure as shown in Figure 3.6a. The total dissipated power in the bare brain is found to be 4.591×10^{-6} W which is about 43% higher than the case of the brain surrounded by the bony structure. This example implies that the surrounding bony structure around the brain tends to reduce the induced EM heating inside the brain.

Figure 3.7a shows the distribution of SARs in the same human head of Figure 3.6a induced by a plane EM wave of 2450 MHz with a vertically polarized electric field of 1 V/m. ε_r and σ for the brain and eyes are assumed to be 47 and 2.21 S/m, respectively, while ε_r and σ for the surrounding bony structure are assumed to be 5.5 and 0.15 S/m, respectively. At this frequency, the induced field is mainly concentrated near the front surface of the head, and thus, induced SARs in the brain are generally very low. The interesting point to observe is the SAR induced inside the eyes. Even though the eyes are located in the front surface of the head and the EM wave is directly incident upon them, the induced SAR inside the eyes is very small compared with that in the surrounding bony structure. The total dissipated power in

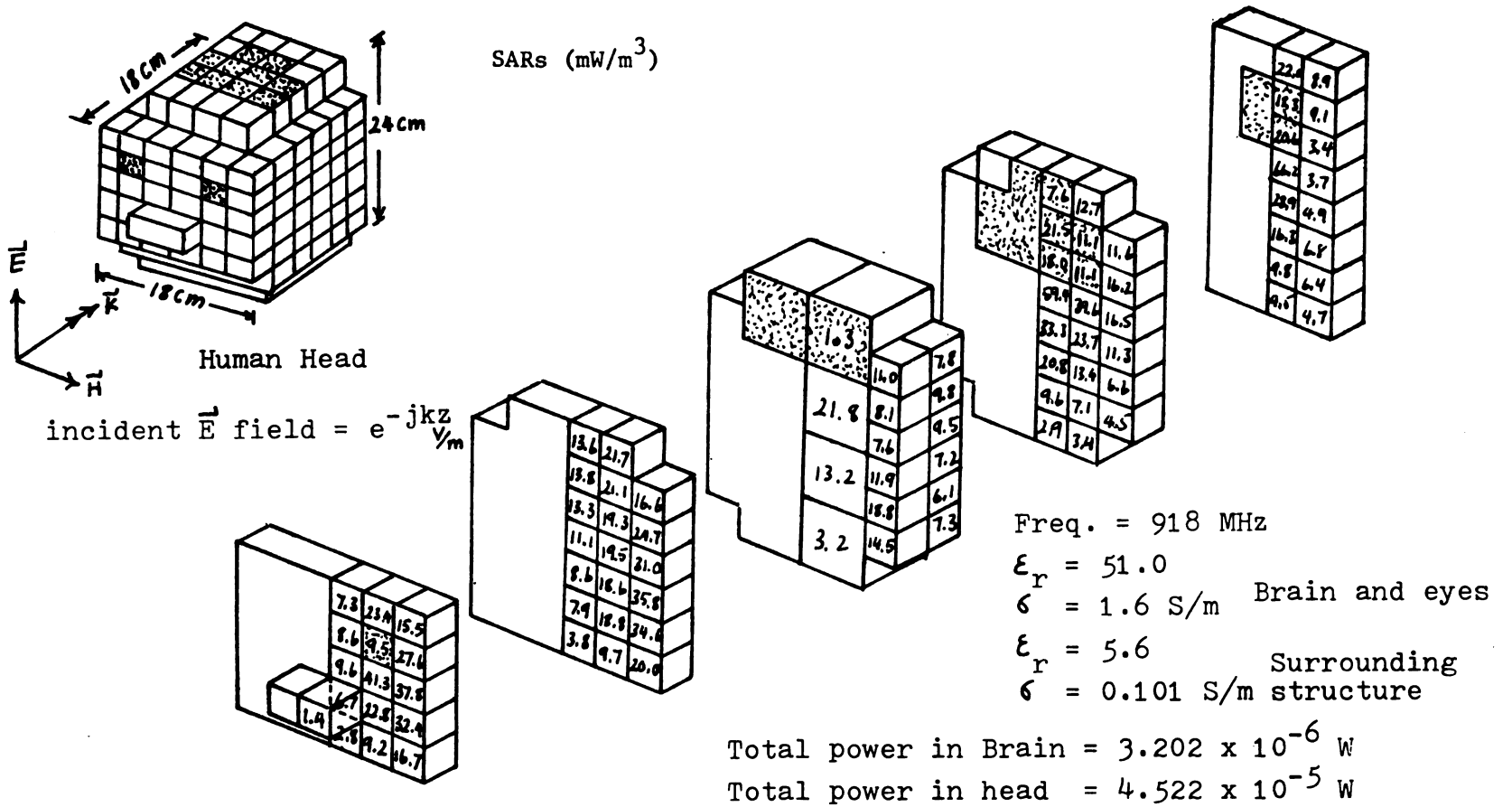

Figure 3.6a. Distribution of SARs inside a human head induced by a plane EM wave of 918 MHz with a vertically polarized electric field of 1 V/m.

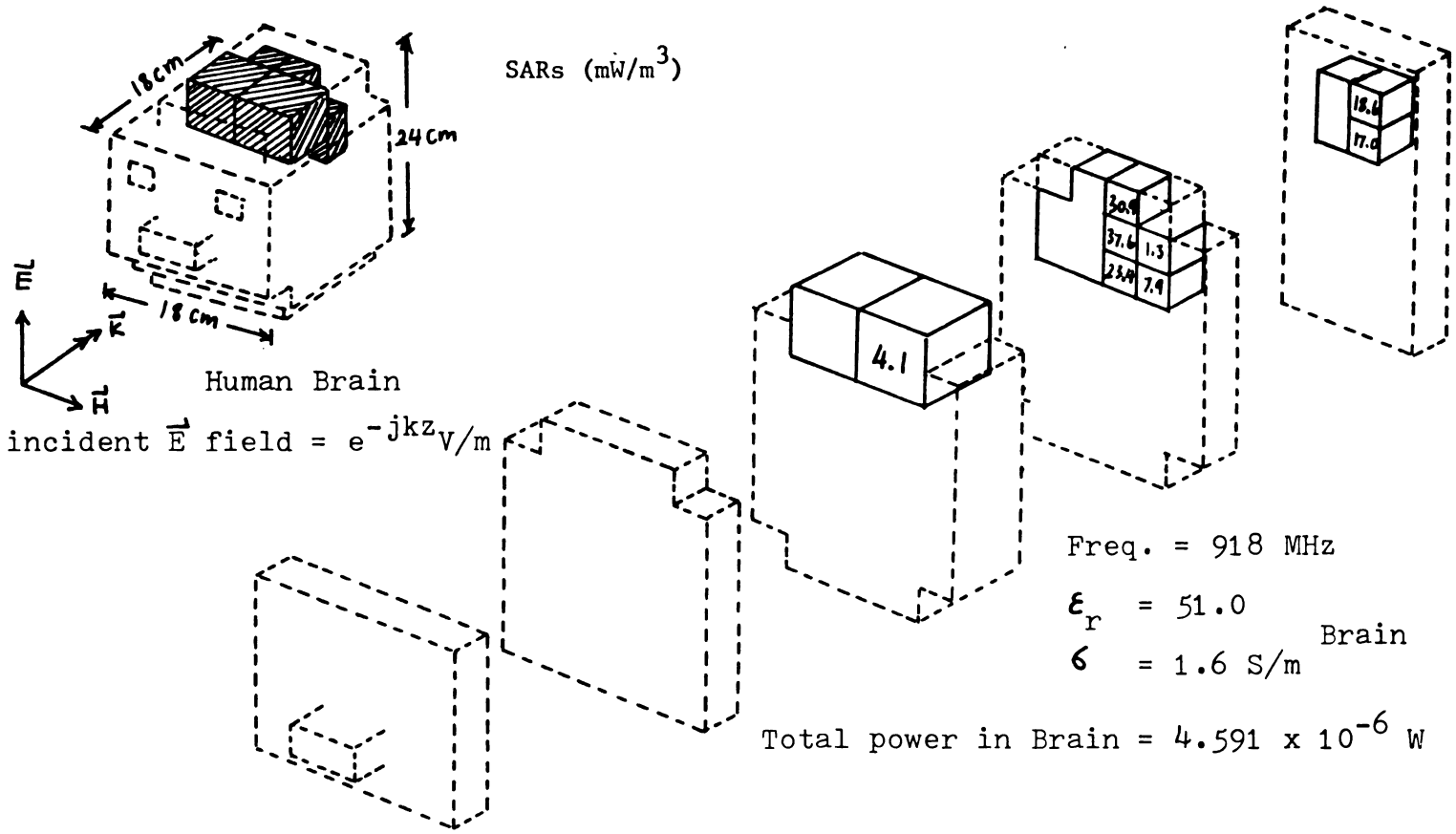

Figure 3.6b. Distribution of SARs inside a human brain, without the surrounding bony structure, induced by a plane EM wave of 918 MHz with a vertically polarized electric field of 1 V/m.

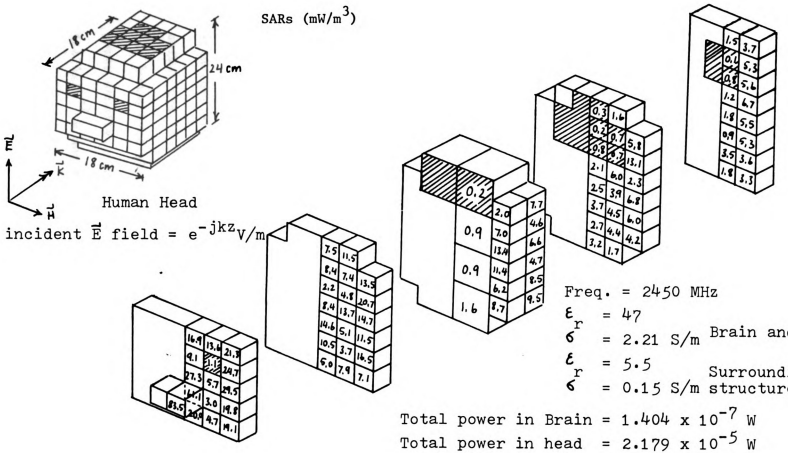

Figure 3.7a. Distribution of SARs inside a human head induced by a plane EM wave of 2450 MHz with a vertically polarized electric field of 1 V/m.

the brain at this frequency is 1.404×10^{-7} W and that in the head is 2.179×10^{-5} W. These values are much smaller compared with the case of 918 MHz.

When the bare brain without the surrounding bony structure is immersed in the same EM wave of 2450 MHz, the induced SARs inside the brain are shown in Figure 3.7b. These values are somewhat greater than the case of Figure 3.7a, but they are still very low compared with the case of 918 MHz. The total dissipated power in the bare brain is found to be 4.20×10^{-7} W.

For the last example, we consider an animal head exposed to a plane EM wave of 2450 MHz because this frequency is known to excite a resonance in a brain with a radius of about 3 cm. Figure 3.8a shows the distribution of SARs inside an animal head, with dimensions of 9x9x12 cm, induced by a plane EM wave of 2450 MHz with a vertically polarized electric field of 1 V/m. ε_r and σ for the brain, eyes and the surrounding bony structure are assumed to be the same as the case of Figure 3.7a. From Figure 3.8a, it is observed that the induced SARs inside the animal brain are quite high and are in the same order of magnitude as the induced SARs inside the human brain when it is exposed to an EM wave of 918 MHz. The SARs in the surrounding bony structure are even higher than the SARs in the brain. The SAR in the animal eye is 9.6 mW/m^3, which is about 10 times higher than that in the human eyes when they are exposed to a 918 MHz EM wave of the same power density. The total power dissipated in the animal brain is 6.814×10^{-7} W and that in the animal head is 9.411×10^{-6} W.

When the bare animal brain without the surrounding bony structure

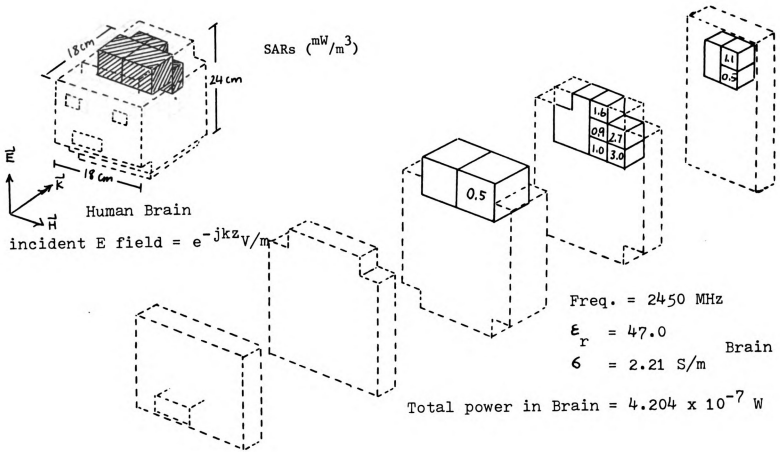

Figure 3.7b. Distribution of SARs inside a human brain, without the surrounding bony structure, induced by a plane EM wave of 2450 MHz with a vertically polarized electric field of 1 V/m.

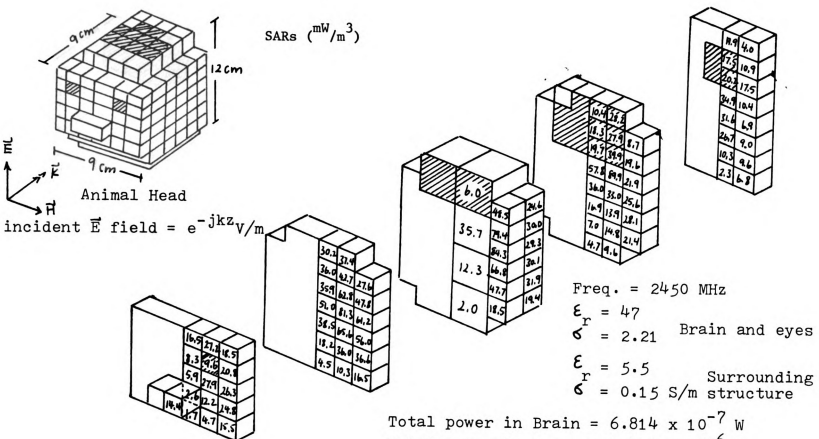

Figure 3.8a. Distribution of SARs inside an animal head induced by a plane EM wave of 2450 MHz with a vertically polarized electric field of 1 V/m.

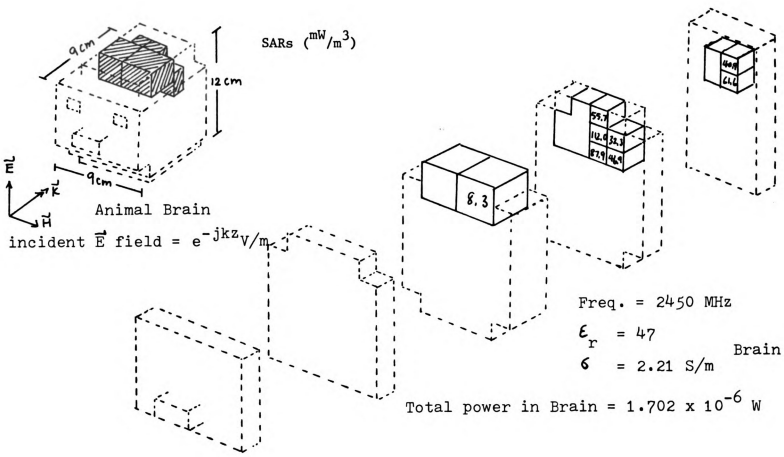

Figure 3.8b. Distribution of SARs inside an animal brain, without the surrounding bony structure, induced by a plane EM wave of 2450 MHz with a vertically polarized electric field of 1 V/m.

is exposed to the same EM wave of 2450 MHz, the induced SARs inside the brain are shown in Figure 3.8b. It is observed that the induced SARs in the bare brain is much higher than the case of Figure 3.8a. The total power dissipated in the bare animal brain is found to be 1.702×10^{-6} W which is more than twice the value of the case shown in Figure 3.8a. From this example, it appears that the surrounding bony structure has a significant effect on the induced EM heating in the animal brain when the animal head is exposed to 2450 MHz EM wave.

To summarize the findings in this section, it appears that the bony structure surrounding the brain tends to reduce the induced EM heating in the brain. The induced EM heating in the brain calculated on the realistic model of a brain within a head is significantly different from the results obtained with an idealistic model of a spherical brain. The induced EM heating in eyes is found to be relatively low compared with that in the surrounding bony structure.

CHAPTER 4

INDUCED EM FIELDS INSIDE THE CUBICAL BODIES

EXPERIMENTAL VERIFICATION

To confirm the accuracy of the tensor integral equation, a series of experiments have been conducted to measure the induced electric field inside the cubic boxes with different size. The phantom materials of varying conductivity were used to model the biological body (phantom model). The phantom models were exposed to a maximum electric field and a maximum magnetic field of a standing EM wave which was created in front of the reflector.

The accuracy of the theory has been checked by comparing the induced electric field inside the phantom cubic boxes with the corresponding experimental results.

4.1 Experimental Set Up

The set up for this experiment is shown in Fig. 4.1. The experiment was conducted inside a large microwave anechoic chamber in which a standing EM wave was created by radiating an EM wave upon a metallic reflector. Standing waves of the electric field $\vec{E}^i$ and the magnetic field of $\vec{H}^i$ set up in front of the reflector are depicted in Fig. 4.1. The electric field of the wave is polarized horizontally and the magnetic field is vertically polarized.

When the phantom cube is placed at the location of a maximum electric field, the impressed electric field on the cube is

$$\vec{E}^i = \hat{x}\, E^i_{max} \cos kz \qquad (4.1)$$

where z = 0 corresponds to the center of the cube. This symmetrically impressed electric field will excite a linear electric mode of induced electric field in the cube.

On the other hand, when the cube is placed at the location of a minimum electric field, or a maximum magnetic field, the impressed electric field on the cube is

$$\vec{E}^{i} = \hat{x}\, E^{i}_{max} \sin kz \qquad (4.2)$$

This impressed electric field is antisymmetrical with respect to the center of the cube, z = 0, and it will excite a circulartory magnetic mode of induced electric field in the cube. It is noted that this magnetic mode can be considered as excited by the magnetic field of the EM wave, from a different point of view.

4.2 Construction of Probe

The main difficulty in the direct measurement of the induced electric field in a phantom model or biological body is the availability of a workable, implantable electric field probe. Although a miniature electric field probe, capable of measuring the electric field from 0.915 to 10 GHz., has been reported by Bassen et al. (1975), the frabication of this probe requires thin-film technique and it is not commercially available. There is a need for an implantable electric field probe which can be constructed inexpensively and handled ruggedly for researchers in the bioelectromagnetic area. In this study such a probe has been developed and used in experiments of measuring induced electric field inside a biological body.

A conventional electric field probe for measuring the electric fields of EM waves consists of a short dipole loaded with a microwave diode and connected with a pair of very thin, high resistive wires. This probe can be used to measure the electric field of an EM wave in space by orientating its lead wires perpendicular to the electric field vector to minimize the induced current in the lead wires, or to minimize the interference caused by the lead wires. However, when implantable electric field probe loaded with a microwave diode is inserted into a finite conducting body to measure the internal electric field, a great difficulty is usually encountered. The situation is depicted in Fig. 4.2a which shows that the electric field on the body surface is much higher than the internal electric field and is mainly perpendicular to the surface, and in parallel with the lead wires. Thus, while the probe is excited by a weak internal electric field, the strong electric field on the body surface can induce a large current on the lead wires over the section adjacent to the probe. Unless the probe system is perfectly symmetrical, the antisymmetrical component of the induced current on the lead wires will be detected by the diode and adds a very large noise to the probe output. It is also found that this noise can not be minimized sufficiently with a pair of very thin, high resistance wires placed very close or twisted around.

A scheme to overcome this difficulty is shown in Fig. 4.2b. In this scheme, the section of lead wires adjacent to the probe is constructed with two series of lumped resistors of 3 KΩ. This large resistance minimizes the current induced in the lead wires by the strong surface electric field and, consequently, minimizes the noise

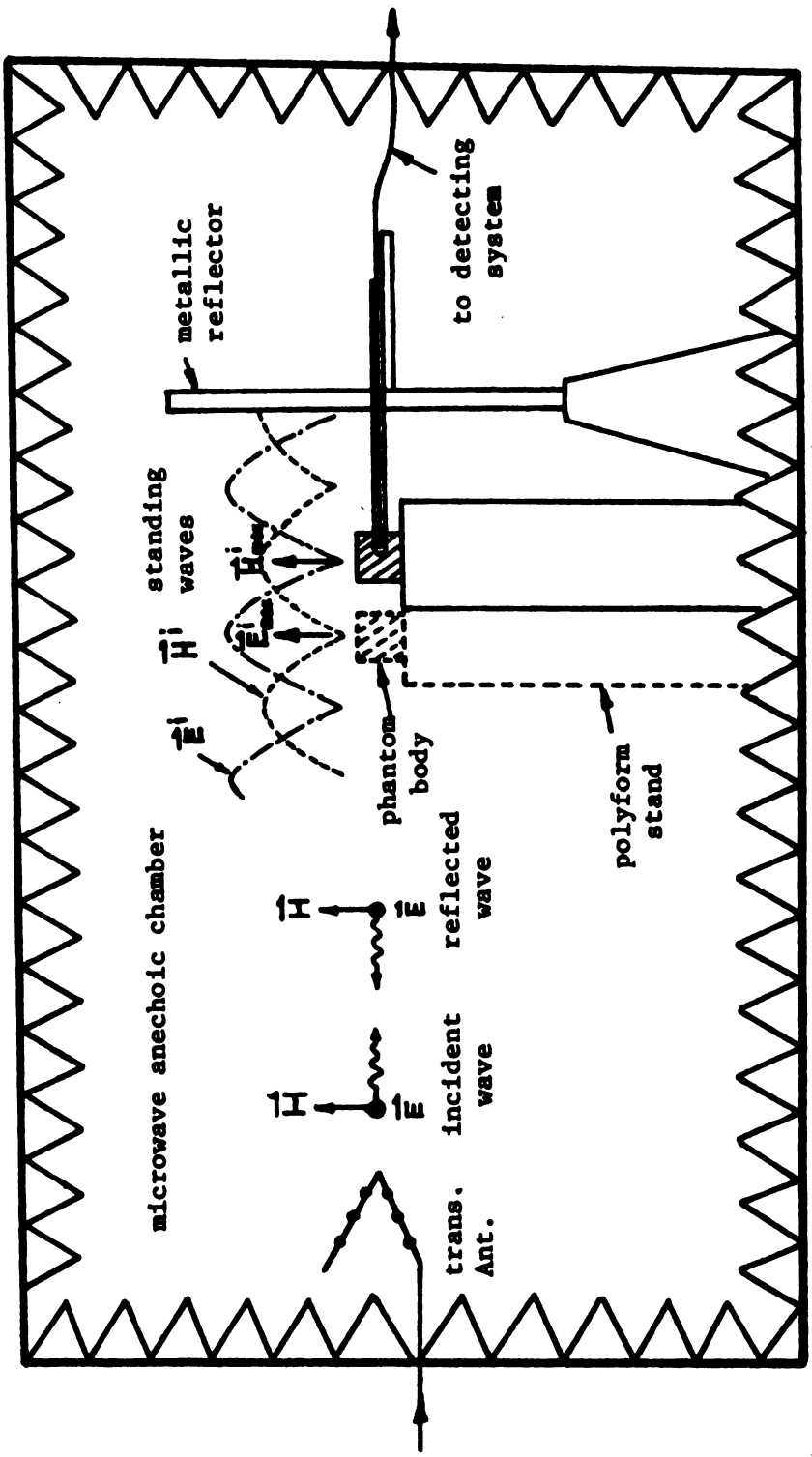

Figure 4.1. The schematic diagram of the experimental setup for the measurement of induced electric field inside the phantom model.

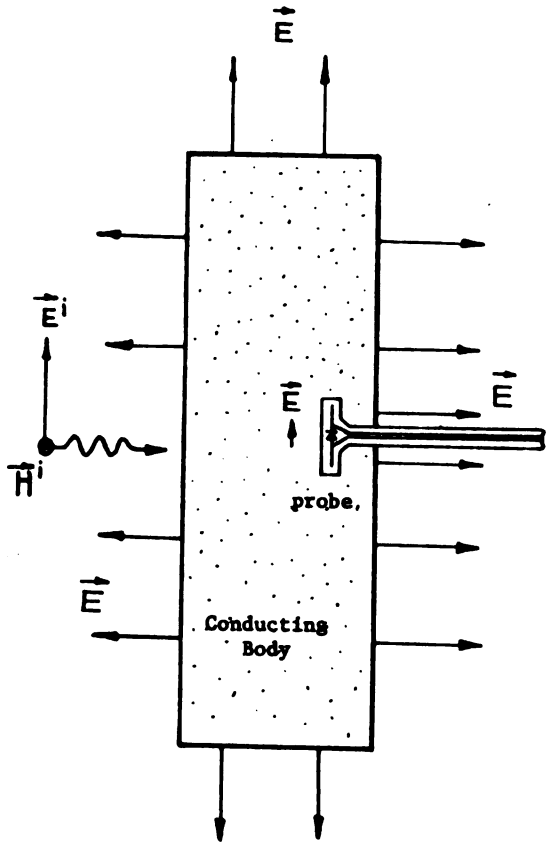

Fig. 4.2a
An implantable electric field probe
immersed inside a conducting body

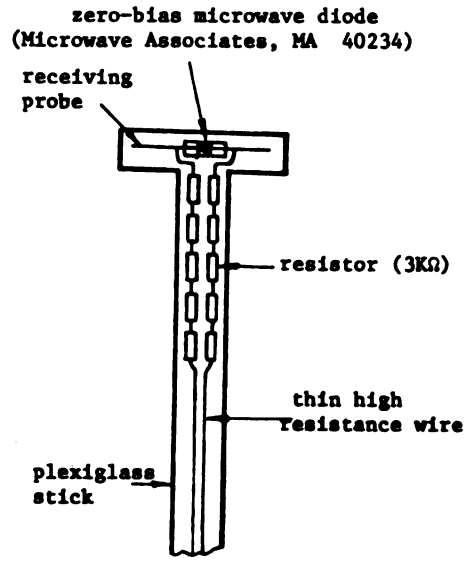

Fig. 4.2b.
An implantable electric field probe
with interference-free lead wires.

component of the probe output signal. The probe itself is made from a zero-bias microwave diode (Microwave Associates, MA 40234). The probe and the lead wire system are encased in a plexiglass stick with the help of epoxy glue. The probe is very rugged and inexpensive and its dimension is about 1 cm.

4.3 Theoretical and Experimental Results

The experimental results on the induced electric fields inside the cubical phantom models are compared with the theoretical values of the induced electric fields obtained from the tensor integral equation method.

The cubical phantom model used in the study is depicted in Fig. 4.3. For the theoretical analysis, one eighth of the cube is divided into 27 cubic cells.

Figure 4.4a shows the case of a cubical phantom model of 2x2x2 cm placed at the location of a maximum electric field of a 750 MHz standing wave in front of the reflector. The dielectric constant and conductivity are assumed to be 50 and 4.5 S/m, respectively. The numerical results on the X-component of the induced electric fields along the Z-axis inside the cube are plotted in this figure. The results show a linear electric mode of induced electric field which is rather uniform in the cube.

In the corresponding experiment, a phantom model of a cubic box with dimension 2x2x2 cm was constructed with thin plexiglass filled with phantom material of the same dielectric constant and conductivity as above ($\varepsilon_r = 50$, $\sigma = 4.5$ S/m). The X-component of the induced electric field has been probed at a 2 mm interval along the z-axis.

By inserting the probe from the back surface along z-axis and taking the data every increment of 2 mm until the probe reaches the front surface. The experimental results of the x-components of the induced electric fields along the z-axis inside the cube were also plotted in Fig. 4.4a. The experimental results compare very well with the theory for this linear electric mode of induced electric field inside the cube.

In Fig. 4.4b, we consider the same cube but now the cube is located at the location of the minimum electric field. In the theoretical calculation, the dielectric constant and conductivity are assumed to be the same as before and again one eighth of the cube is divided into 27 cubic cells. The impressed field for this case is $\vec{E}^i = \hat{x}\, E^i_{max} \sin kz$ with the minimum electric field located at the center of the cube. The same experimental procedure was used to measure the induced electric field. The theoretical and experimental results are plotted in the same figure for comparison. A good agreement is obtained between theory and experiment and these results show a circulatory magnetic mode of induced electric field excited in the cube.

In Fig. 4.5a, we consider a phantom cube with dimensions of 4x4x4 cm, placed at the location of a maximum electric field of 750 MHz standing wave. In the numerical calculation, the same dielectric constant and conductivity ($\varepsilon_r = 50$, $\sigma = 4.5$ S/m) are assumed and one eighth of the cube is divided into 27 cubic cells. In this experiment, a phantom material with the same dielectric constant and conductivity was packed in the cubic plexiglass box of size 4x4x4 cm. The x-component

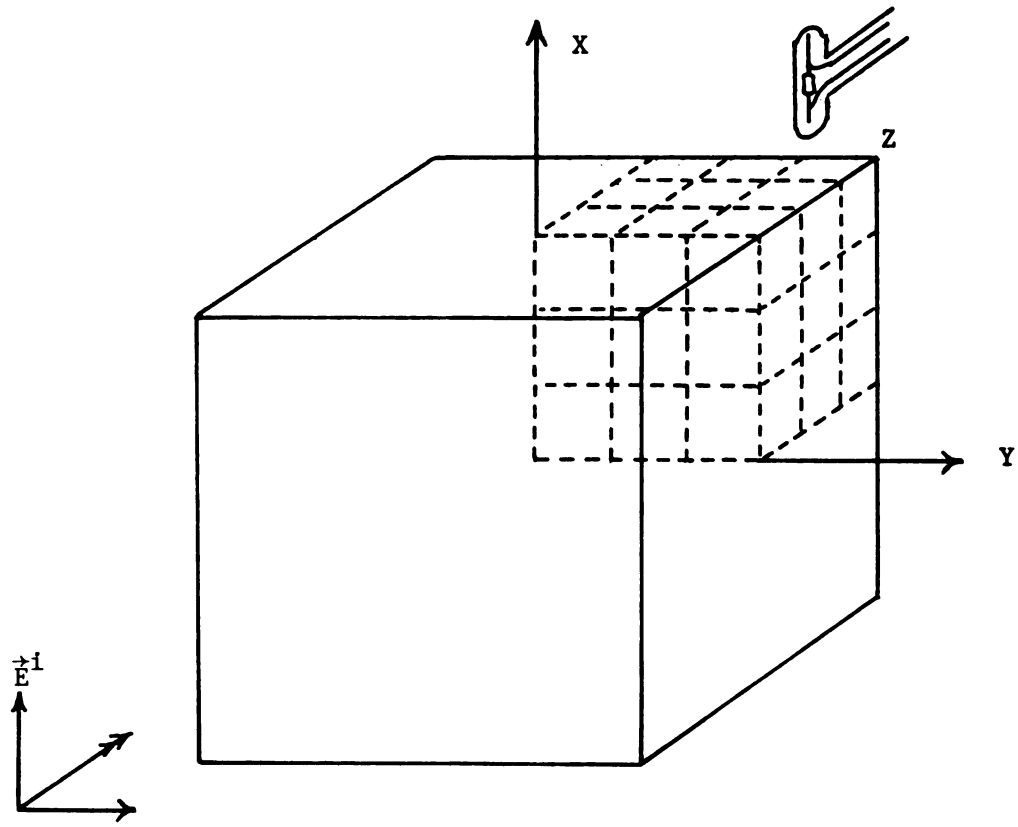

Figure 4.3. A cubical phantom model is illuminated by an EM wave. One eighth of the cube is divided into 27 cubic cells.

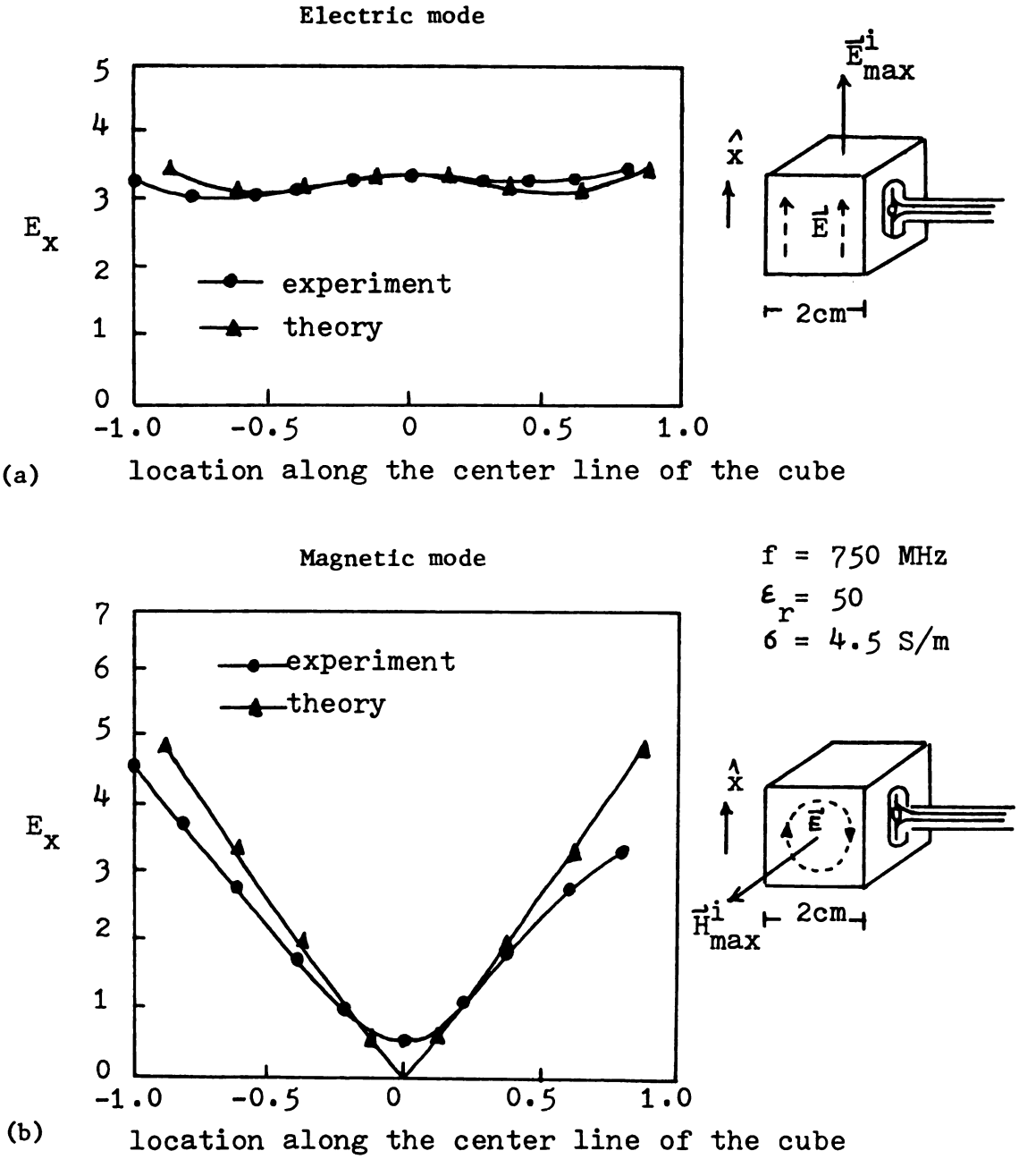

Figure 4.4. Theoretical and experimental results of the x-components of the induced electric field, E_x, along the z-axis of the 2-cm cube, placed at the locations of a maximum electric field and a maximum magnetic field of a 750 MHz, EM standing wave.

of the induced electric field was probed along the z-axis. Theoretical and experimental results show a good agreement for this case. In Fig. 4.5b, the same phantom cube is placed at the location of a minimum electric field. For this case a good agreement is again obtained between experiment and theory.

From these two examples of 2 cm cube and 4 cm cube, it is found that the magnetic mode becomes much greater than the electric mode in the larger cube.

Next we will study the effect of the conductivity of the biological system on the induced electric field inside the body. We consider a 2x2x2 cm phantom cubic with the dielectric constant and conductivity of 50 and 3.0 S/m, respectively. In the numerical calculation, one eighth of the cube was divided into 27 cubic cells and the induced electric field inside the cube was calculated. In the experiment, the field probe was inserted into the body along the z-axis to measure the x-component of the induced electric field along the z-axis. Fig. 4.6a shows the experimental and theoretical results when the cube was placed at the location of a maximum electric field of a 750 MHz standing wave. Fig. 4.6b shows the experimental and theoretical results when the cube was placed at the location of a maximum magnetic field of the same standing wave. Both results show a good agreement between theory and experiment. From these results we observe that when the conductivity decreases the linear electric mode of the induced electric field becomes greater than the circulatory magnetic mode of the induced electric field in the cube.

After three examples have been checked at 750 MHz, we proceeded

(

E_1

(b)

Fig

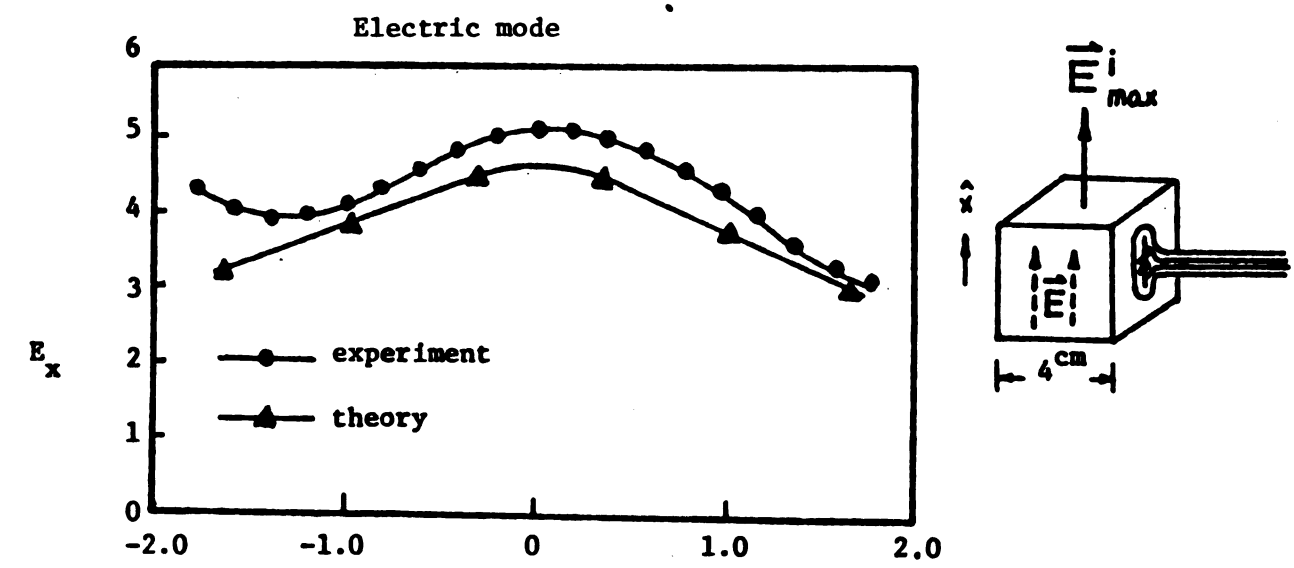

(a) location along the center line of the cube

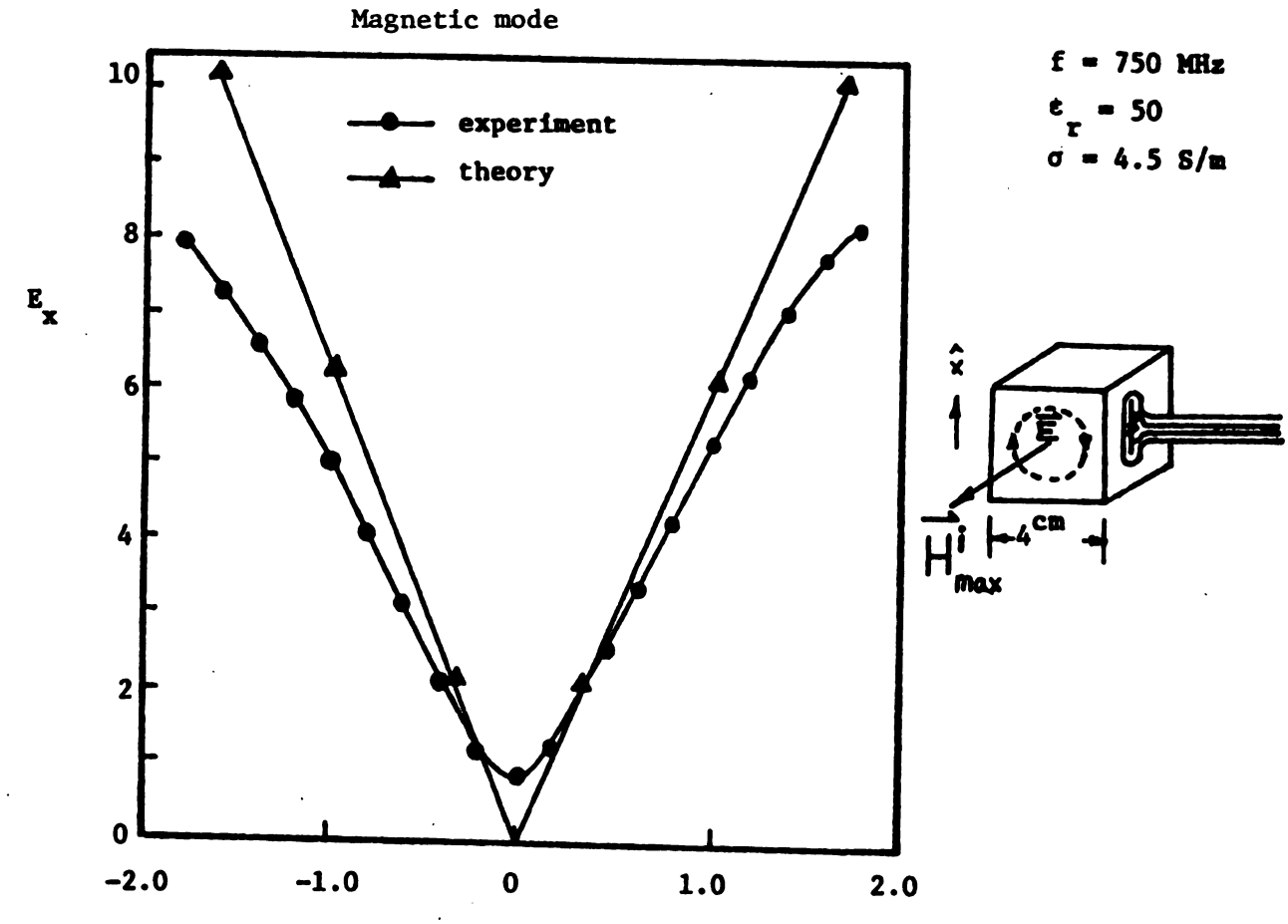

(b) location along the center line of the cube

Figure 4.5 Theoretical and experimental results of the x-components of the induced electric field, E_x, along the z-axis of the 4-cm cube, placed at the locations of a maximum electric field and a maximum magnetic field of a 750 MHz, EM standing wave.

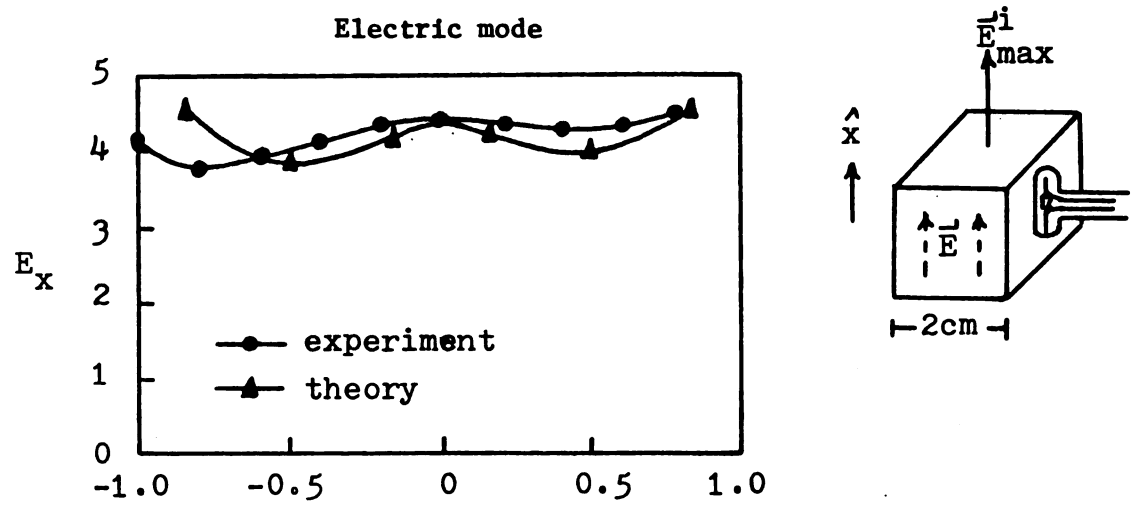

(a)

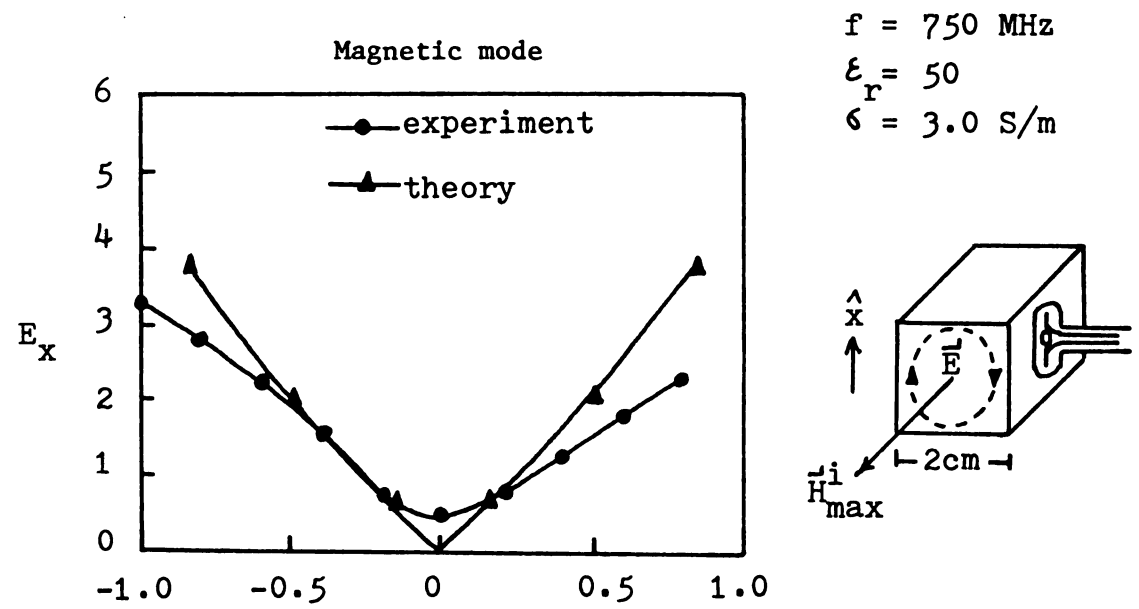

(b)

Figure 4.6 Theoretical and experimental results of the x-components of the induced electric fields, E_x, along the z-axis of the 2-cm cube, placed at the locations of a maximum electric field and a maximum magnetic field of a 750 MHz, EM standing wave.

to check the validity of the theory at a high frequency of 1 GHz. The phantom cube was exposed to 1 GHz standing wave in the experiment.

Figs. 4.7a and 4.7b show the theoretical and experimental results on the x-components of the induced electric fields along the z-axis of the phantom cube of 2x2x2 cm when the cube is placed at the maximum electric field location and the maximum magnetic field location of the 1 GHz standing wave, respectively. The dielectric constant and conductivity are assumed to be 50 and 4.5 S/m, respectively. The results show that the theory agree very well with the experiment.

Figures 4.8a and 4.8b show the theoretical and experimental results on the x-components of the induced electric fields along the z-axis of the phantom cube of 4x4x4 cm when the cube is placed at the maximum electric field location and the maximum magnetic field location of 1 GHz standing wave, respectively. The dielectric constant and conductivity are assumed to be 50 and 1.62 S/m, respectively. The agreement between experiment and theory at this frequency is only fair because the electrical dimension of the cube becomes larger in this case.

From these two examples we also observe that when the cube becomes larger the magnetic mode tends to dominate the electric mode, and when the conductivity decreases the linear electric mode tends to increase in magnitude.

4.4 Summary

After the accuracy of our theory has been checked with Mie theory in Chapter 3, it was reconfirmed in this chapter by comparing it with a series of experimental results on the induced electric field measured in phantom cubes exposed to EM standing waves. Up to this

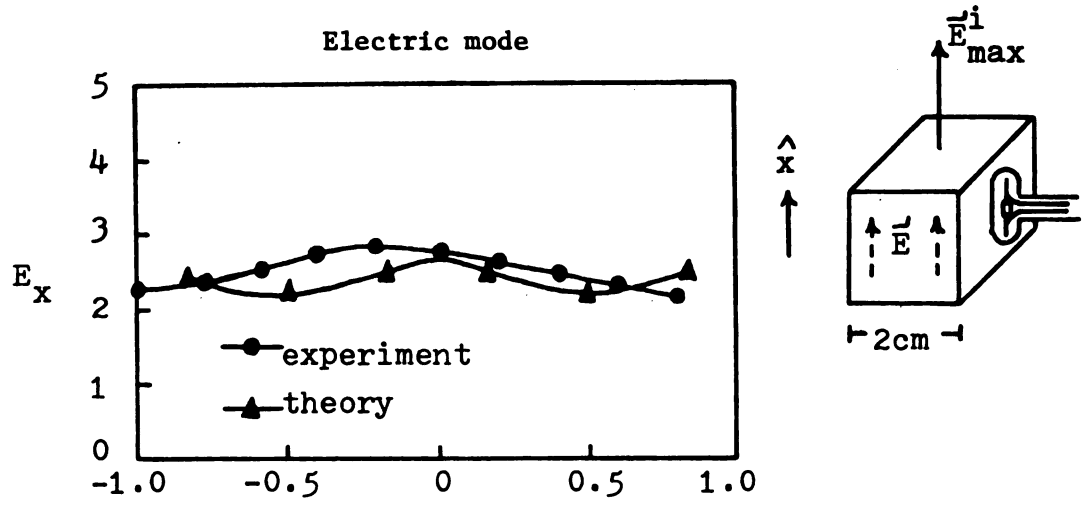

(a) location along the center line of the cube

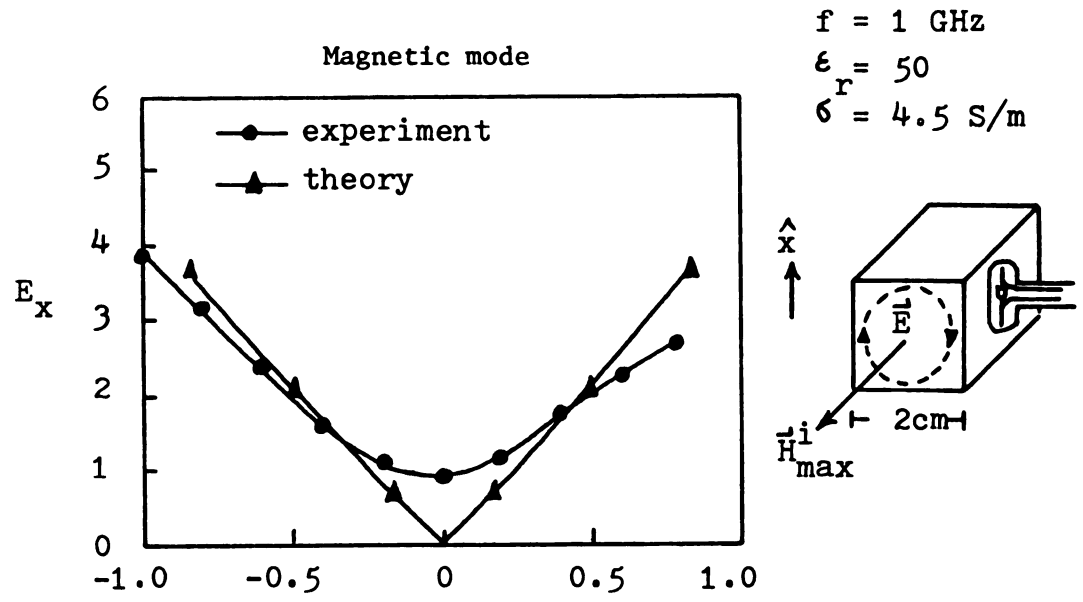

(b) location along the center line of the cube

Figure 4.7 Theoretical and experimental results of the x-components of the induced electric fields, E_x, along the z-axis of the 2-cm cube, placed at the locations of a maximum electric field and a maximum magnetic field of a 1 GHz, EM standing wave.

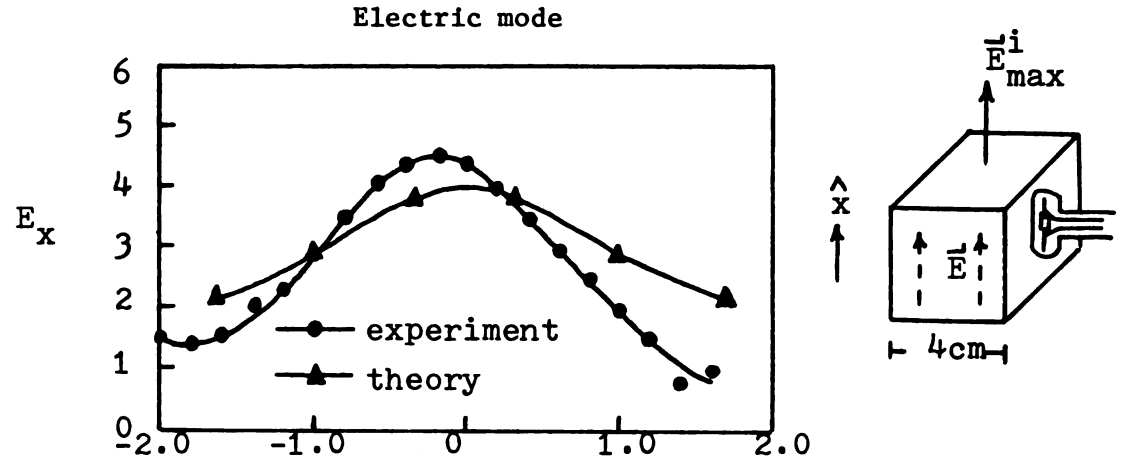

(a) location along the center line of the cube

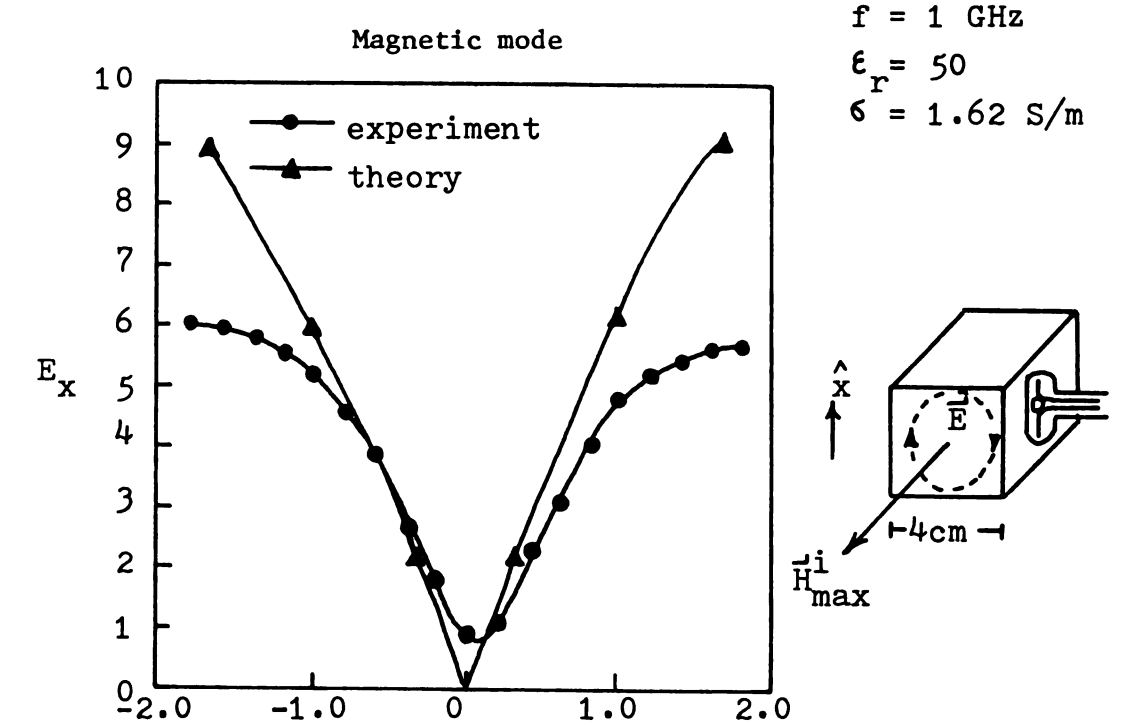

(b) location along the center line of the cube

Figure 4.8. Theoretical and experimental results of the x-components of the induced electric field, E_x, along the z-axis of the 4 cm cube, placed at the locations of a maximum electric field and a maximum magnetic field of a 1 GHz, EM standing wave.

point the accuracy of our theory has been established. We will use our theory to predict the induced electric field inside a human body with a realistic model in the next chapter. Also in this chapter we observe that the circulatory magnetic mode of the induced electric field has a significant effect in a large body at a low frequency.

CHAPTER 5

INDUCED EM FIELDS INSIDE HUMAN BODIES

The theoretical quantification of the induced electric field and the specific absorption rate (SAR) of EM energy inside a realistic model of human body irradiated by EM waves has been reported by Chen and Guru (10,11) and by Gandhi et al. (12). Experimentally, the induced SARs was determined indirectly by measuring the temperature distribution in an irradiated phantom model of man with a thermographical method by Guy et al. (14) or by a liquid-crystal temperature probe by Gandhi et al. (13). The temperature distribution in a phantom model may not correspond to the true distribution of the induced SARs because of the heat dissipation. A direct measurement of the induced electric field inside a phantom model of man should provide a more accurate distribution of the induced SARs.

The main difficulty in the direct measurement of the induced electric field in a phantom model of man or in a biological body is the availability of a workable, implantable electric field probe. We have described an implantable electric field probe which can be constructed inexpensively and handled ruggedly in Section 4.2. We have used this field probe to measure the induced electric field inside a phantom model of human body. Characteristics of the probe were checked by measuring the induced electric fields in small phantom cubes in Chapter 4. The measured induced electric fields with this probe were confirmed by theoretical results, and, thus, a good working condition for this probe was assured.

5.1 Experimental set up

The schematic diagram of the experimental set up for measuring the induced electric field in the phantom model of human body is shown in Fig. 5.1. The model was placed in a large microwave anechoic chamber and was irradiated by a travelling EM wave of 500 to 3000 MHz incident normally from front to back. An array antenna was used as a radiating source for the range of 500 to 1000 MHz and a horn antenna was used as a radiating source for the range of 1000 to 3000 MHz. A phantom model of man with 1/5 dimension of a typical man was constructed with thin plexiglass and filled with phantom material of appropriate conductivity and permittivity. Induced electric fields were probed over 28 locations in one side of the model. Detailed dimensions of the model are depicted in Fig. 5.2. Since the scaling factor of 5 was used in the model, thus, to simulate the actual human body the conductivity of the phantom model needs to be five times that of the human body and, at the same time, the model should have the same permittivity as the human body.

5.2 Theoretical and Experimental results

The theoretical and experimental results on the induced electromagnetic fields inside the phantom model of human body are shown in Figs. 5.3 to 5.8.

Figure 5.3 shows the relative distribution of measured induced electric field inside the phantom model of the human body for the case of 2500 MHz., conductivity and dielectric constant are 7.4 S/m and 50, respectively. In this experiment, a field probe was inserted into the body through the hole in the back surface and measured the

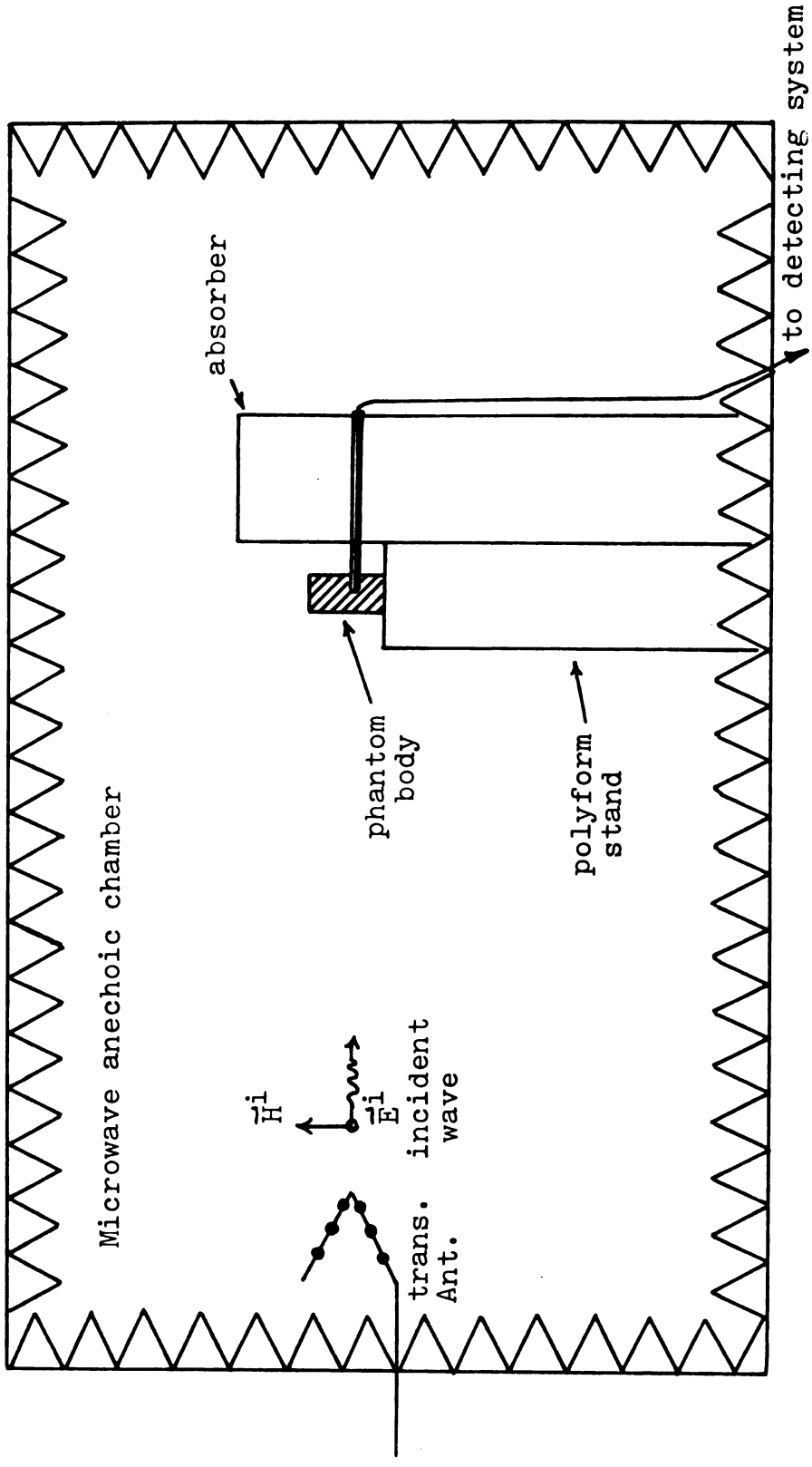

Figure 5.1. Experimental setup for measuring the induced electric field inside a phantom model of human body.

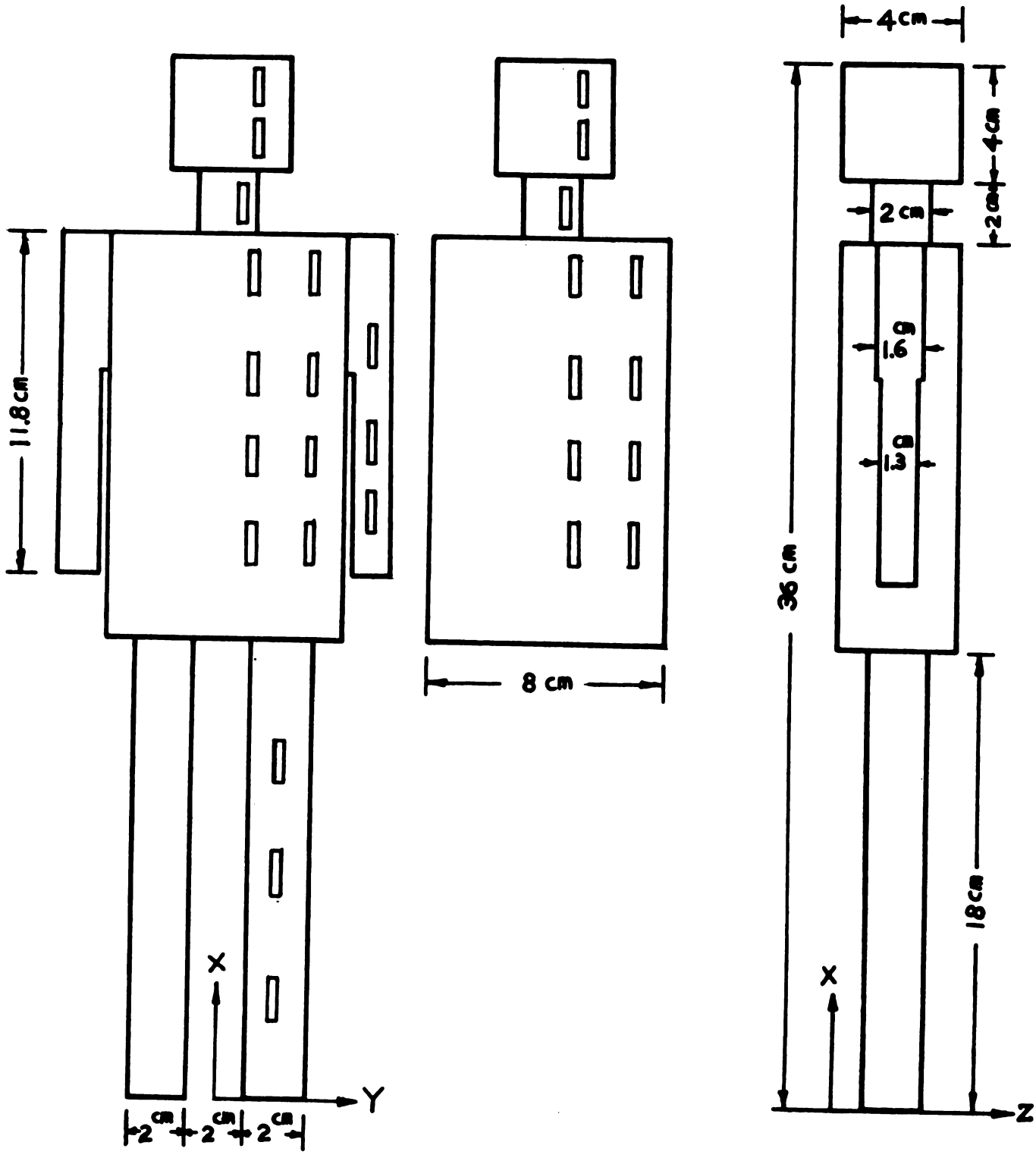

Figure 5.2. Geometry and dimensions of the phantom model of man.

induced electric field in the back layer first and then front layer by moving the probe further inside the body. The measurement was repeated at each of the 28 locations in the body. Figure 5.4 shows the distribution of corresponding theoretical results obtained from the tensor integral equation method. The theoretical results were obtained when the geometry of the phantom model was subdivided into 104 cubic cells of various sizes in the numerical calculation. Incident EM wave was assumed to be a plane wave travelling in the +z direction with a vertically polarized electric field.

Comparing Figs. 5.3 and 5.4, a quanlitative agreement is obtained between experiment and theory: the maximum field is found in the neck, and other high field regions in the arms, the legs, and the front part of the head. It is noted that this case simulates the case of a typical man with σ = 1.48 S/m and ε_r = 50 irradiated by an EM wave of 500 MHz.

Figures 5.5 and 5.6 show the relative distributions of measured induced electric field and theoretical induced electric field inside the phantom model of human body with σ = 7.0 S/m and ε_r = 50 irradiated by a travelling EM wave of 2000 MHz. Theoretical results were obtained with the 104-cell model as the previous case. A quanlitative agreement is again obtained between experiment and theory: the maximum field is found in the lower part of the arm, and other high field regions are found in the neck, the front part of the head and the legs.

Figures 5.7 and 5.8 show the relative distributions of experimental and theoretical results on the induced electric fields in a phantom

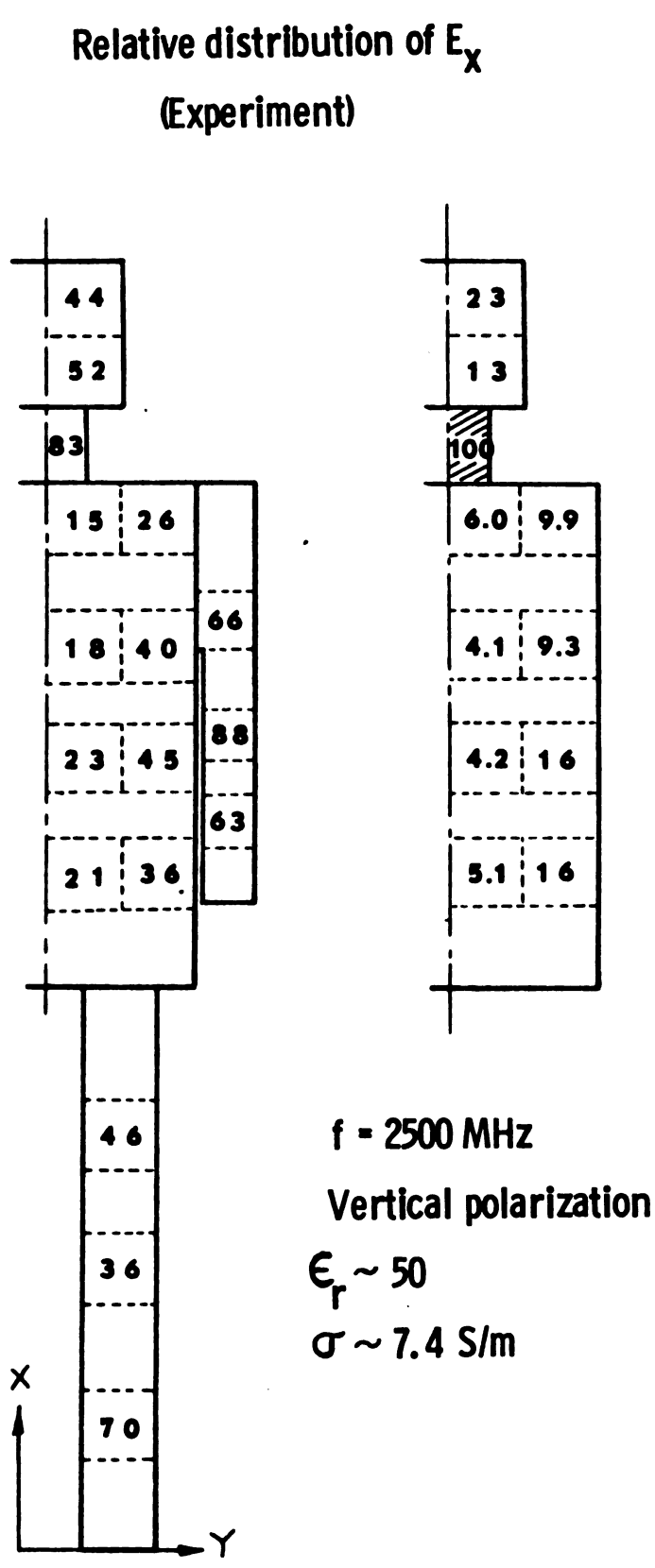

Figure 5.3 Relative distribution of the x-components of the measured induced electric fields inside the phantom model of man, excited by a vertically polarized, travelling EM wave of 2500 MHz at normal incidence.

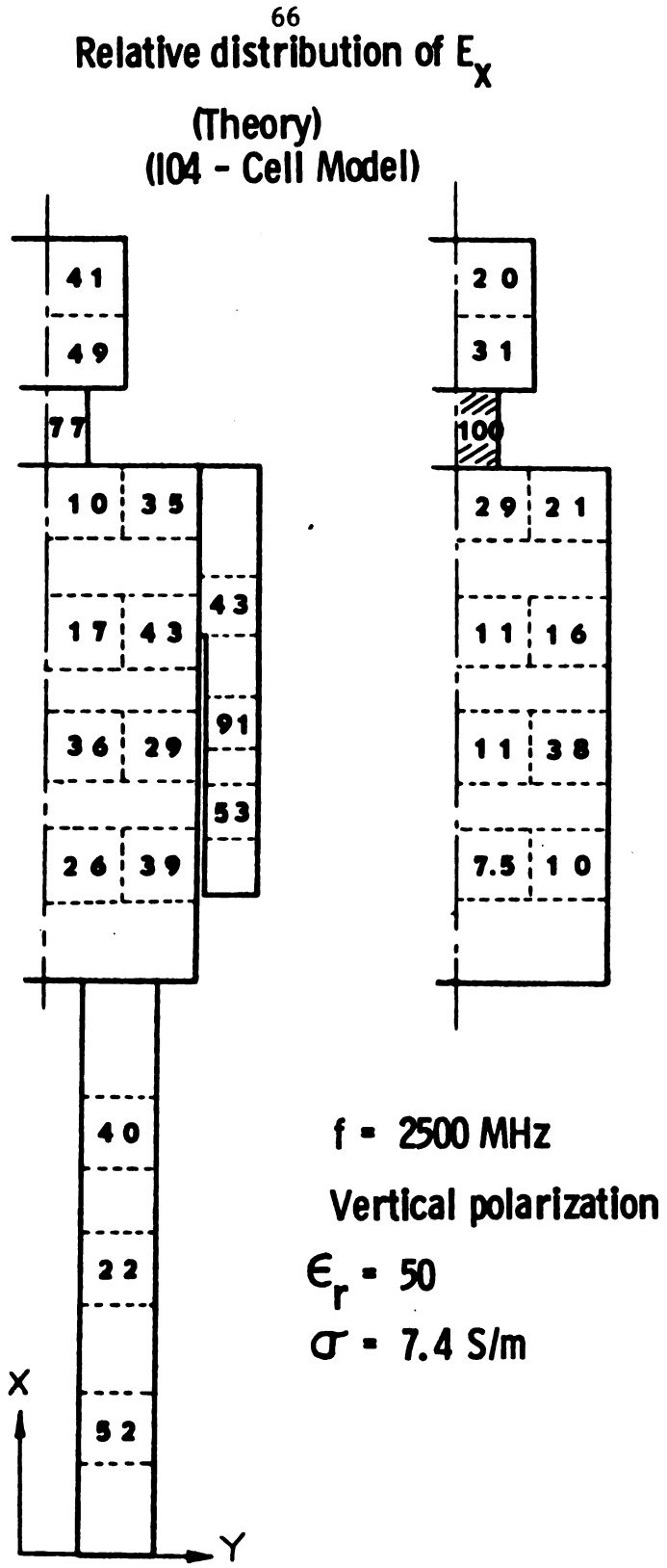

Figure 5.4. Relative distribution of the x-components of theoretical induced electric fields inside the phantom model of man, excited by a vertically polarized, travelling EM wave of 2500 MHz at normal incidence (104-cell model).

model of human body with σ = 4.5 S/m and ε_r = 50 irradiated by a travelling EM wave of 500 MHz. It is noted that theoretical results shown in Fig. 5.8 are obtained when the body is subdivided into 246 cubic cells of various sizes. A larger number of cells, or a finer cell subdivision, was needed to produce a set of theoretical results which agreed quanlitatively with the experimental results at 500 MHz. This point will be discussed again in the next section. We observe a quanlitative agreement between experiment and theory in Figs. 5.7 and 5.8: at 500 MHz., the maximum field point moves to the thigh, and high field regions are found in the arm and the back side of the torso. A disagreement between theoretical and experimental results is found in the neck.

5.3 Discussion

In the course of our study on the induced electric field in a phantom model of man, it was found that the agreement between experiment and thory tended to deteriorate as the frequency is lowered. This phenomenon seemed to contradict the thinking that at a lower frequency, theoretical results should be more accurate because the cell size would be electrically smaller. After a careful examination of this phenomenon we have found the possible reason. When a phantom body is irradiated by a travelling EM wave with an impressed electric field,

$$\vec{E}^i = \hat{x}\, E^i_{max}\, e^{-jkz} = \hat{x}\, E^i_m \cos kz - \hat{x}j\, E^i_m \sin kz \qquad (5.1)$$

an electric mode and a magnetic mode of induced electric field are

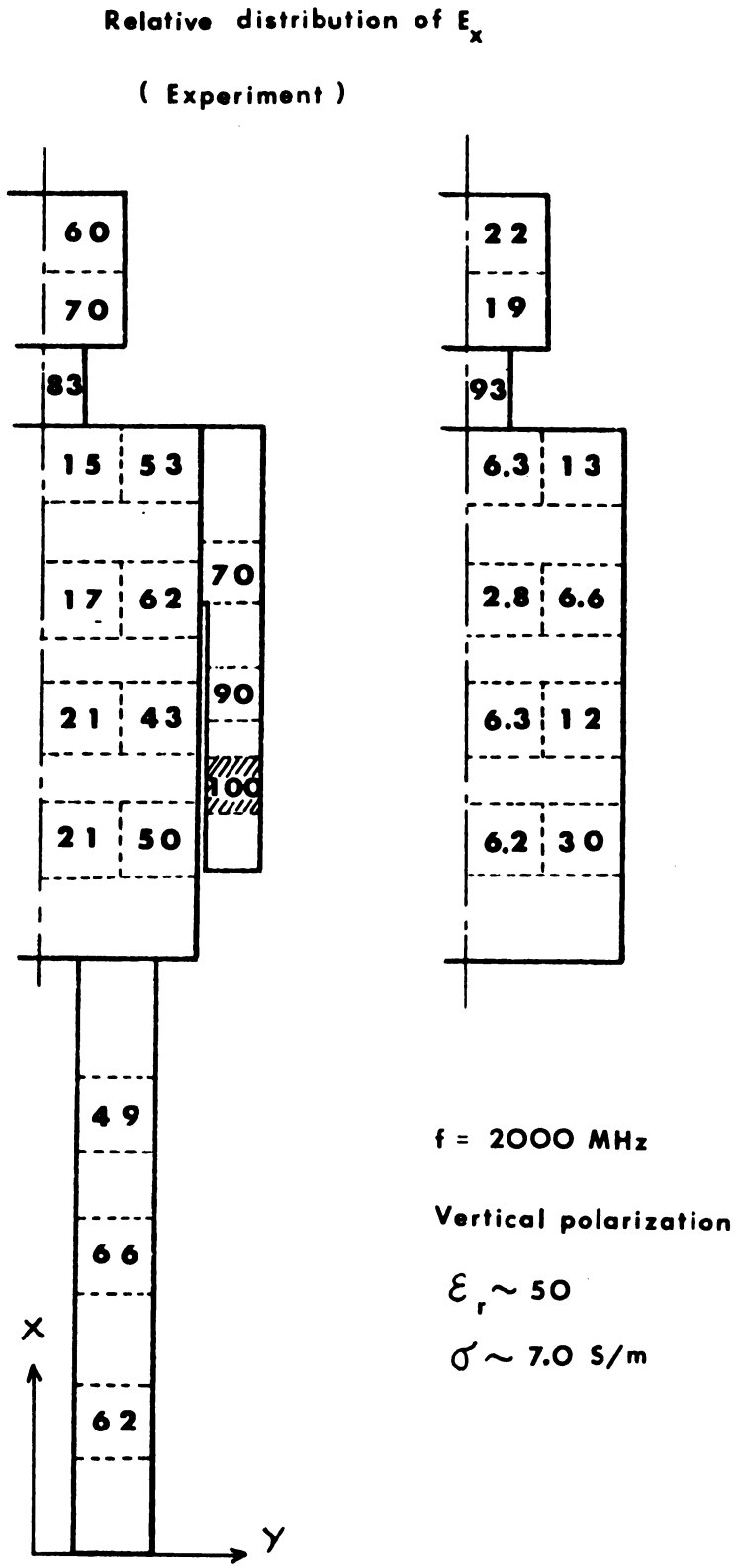

Figure 5.5 Relative distribution of the x-components of the measured induced electric fields inside the phantom model of man, excited by a vertically polarized, travelling EM wave of 2000 MHz at normal incidence.

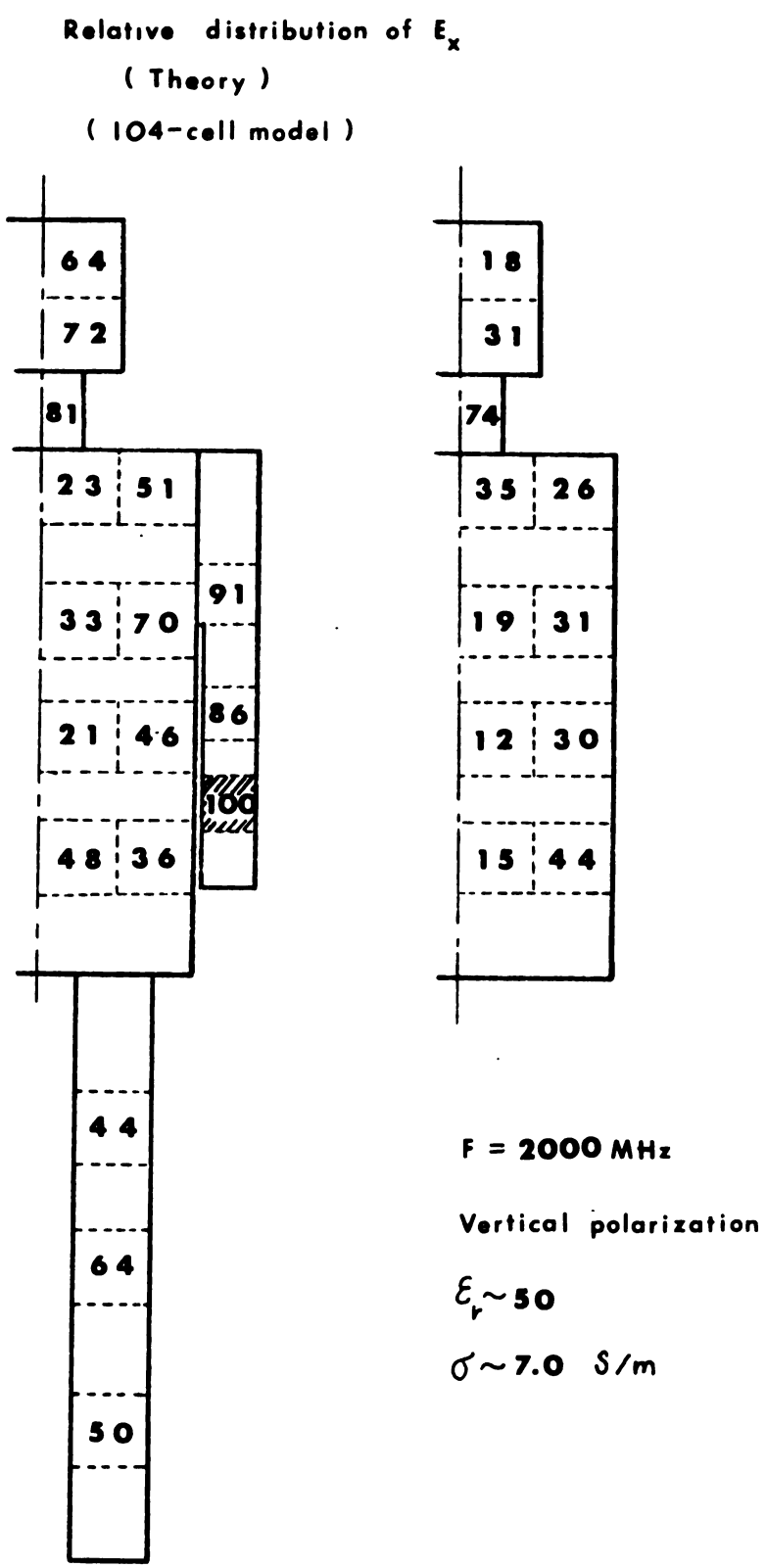

Figure 5.6. Relative distribution of the x-components of theoretical induced electric fields inside the phantom model of man, excited by a vertically polarized, travelling EM wave of 2000 MHz at normal incidence (104-cell model).

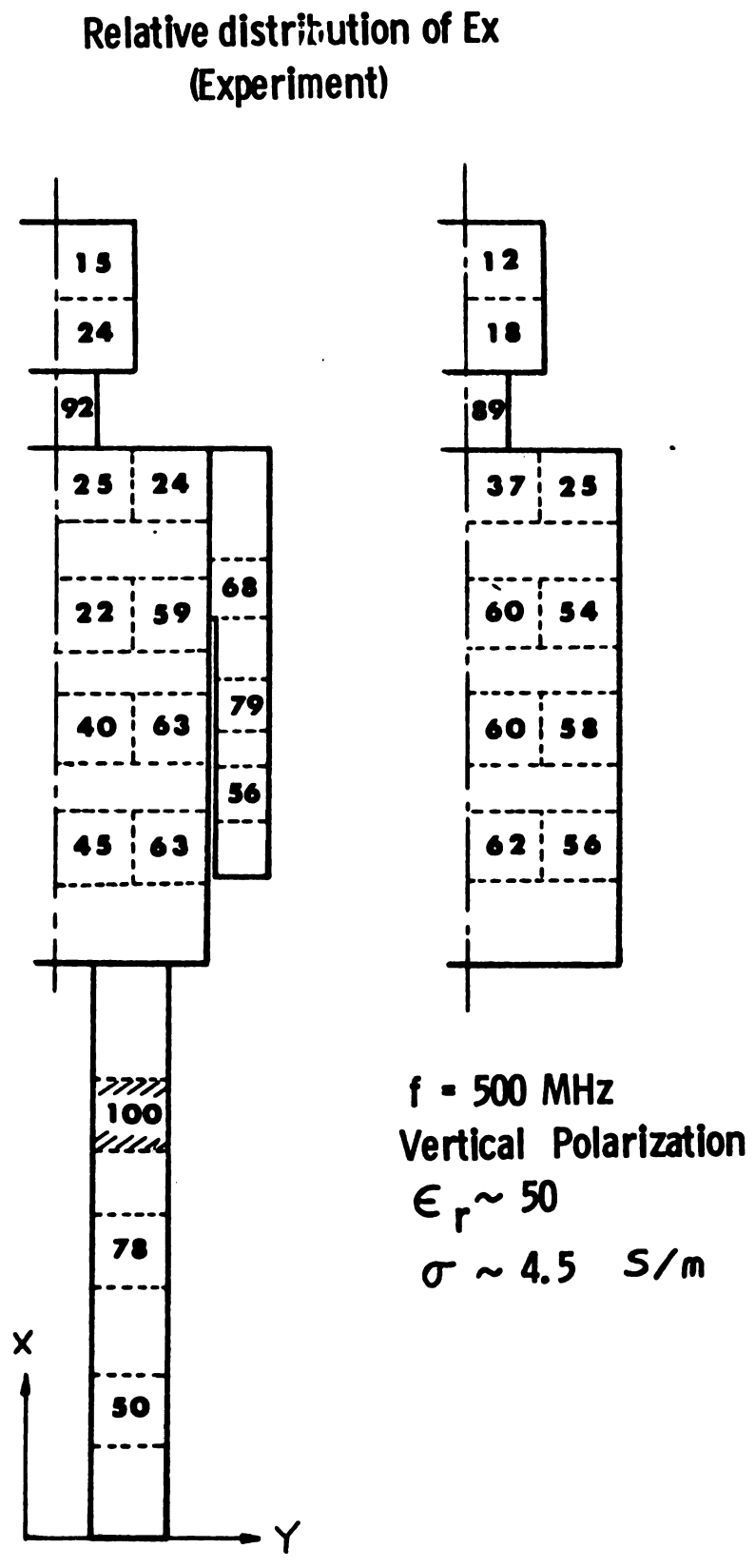

Figure 5.7. Relative distribution of the x-components of the measured induced electric fields inside the phantom model of man, excited by a vertically polarized, travelling EM wave of 500 MHz at normal incidence.

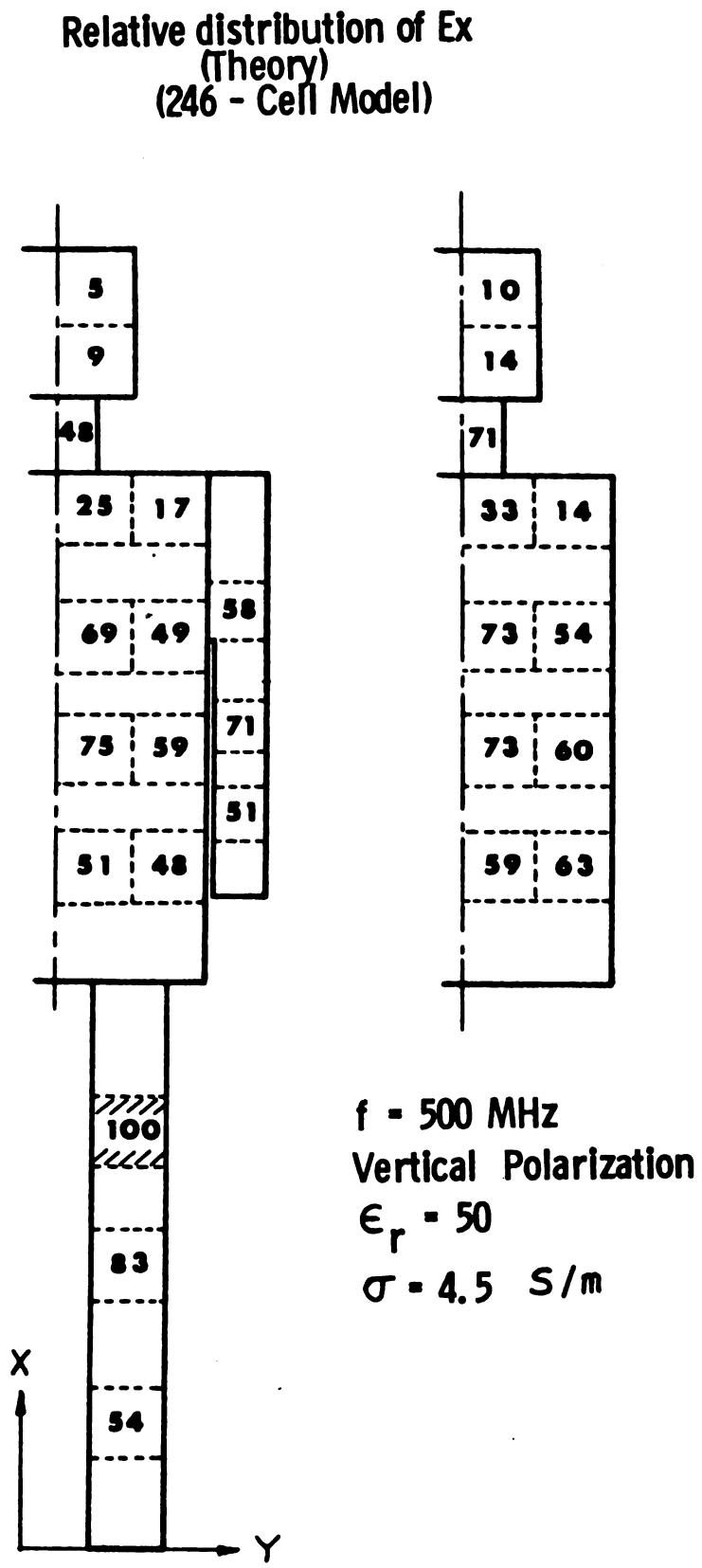

Figure 5.8. Relative distribution of the x-components of theoretical induced electric fields inside the phantom model of man, excited by a vertically polarized, travelling EM wave of 500 MHz at normal incidence (246-cell model).

both excited in the body. For the phantom model of man we used in the experiment, the magnetic mode of induced electric field starts to dominate the electric mode as the frequency becomes lower than 1000 MHz. The electric mode of induced elctric field is linear in nature, and its numerical results converge well. On the other hand, the magnetic mode of induced field is circulartory, and we often encounter the difficulty of numerical convergence. Thus, for a specific cell subdivision, the accuracy of the numerical results on the electric mode of induced electric field is higher than that of the magnetic mode. If the magnetic mode becomes dominant in the total induced electric field, a finer cell subdivision is needed to produce accurate results on the induced electric field. This is the possible reason for the phenomenon we have observed in the 500 MHz case, in which a 246-cell model is needed to yield a set of theoretical results which agreed with the experimental results.

To demonstrate this phenomenon further, two examples are given in Figs. 5.9 and 5.10. Figure 5.9 shows the x-components of the induced electric fields, $|E_x|$, inside a 4-cm phantom cube with $\sigma = 4.5$ S/m and $\epsilon_r = 50$, excited by a symmetrically impressed electric field of $\vec{E}^i = \hat{x} \cos kz$ at 750 MHz. With this $\vec{E}^i$, an electric mode of electric field is induced inside the cube. In the upper part of Fig. 5.9 is shown the distributions of $|E_x|$ within 1/8 of the cube, obtained when the cube is subdivided into 216 cubic cells. In the lower part of Fig. 5.9, the distribution of $|E_x|$ within 1/8 of the cube, obtained with the 512-cell subdivision, is shown. Comparing these two sets of numerical results, we observe an excellent convergence for the

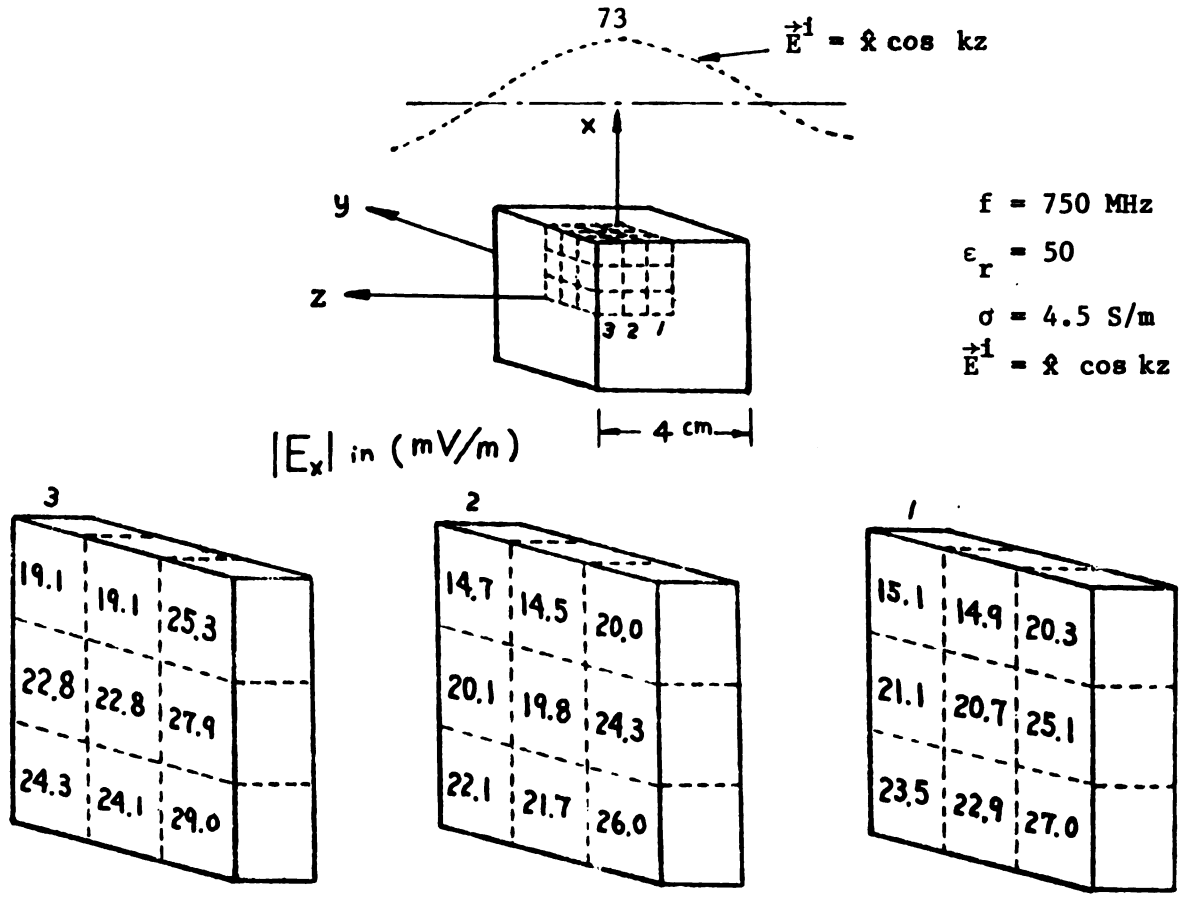

(216-cell subdivision)

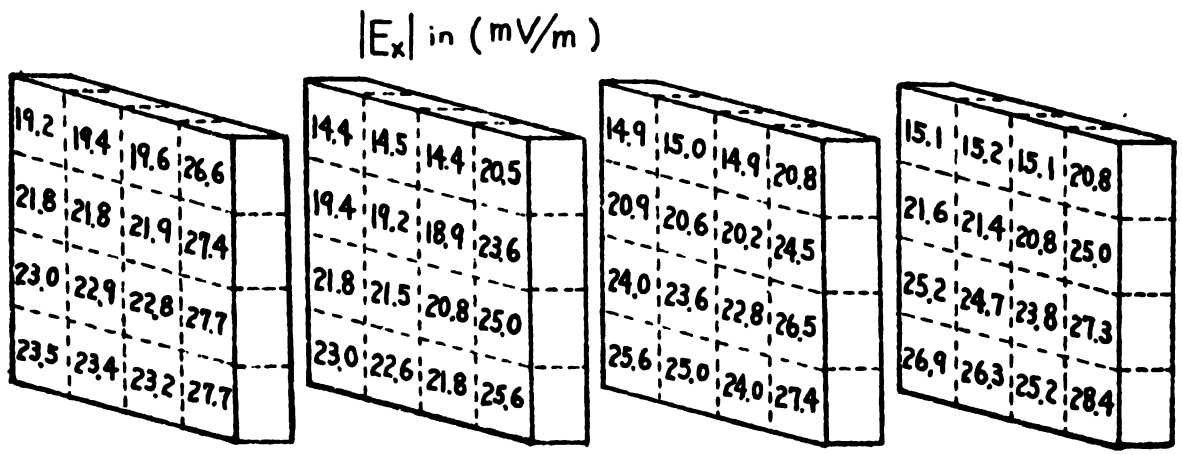

(512-cell subdivision)

Figure 5.9. Distribution of the x-component of the induced electric fields (the electric mode) excited by a symmetrically impressed electric field in a 4-cm phantom cube, and the comparison of numberical results based on the 216-cell subdivision and the 512-cell subdivision.

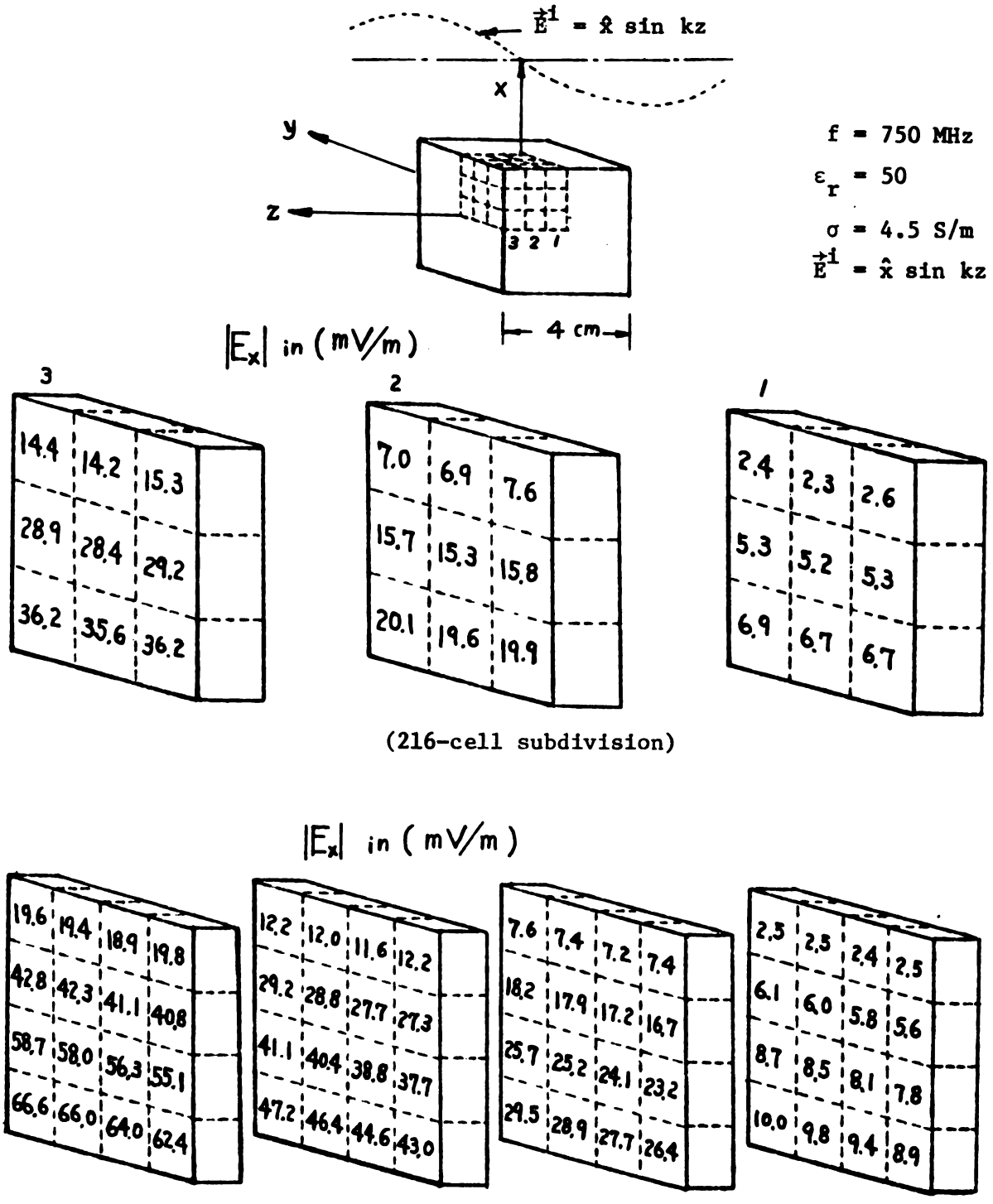

Figure 5.10. Distribution of the x-component of the induced electric fields (magnetic mode) excited by an antisymmetrically impressed electric field in a 4-cm phantom cube, and the comparison of numerical results based on the 216-cell subdivision and the 512-cell subdivision.

numerical results for the electric mode of induced electric field.

Figure 5.10 shows the distribution of the x-components of the induced electric fields, $|E_x|$, inside the same 4-cm cube excited by an antisymmetrically impressed electric field of $\vec{E}^i = \hat{x} \sin kz$ at 750 MHz. Two sets of numerical results for $|E_x|$ are given in Fig. 5.10 for the 216-cell subdivision and the 512-cell subdivision. It is observed that the results for the 512-cell subdivision deviate significantly from that of the 216-cell subdivision, especially at the outer layer of the cube. This implies a poor numerical convergence, thus, to produce accurate results for the magnetic mode of induced electric field the cell size should be smaller compared with the case of the electric mode shown in Fig. 5.9.

CHAPTER 6

INDUCED EM FIELDS IN HETEROGENEOUS BIOLOGICAL SYSTEM AND APPLICATION TO HYPERTHERMIA CANCER THERAPY

In Chapter 3-5, the induced electric field inside an irradiated homogeneous biological system has been studied. In this chapter, we proceede to check the validity of the theory when applied to a heterogeneous biological system. We have conducted experiments to varify the theory, and then applied the theory to the hyperthermia cancer therapy.

6.1 Comparison of experiment and theory in a heterogeneous biological system

Two sets of experimental and theoretical results on the induced electric fields in two different heterogeneous biological systems are compared. We used the same experimental set up as we did for measuring the induced electric field in the phantom model of human body. An array antenna was used as a radiating source at 600 MHz. A phantom model of rectangular box with dimensions of 6x12x2 cm was constructed with thin plexiglass and filled with phantom material of appropriate conductivity and permittivity. A tumor (heterogeneity) was assumed to be a part of the body (phantom material) that has a conductivity differs from that of the body. As this experimental model was irradiated, induced electric fields were probed over 18 locations in one side of the body. Detailed dimensions of the model are depicted in Fig. 6.1.

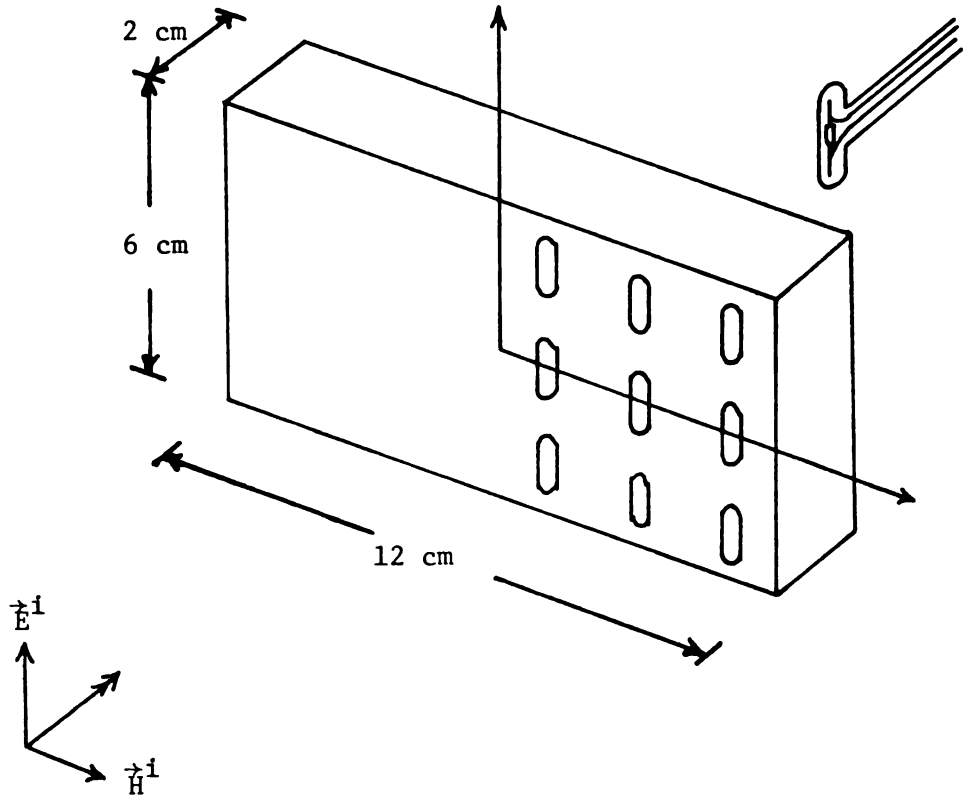

Figure 6.1. Geometry and dimensions of the phantom model.

Figures 6.2 (a) and (b) show the theoretical and experimental results of the induced electric field at the tumor inside the phantom model varying as a function of the tumor conductivity. The tumor with dimensions of 2x4x2 cm is embedded in the center of the body as shown in the upper right hand corner of Fig. 6.2. At this frequency, conductivity and dielectric constant of the body are assumed to be 4.5 S/m and 70, respectively. Four different tumor conductivities have been considered while the dielectric constant of the tumor is assumed to be equal to that of the body. In the experiment, each time a phantom material of 2x4x2 cm dimensions with appropriate tumor conductivity was packed at the center of the body (box) and then the rest of the body was filled with a phantom material with conductivity and dielectric constant equal to that of the body. The induced electric fields were probed over 18 locations in one side of the body, nine locations in the front and the back layer, respectively. Only the induced electric fields at the tumor were plotted as a function of the tumor conductivity because the induced electric fields elsewhere were only slightly changed when the tumor conductivity was changed. Figures 6.2 (a) and (b) show that the induced electric fields at the tumor in the front and the back layer decrease as the tumor conductivity is increased from 2.0 S/m to 6.5 S/m. Corresponding theoretical results on the induced electric fields at the tumor and other parts of the body were generated. A good agreement between theory and experiment was obtained.

In Figures 6.3 (a) and (b), the same phantom model is considered but the location and size of the tumor are changed. Two tumors each with dimensions of 2x2x2 cm are embedded inside each half of the body

Freq. = 600 MHz $\quad \sigma = 4.5$ S/m

$\vec{E}^i = \hat{x}\, e^{-jk_o z} \quad \varepsilon_r = 70$

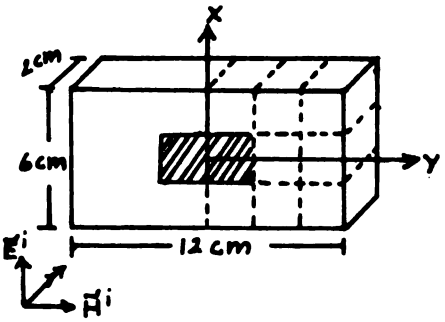

(a) Front layer at x=0 cm, y=1 cm, z=0.5 cm

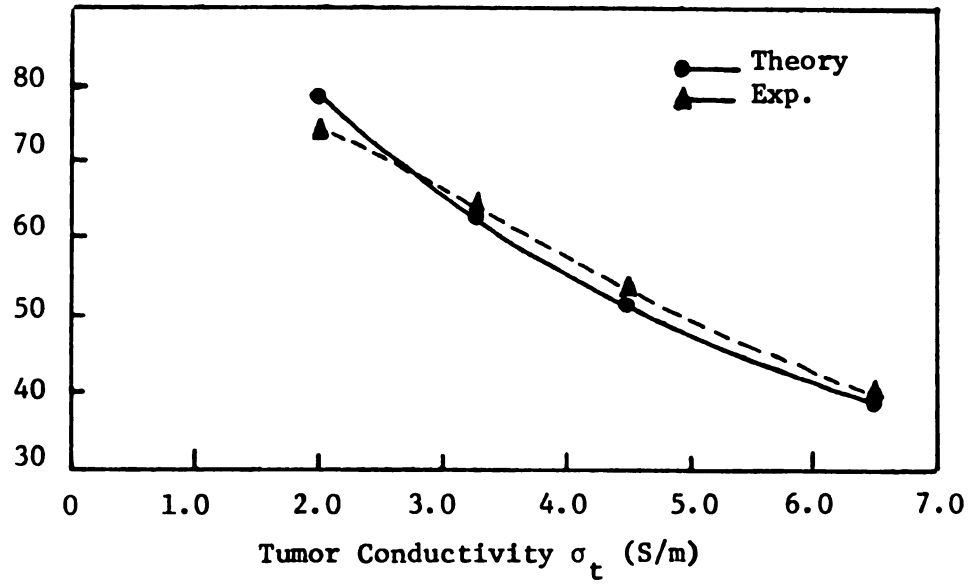

(b) Back layer at x=0 cm, y=1 cm, z=1.5 cm

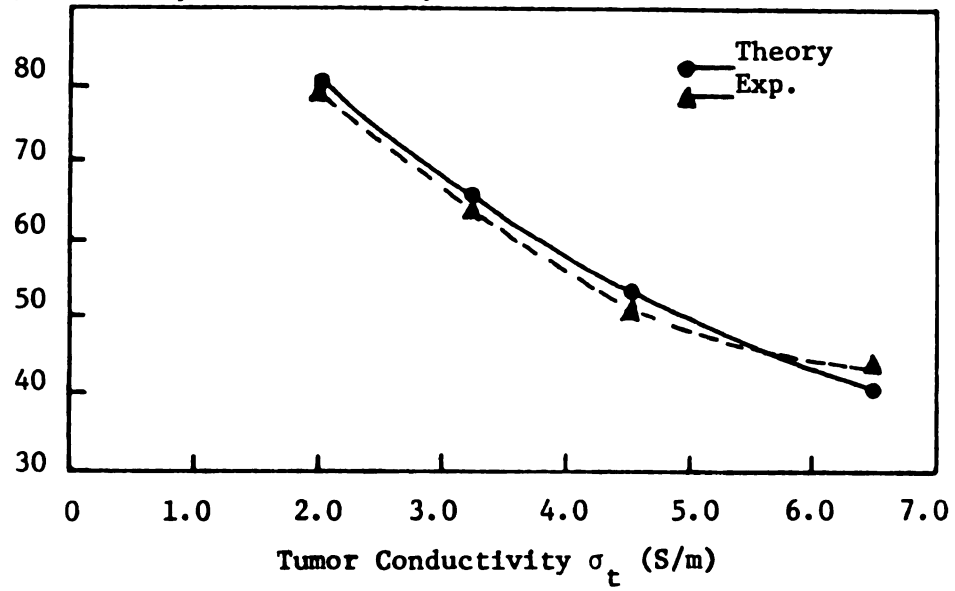

Figure 6.2. Theoretical and experimental results of the x-components of the induced electric field, E_x, at the tumor as a function of the tumor conductivity, excited by a vertically polarized, travelling EM wave of 600 MHz at normal incidence.

Freq. = 600 MHz $\quad \sigma = 4.5$ S/m

$\vec{E}^i = \hat{x}\, e^{-jk_o z} \quad \varepsilon_r = 70$

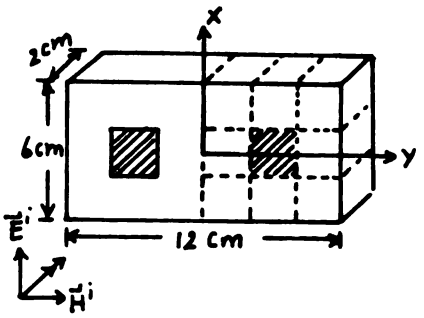

(a) Front layer at x=0 cm, y=3 cm, z=0.5 cm

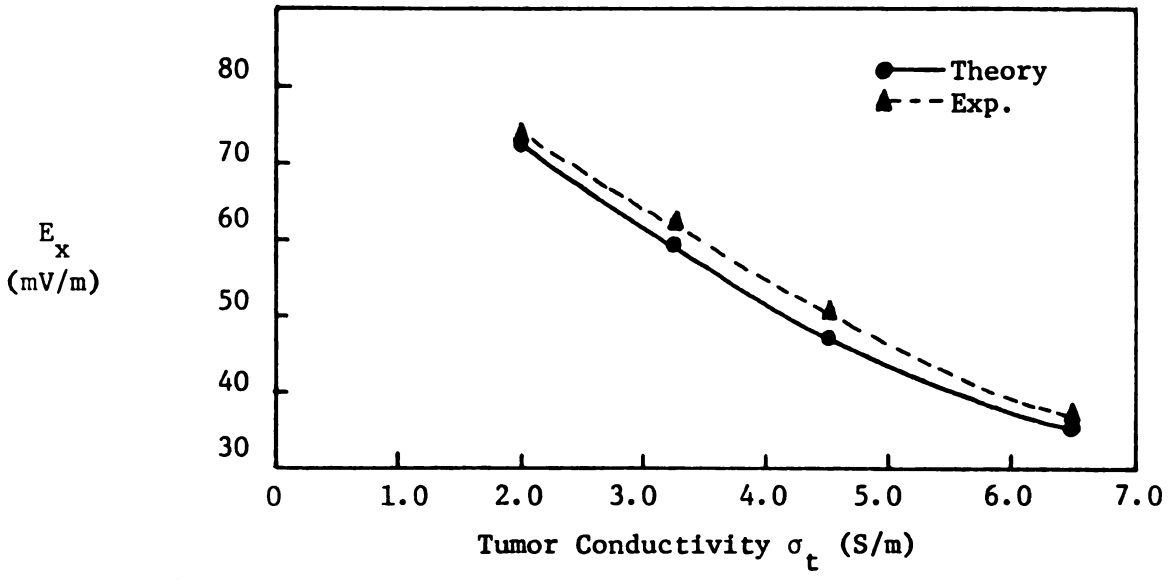

(b) Back layer at x=0 cm, y=3 cm, z=1.5 cm

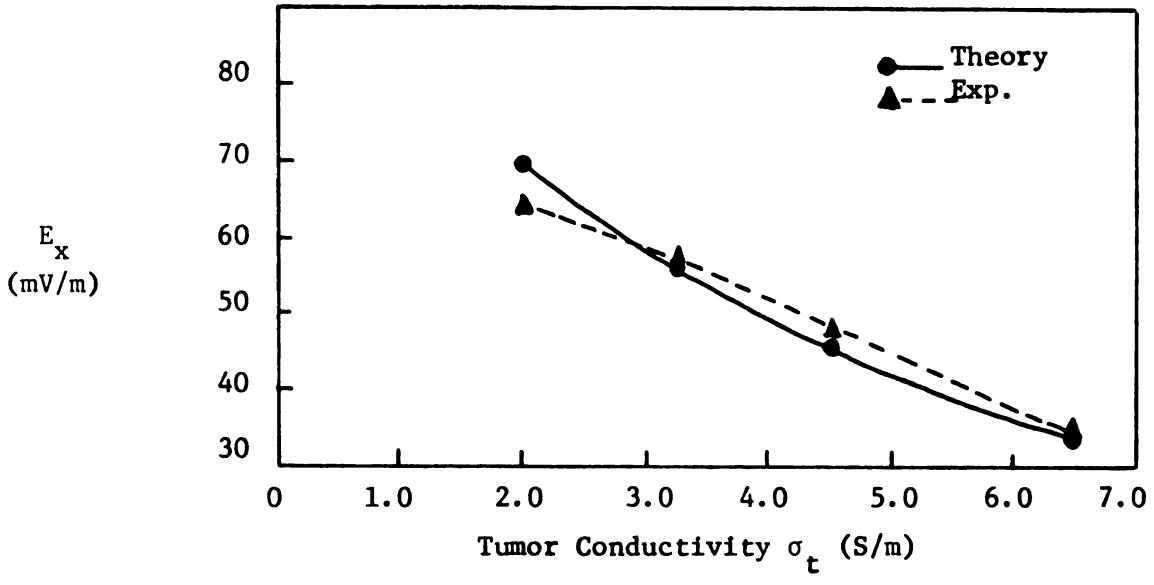

Figure 6.3. Theoretical and experimental results of the x-components of the induced electric field, E_x, at the tumor as a function of the tumor conductivity, excited by a vertically polarized, travelling EM wave of 600 MHz at normal incidence.

as shown in the upper right hand corner of Figure 6.3. Conductivity and dielectric constant of the body are assumed to be 4.5 S/m and 70, respectively. Again four different conductivities of the tumor have been considered. Figures 6.3 (a) and (b) show the theoretical and experimental results of the induced electric fields at the tumor in the front and the back layer, respectively, as a function of the tumor conductivity. A good agreement is again obtained between experiment and theory for this case.

6.2 Hyperthermia in animal and human bodies induced by EM fields

One of the promising therapies for cancer is that of hyperthermia in combination with chemotherapy or ionizing radiations. When the temperature of a tumor is raised a few degrees above that of surrounding tissues, accompanying chemo- or radio- therapy has been found to be effective in treating the tumor (15,16,17). In the combined cancer therapy, the objective is to find a noninvasive method by which to heat the tumor without overheating other parts of the body.

A convenient means of heating embedded tumors in a biological body noninvasively is to utilize the EM radiation. When an EM field of a certain frequency is applied in a particular manner to a biological body with an embedded tumor, it is difficult to predict the distribution of the induced field inside the body because the body with the tumor represents electrically a finite heterogeneous body. Thus, it is a non-trivial engineering problem to construct an effective scheme for local EM heating. In general, an effective local EM heating of embedded tumor depends on the following factors: (i) the type of EM irradiation, part-body or whole-body; (ii) the frequency of the EM field; (iii) the

type of applied field, electric, magnetic or electromagnetic; (iv) the location of the tumor in the body; (v) the conductivity and permittivity of the tumor relative to that of the surrounding tissues; and (vi) the heat diffusion from the tumor.

The purpose of this study is to theoretically predict the heating pattern induced inside the body with the tumor when it is irradiated by various EM fields under certain schemes, some of which are commonly used for the hyperthermia purpose. From these theoretical results, the effectiveness of various EM heating schemes can be assessed. We will theoretically quantify the induced electric field and the specific absorption rate (SAR) of the EM energy in the theoretical model of a biological body with an embedded tumor under various schemes of EM irradiation. The scheme which can induce a localized high SAR in the tumor while maintaining low SARs in the surrounding tissues is considered to be an effective scheme. In the present study, the heat diffusion from the tumor will not be considered. It is well known that the heat diffusion from the tumor is poor because of a sluggish blood supply to the tumor. This phenomenon is advantageous from the viewpoint of maintaining hyperthermia at the tumor.

We consider, first, the part-body irradiation with HF electric fields. We found that this scheme is effective for internal tumors, especially those with lower conductivities. We also found that this scheme of irradiation cannot selectively heat surface tumor. Secondly, we consider the irradiation with microwave or UHF EM fields. At these frequency ranges, application of a localized EM radiation at the tumor may create hot spots at various locations away from the tumor, instead of heating the tumor.

6.3 Theoretical model of a biological body with tumor

In this study, we use biological bodies of simple geometries to simulate animal and human bodies with embedded tumors. The body is considered to be homogeneous with certain electrical properties and the tumor is assumed to be a local region with a conductivity that differs from that of the surrounding tissue. The permittivity of the tumor is assumed to be the same as that of the surrounding tissue. These assumptions are supported by recent *in vivo* measurements of electrical properties of tumors in mice by Bordette *et al.* (18). Another reason for the assumption of the same permittivity for the body and for the tumor is that effect of the permittivity on the induced electric field in the body is insignificant, especially in the lower frequency ranges.

The body is assumed to be partially or wholly irradiated by EM energy of various frequency ranges including HF, VHF, UHF, and microwave.

The first step of our study is to determine the induced electric field inside a heterogeneous body, consisting of a homogeneous body with an embedded tumor of different electrical properties, as induced by the applied EM field. After this quantity is obtained, the SAR of EM energy in the tumor and at any other point of the body are determined. An effective EM heating should induce a localized, high SAR in the tumor and low SARs in the surrounding tissues.

6.4 Part-Body Irradiation with HF Electric Field

The electric fields of the HF range (3 to 30 MHz) maintained between two capacitor-plate electrodes have been used to heat embedded

tumor in animals (19) and in human bodies (20). We will analytically show that this scheme of EM heating is very effective for internal tumors embedded in the central part of the body, however, this scheme cannot provide a selective heating for surface tumors. We will also show that the tumor conductivity relative to that of the surrounding tissue plays an important role in this type of EM heating.

The first example is a simulated animal body with the dimensions of 6x6x12 cm having a tumor of 2x2x4 cm located at the center of the body and under the partial irradiation of a uniform electric field as shown in Fig. 6.4. A uniform electric field ($\vec{E}^i$) of 1 V/m (max. value) at 15 MHz is applied across the top and bottom of the body and only over the area of tumor (2x4 cm).

For the numerical calculation of the absorbed power density, the body is divided into 27 2-cm cubic cells as shown in Fig. 6.4. The tumor occupies the 13th cell and its image and has a conductivity (σ_t) of 0.31 S/m while the conductivity of the body (σ) is 0.62 S/m. The dielectric constant (ε_r) of the tumor and the body is assumed to be 150.

The distribution of SARs in this simulated biological body is shown in Fig. 6.5. The SAR in the tumor reaches a maximum value of 150.9$\mu W/m^3$ while the immediate neighboring cells, the 10th and the 16th cell, only have a value of 44.8 $\mu W/m^3$. If the tumor conductivity is increased from 0.31 S/m to 0.496, 0.62, 0.744, and 1.24 S/m, the SAR in the tumor will decrease from 150.0 $\mu W/m^3$ to 103.7, 84.9, 71.7 and 43.8 $\mu W/m^3$, respectively. The results for this case are summarized in Fig. 6.6. The absorbed power density at other parts of the body is only altered slightly by the change in the tumor conductivity.

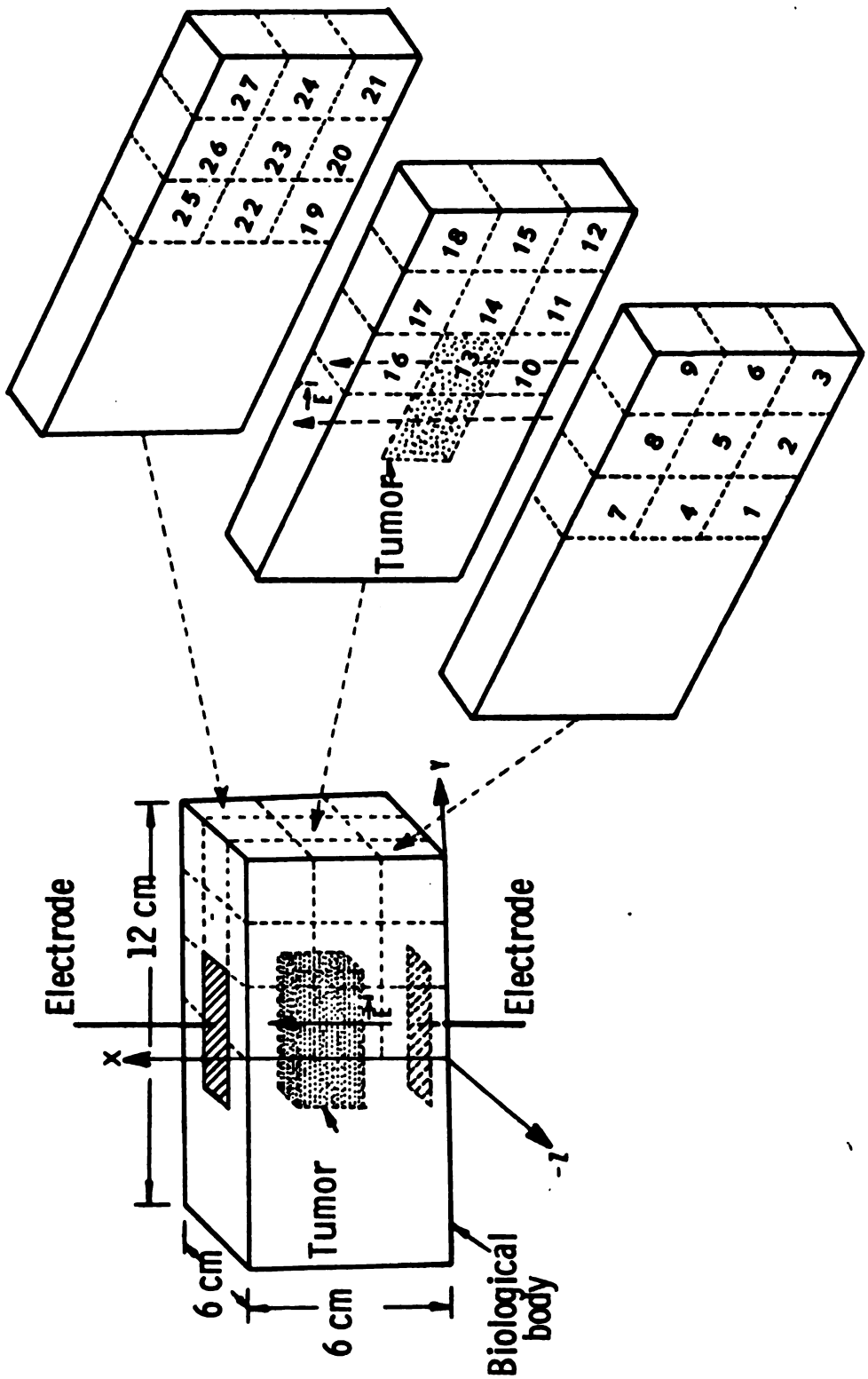

Figure 6.4. A simulated biological body (6x6x12 cm) with an embedded tumor (2x2x4 cm) irradiated by a uniform electric field (E^i) of 1 V/m (max. value) at frequency (f) across the top and bottom of the body and over the area of the tumor. The uniform electric field is maintained by two capacitor-plate electrodes.

When $\sigma_t = \sigma$, the SAR in the tumor is about twice that of the surrounding tissue. If $\sigma_t = 0.5\sigma$, the SAR in the tumor can be about four times that of the surrounding tissue. The important point not to overlook is that even the tumor conductivity is considerably higher than that of the surrounding tissue, the SAR in the tumor is still higher than that in the surrounding tissues. This result implies that an electric field of the HF range maintained by a capacitor-plate applicator can be used to selectively heat the internal tumors of various kinds as long as the tumor is located in the central part of the body.

The examples show in Figs. 6.4 to 6.6 are for a simulated animal body with an internal tumor. The case of a human body with an internal tumor is considered next. Figure 6.7 depicts a human body with an internal tumor of 5x5x5 cm embedded inside the upper torso. A uniform electric field of 15 MHz with the intensity of 1 V/m maintained by a capacitor-plate applicator is applied over the tumor area across the body as shown. For the numerical calculation of the induced electric field, only a volume of the body with dimensions of 15x15x20 cm centered around the tumor is considered because the fringe field is small in other parts of the body. This volume of the body is divided into 36 5-cm cubic cells stacked in four layers, and with the tumor occupying the center cell of the second layer. For this particular example, we assume that $\sigma_t = 0.5 \quad \sigma = 0.31$ S/m, and $\varepsilon_r = 150$. From the distribution of SARs shown in Fig. 6.7, it is observed that the SAR in the tumor reaches a maximum value of 417.8 $\mu W/m^3$ while that in the cells immediately above and below the tumor are 98.2 $\mu W/m^3$

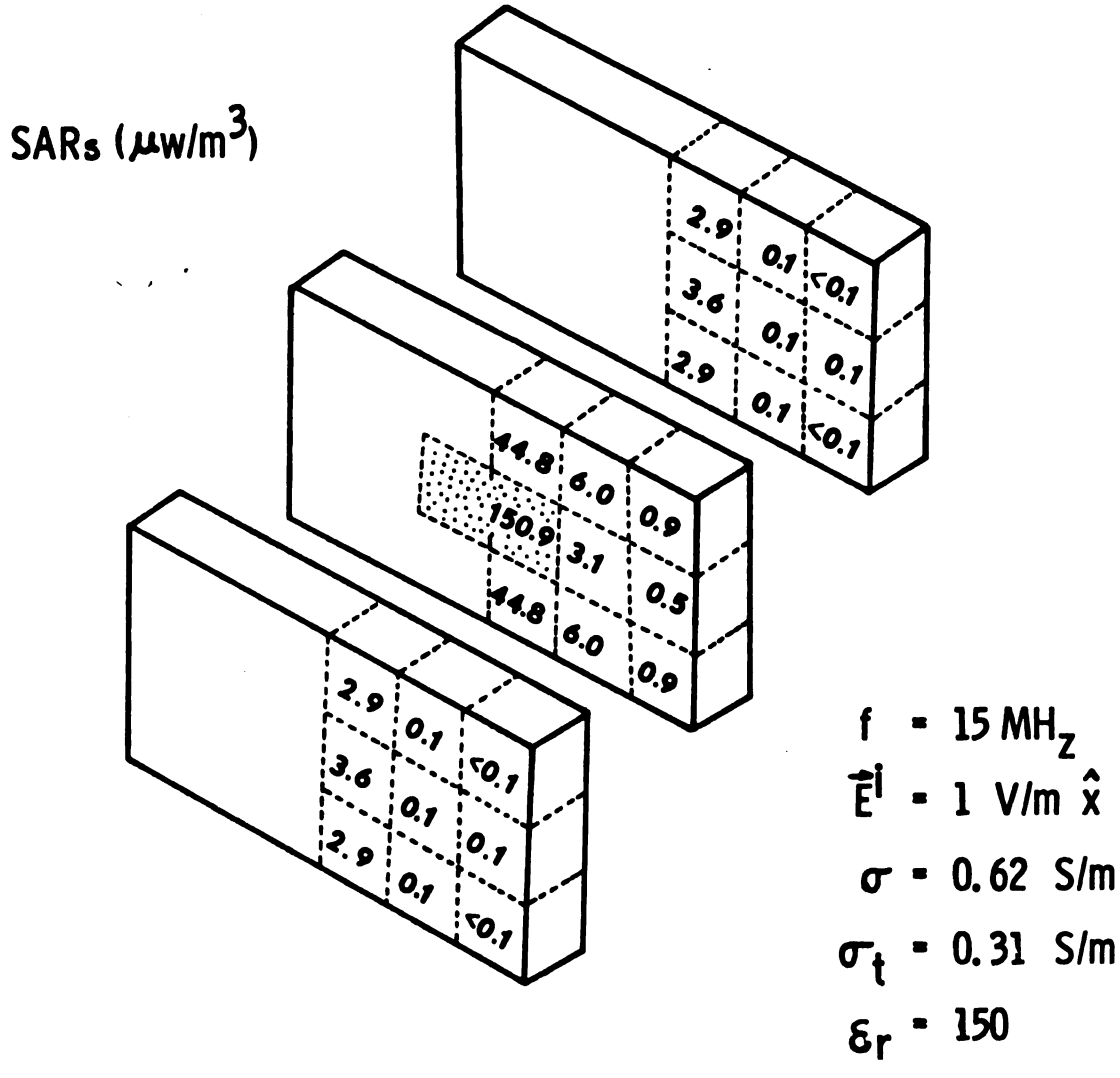

Figure 6.5 Distribution of SARs inside a simulated biological body of Fig 6.4 when f = 15 MHz, $\vec{E}^i$ = 1 V/m, σ = 0.62 S/m, σ_t = 0.31 S/m, and ε_r = 150.

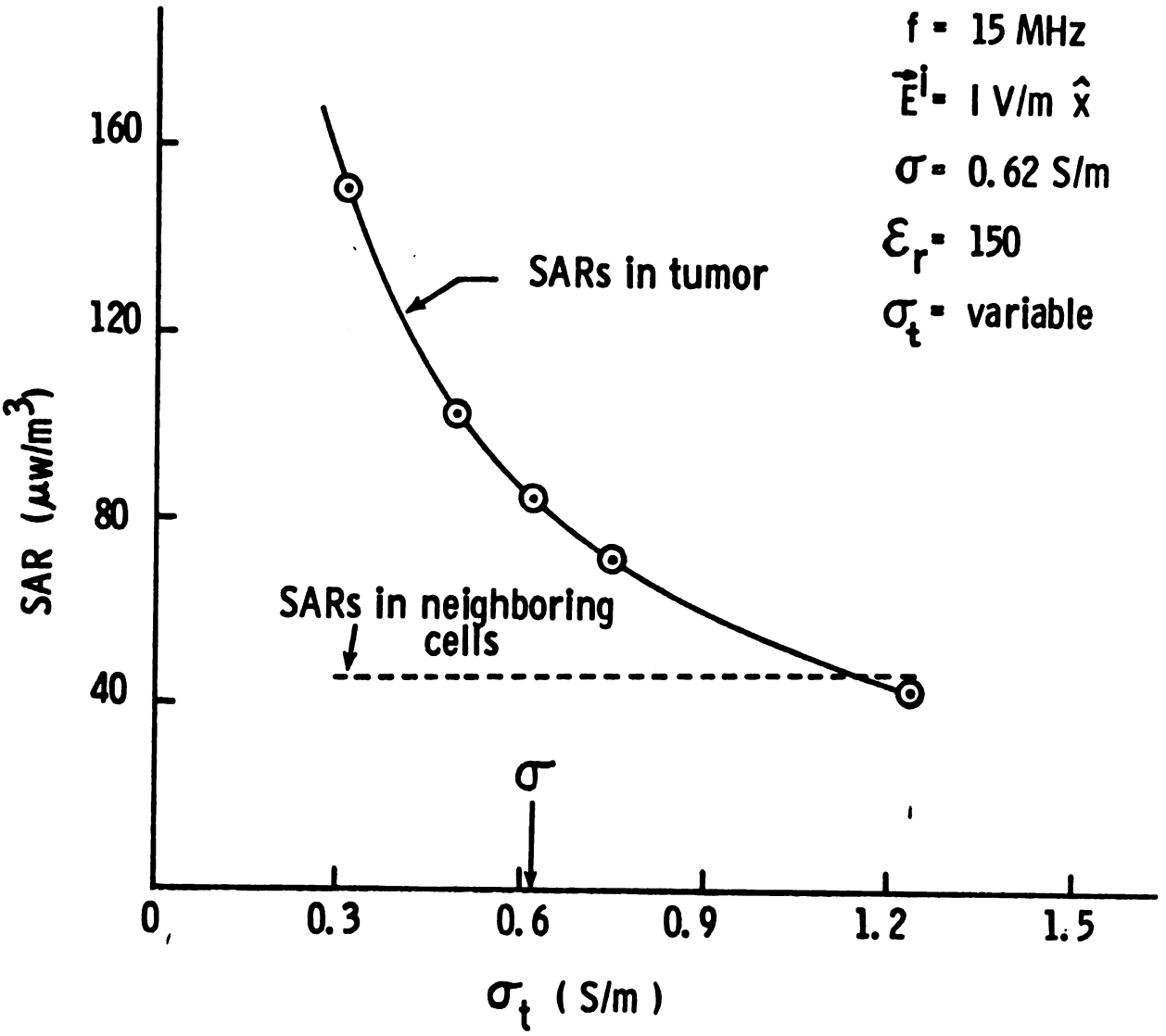

Figure 6.6. SAR in the tumor and in the neighboring cells varying as a function of the tumor conductivity (σ_t) for the case of f = 15 MHz, $\vec{E}^i$ = 1 V/m $\hat{x}$, σ = 0.62 S/m and ε_r = 150.

and 234.1 $\mu W/m^3$, respectively. The fringe field in the vicinity of the tumor is insignificantly small. We have also calculated the SAR in the tumor for different tumor conductivities: when $\sigma_t = \sigma = 0.62$ S/m, the SAR in the tumor is 235.9 $\mu W/m^3$, and if $\sigma_t = 2\sigma = 1.24$ S/m, the SAR in the tumor becomes 121.9 $\mu W/m^3$. From these results, one observes that an embedded tumor inside a human body can also be selectively heated by a HF electric field produced by a simple capacitor-plate applicator.

Up to this point, we have demonstrated that a uniform electric field in the HF range can be used to selectively heat an internal tumor embedded inside an animal or a human body. We will now show that this type of electric field can not be utilized to selectively heat surface tumors because it heats the tissue immediately below the tumor excessively.

Figure 6.8 shows the distribution of SARs in the simulated animal body depicted in Fig. 6.4, but with the tumor located in the middle of the upper body surface, when the same uniform electric field of 15 MHz with the intensity of 1 V/m is applied over the tumor area and across the body. For this example, we assume that $\sigma_t = 0.5\sigma = 0.31$ S/m and $\varepsilon_r = 150$. It is observed in Fig. 6.8 that the SAR in the tumor is 80.3 $\mu W/m^3$ while that in the cell immediately below the tumor is 84.7 $\mu W/m^3$. If the tumor conductivity is higher than 0.5 σ, the SAR in the tumor decreases further while the SAR in the cell immediately below the tumor remains about 85 $\mu W/m^3$. This phenomenon is summarized in Fig. 6.9. It is observed in Fig. 6.9 that the SAR in the tumor is about the same as that in the neighboring

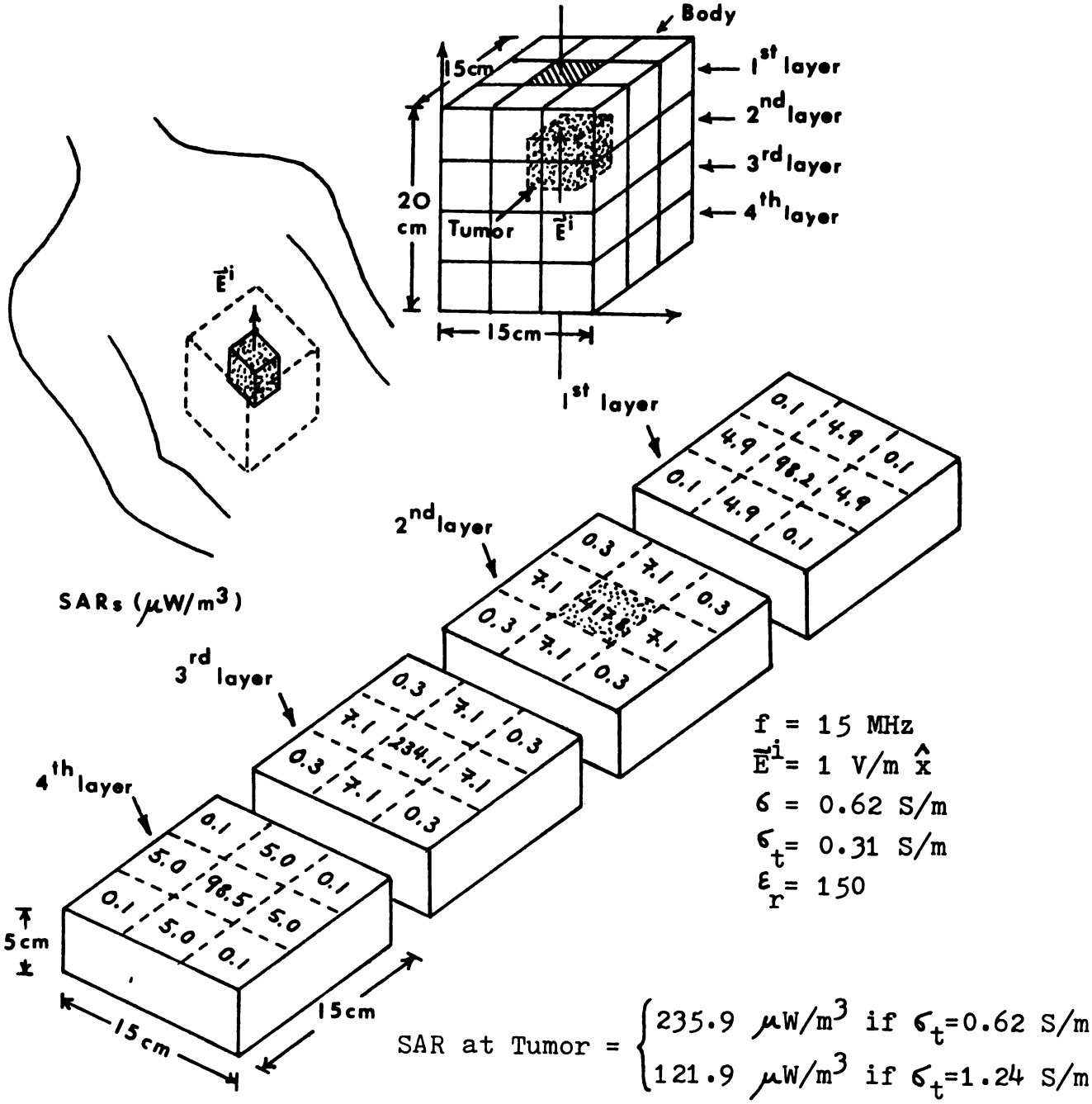

Figure 6.7. Distribution of SARs inside a human body with an embedded tumor when f = 15 MHz, $\vec{E}^i$ = 1V/m $\hat{x}$, σ = 0.62 S/m, σ_t = 0.31 S/m, and ε_r = 150. The SARs in the tumor for the cases of σ_t = 0.62 S/m and σ_t = 1.24 S/m are also given.

cell if $\sigma_t = 0.5\ \sigma$, the SAR in the tumor is reduced to about one half of that in the neighboring cell if $\sigma_t \doteq \sigma$, and if $\sigma_t > \sigma$, the SAR in the tumor decreases further while the SAR in the neighboring cell remains relatively unchanged.

From these results shown in Figs 6.8 and 6.9, it is evident that a uniform electric field in the HF range maintained by a capacitor-plate applicator cannot be utilized to selectively heat a surface tumor without severely heating the tissue immediately below the tumor. This situation may be somewhat improved by increasing the area of the lower electrode of the applicator in such a way that the induced current starting from the upper electrode flows through the tumor and then diffuses into the tissue below the tumor before it reaches the lower electrode. The reduction of the current density in the neighboring tissue will cause a decrease in the SAR and the heating.

6.5 Hyperthermia with Microwave or UHF Irradiation

In this section, we aim to show that EM fields of the UHF to microwave range (e.g. 500 to 4000 MHz) should be carefully applied to a biological body to induce a local heating at the tumor. An improper scheme of irradiation may cause severe heating at locations away from the tumor. This problem is essentially caused by the fact that electrical dimensions of experimental animal such as rats or mice are in the "resonance region" of this frequency range. Thus, hot spots may be induced at unintended locations inside the body even though only the tumor region is irradiated. Figure 6.10 shows the simulated animal body with a surface tumor as considered in Fig. 6.8 being irradiated by a microwave of 2.45 GHz in a waveguide. Assuming

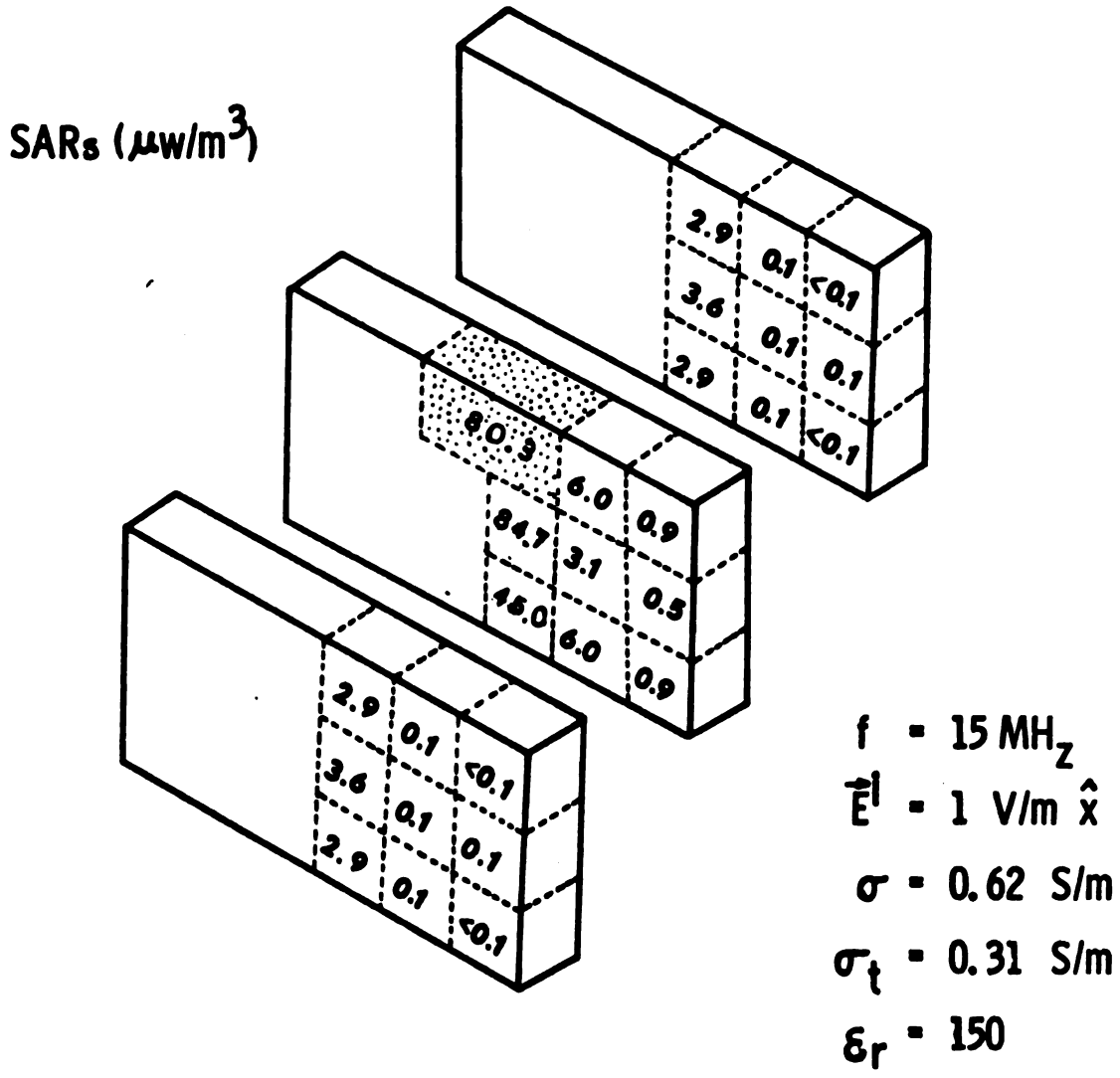

Figure 6.8. Distribution of SARs inside the simulated body of Fig. 6.4, but with the tumor located at the body surface. Parameters are: f = 15 MHz, $\vec{E}^i$ = 1 V/m $\hat{x}$, σ = 0.62 S/m, σ_t = 0.31 S/m and ε_r = 150.

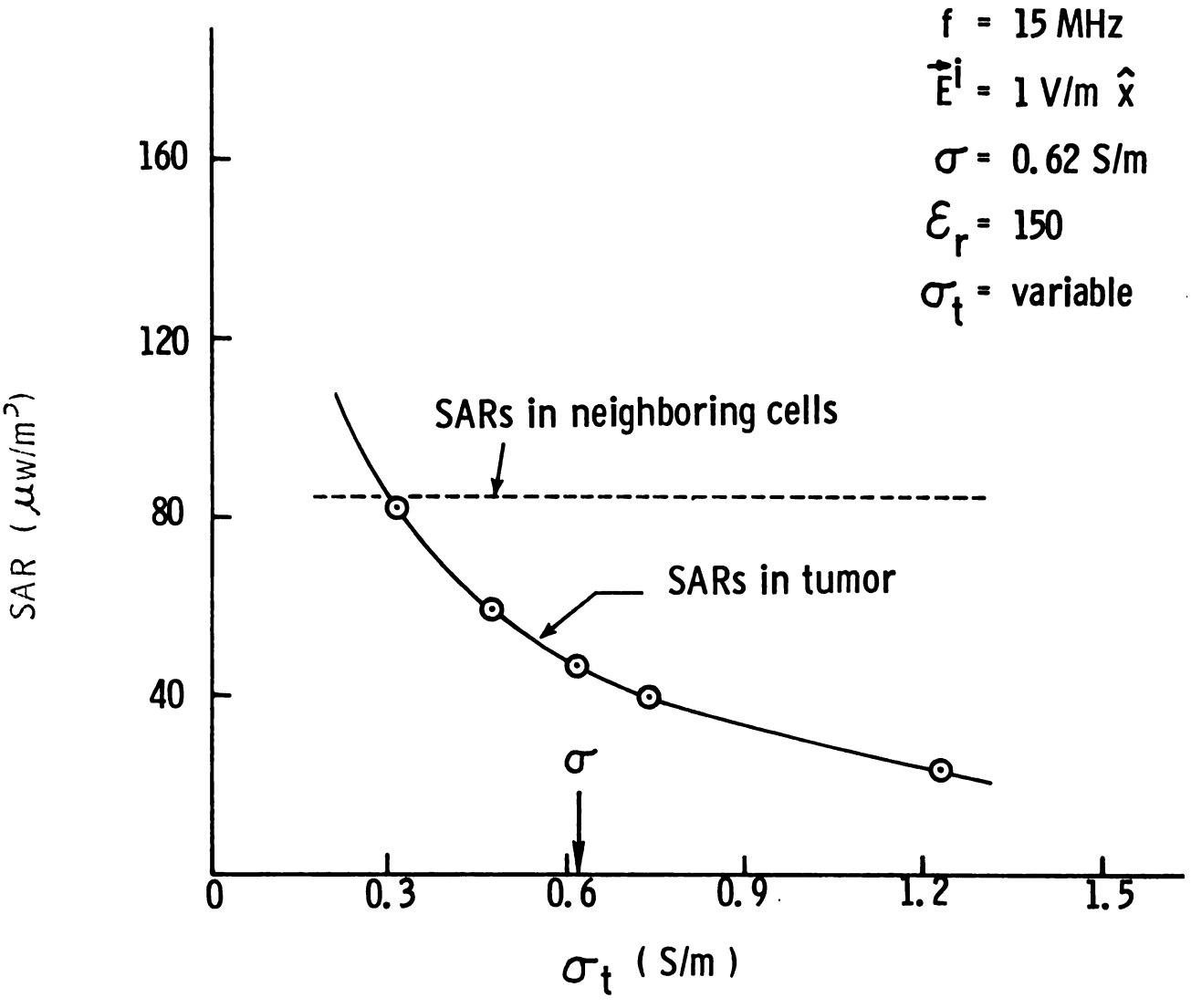

Figure 6.9. SARs in the surface tumor and in the neighboring cells varying as functions of the tumor conductivity (σ_t). Other parameters are: f = 15 MHz, $\vec{E}^i$ = 1 V/m $\hat{x}$, σ = 0.62 S/m and ε_r = 150.

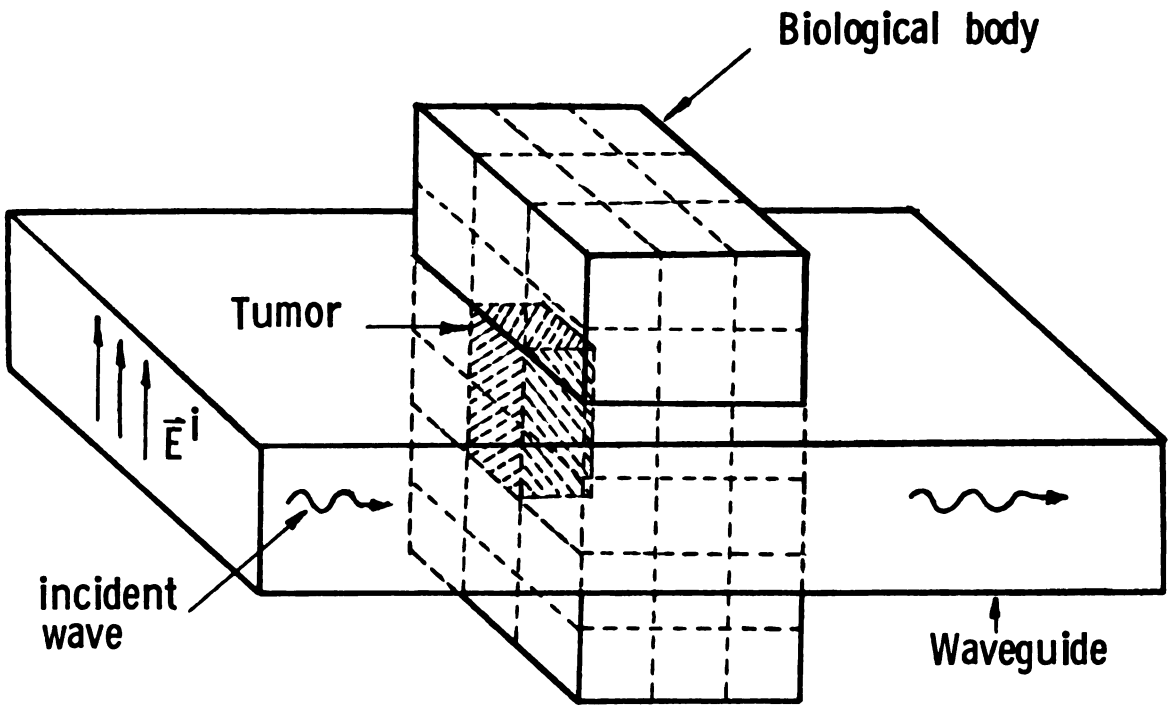

Figure 6.10. The simulated body of Fig. 6.4 with a surface tumor is irradiated by a microwave in a waveguide.

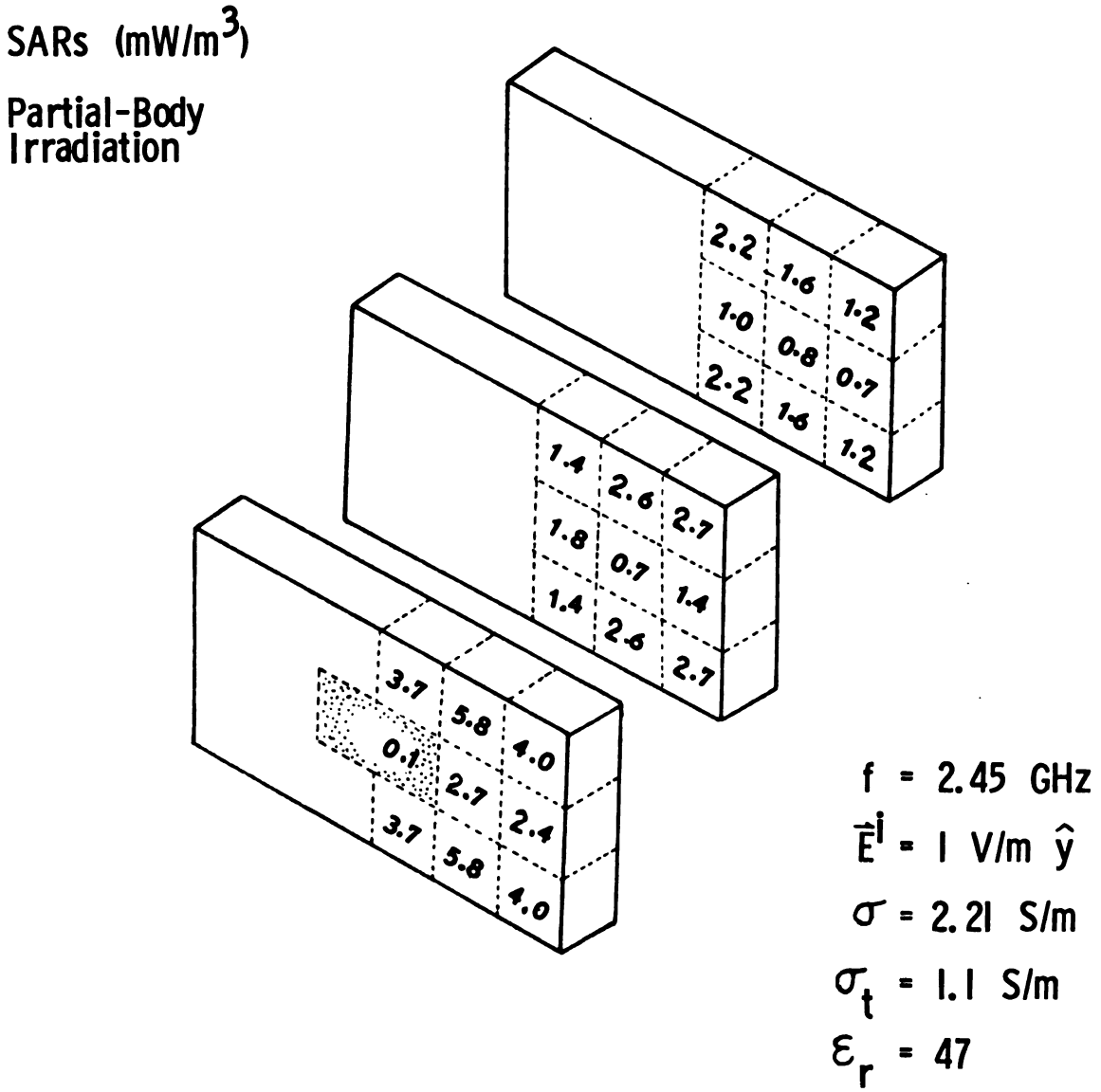

$$\text{SAR at Tumor} = \begin{cases} 0.2 \text{ mW/m}^3 & \text{if } \sigma_t = 2.21 \text{ S/m} \\ 0.3 \text{ mW/m}^3 & \text{if } \sigma_t = 4.42 \text{ S/m} \end{cases}$$

Figure 6.11. Distribution of SARs inside the simulated body of Fig. 6.10. Parameters are: f = 2.45 GHz, $\vec{E}^i$ =1V/m $\hat{y}$, σ = 2.21 S/m, σ_t = 1.1 S/m and ε_r = 47. The SARs in the tumor for the cases of σ_t = 2.21 S/m and σ_t = 4.42 S/m are also given.

that the tumor is placed in the center of the waveguide so that the maximum electric field of TE_{10} mode is incident upon the tumor. For this arrangement only one third of the middle section of the body is irradiated by the microwave. The cells being irradiated are the 1st, the 4th, the 7th, the 10th, the 12th, the 16th, the 19th, the 22nd and the 25th, and their image in the other half of the body (see Fig. 6.4). The incident electric fields to these cells are assumed to be that of TE_{10} mode with an intensity of 1 V/m in the y-direction. We also assume that $\sigma_t = 0.5\ \sigma = 1.1$ S/m and $\varepsilon_r = 47$ at 2.45 GHz. Under this irradiation, the distribution of SARs in the body is shown in Fig. 6.11. It is surprising to observe that the SAR in the tumor is, in effect, a minimum value of 0.1 mW/m^3 instead of an expected maximum. The highest SARs reaching a value of 5.8 mW/m^3 are induced in the regions not irradiated. Other high SARs are also induced in various point of the body. We have also calculated for the cases of $\sigma_t = \sigma = 2.21$ S/m and $\sigma_t = 2\ \sigma = 4.42$ S/m. The SAR in the tumor for these two cases are still very small at 0.2 mW/m^3 and 0.3 mW/m^3, respectively, while high SARs are observed at regions away from the tumor. This unexpected heating pattern is due to the resonance phenomenon induced in a 6x6x12 cm biological body by a 2.45 GHz microwave. This example implies that to irradiate experimental animals such as rats with a microwave of 2.45 GHz, the potential resonance phenomenon should be taken into account. To avoid this phenomenon, the surface tumor may be drawn through a slot on a shielded animal strainer and the microwave is then applied exclusively to the tumor (21). It is also noted that mice irradiated by the

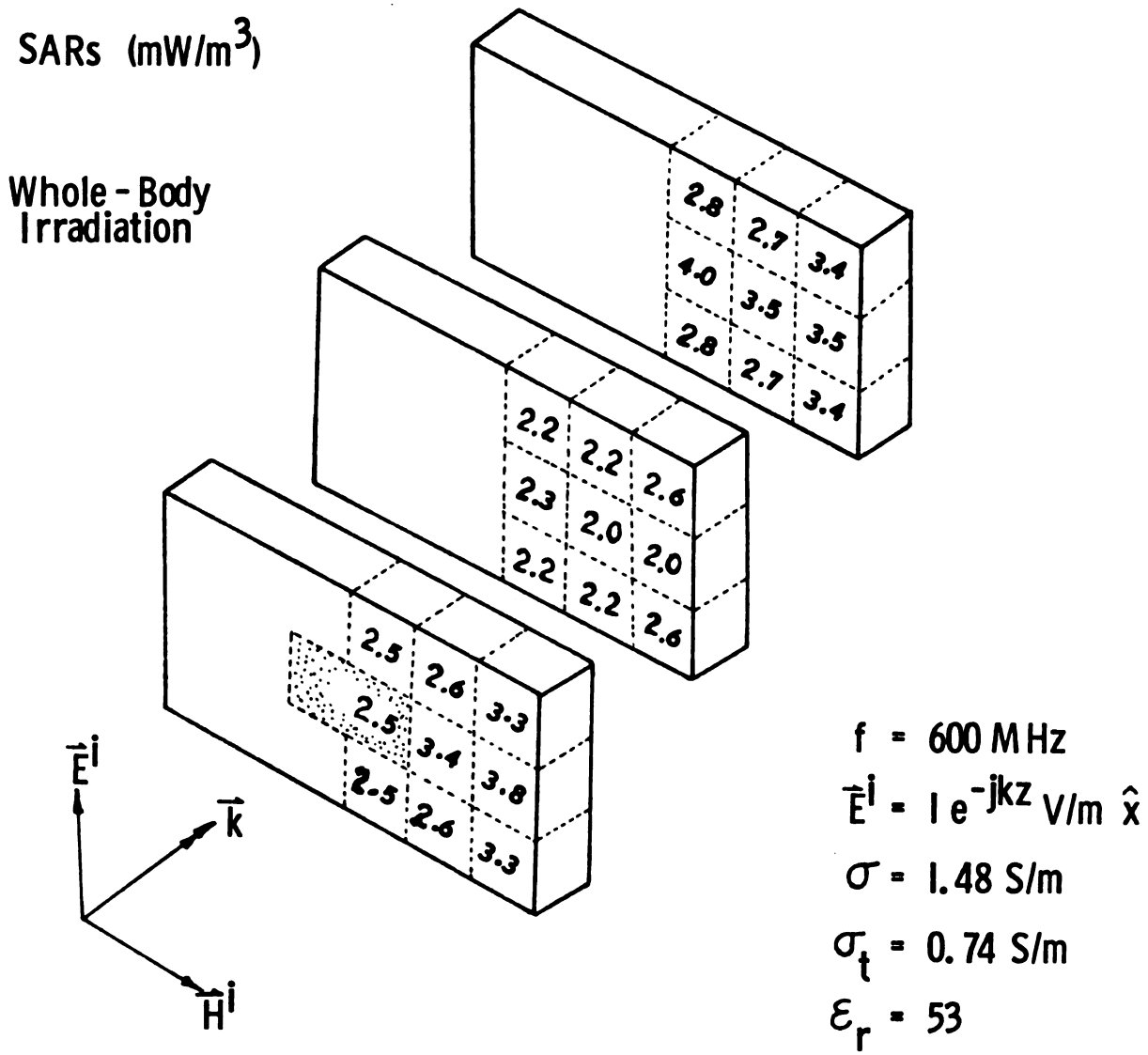

$$\text{SAR at Tumor} = \begin{cases} 3.6 \text{ mW/m}^3 & \text{if } \sigma_t = 1.48 \text{ S/m} \\ 3.5 \text{ mW/m}^3 & \text{if } \sigma_t = 2.96 \text{ S/m} \end{cases}$$

Figure 6.12. Distribution of SARs inside the simulated body of Fig. 6.4 with a surface tumor under the whole-body irradiation. Parameters are: f = 600 MHz, $\vec{E}^i = 1\ e^{-jkz}$ V/m $\hat{x}$, σ = 1.48 S/m, σ_t = 0.74 S/m and ε_r = 53. The SARs in the tumor for the cases of σ_t = 1.48 S/m and σ_t = 2.96 S/m are also given.

scheme of Fig. 6.10 at 2.45 GHz (22) will not exhibit an unexpected heating pattern because mice are electrically much smaller and a resonance is not possible at this frequency.

One example is given to show the distribution of SARs in the same simulated body with a surface tumor induced by a UHF field under the whole-body irradiation. This example is depicted in Fig. 6.12 where a plane EM wave of 600 MHz with an electric field of 1 V/m in the x-direction is incident upon the front surface of the body where the tumor is located. For this example, we assume that $\sigma_t = 0.5\sigma$ = 0.74 S/m and $\varepsilon_r = 53$ at 600 MHz. From Fig. 6.12, one observes a rather uniform distribution of SARs throughout the body with higher SARs induced in the rearside of the body. No peaking of the SAR in the tumor is observed for this case. The SAR in the tumor is increased to 3.6 mW/m^3 if $\sigma_t = \sigma = 1.48$ S/m. However, when $\sigma_t = 2\sigma$ = 2.96 S/m, the SAR in the tumor decreases to 3.5 mW/m^3. The SARs in other part of the body are only affected slightly by the change in the tumor conductivity. From this example, it seems that the maximum SAR in the tumor is obtained when $\sigma_t = \sigma$. However, this scheme of irradiation cannot selectively produce a peak SAR in the tumor even though the electrical properties of the tumor may be significantly different from that of the surrounding tissue.

CHAPTER 7

TENSOR INTEGRAL EQUATION METHOD COMBINED WITH ITERATION TECHNIQUE FOR QUANTIFYING INDUCED EM FIELD IN BIOLOGICAL SYSTEM

7.1 Introduction

The tensor integral equation method has been applied to solve many problems involving the interaction of EM fields with a biological system. Although this method has been powerful in many problems, it has some difficulties. The major difficulty is on the numerical convergence when it is applied to an electrically large body. In order to generate accurate numerical results, it is necessary to divide the body into a large number of electrically small volume cells. This, in turn, leads to an unmanageably large number of unknowns in the numerical calculation. Since a conventional computer may have difficulty in inverting a matrix larger than 300 x 300 due to storage limitation, it is desirable to devise schemes to extend the tensor integral equation method to handle a body consisting of a very large number of cells, while sidestepping the problem of computer storage limitation.

7.2 Theoretical Development

We have developed a scheme which combines an iteration process with the tensor integral equation method. This method is not a simple numerical average process; it is a process consistant with Maxwell's

equations. This method is explained here.

1. As the first step, we subdivide an irradiated body as shown in Fig. 7.1 into N cells, where N is the maximum number of cells which can be handled by the computer with a reasonable cost. We then quantify the induced electric field in the body with this N-cell model based on the tensor integral equation method. The numerical results of this N-cell model will be considered as the first-order solution for the induced electric field.

2. Each of N cells will be subdivided, one at a time, further into 8 subcells as shown in Fig. 7.1. Let us exclude the m^{th} cell from the body temporarily and consider its 8 subcells, $m_1, m_2, \ldots\ldots, m_8$.

3. Next, in the absence of the m^{th} cell, calculate the equivalent incident electric fields at the centers of the 8 subcells, located at $\vec{r}_{m1}$, $\vec{r}_{m2}$, ..., $\vec{r}_{m8}$. The equivalent incident electric field at the center of m_i subcell, or at $\vec{r}_{mi}$, is equal to the sum of the original incident electric field at $\vec{r}_{m_i}$ and the scattered electric field maintained by the first-order induced currents in the N-1 cells (the m^{th} cell excluded) at $\vec{r}_{m_i}$. That is

$$\vec{E}^{inc}_{eq}(\vec{r}_{m_i}) = \vec{E}^{inc}(\vec{r}_{m_i}) + \vec{E}^{s}(\vec{r}_{m_i}) \tag{7.1}$$

and

$$\vec{E}^{s}(\vec{r}_{m_i}) = \int_{V-\Delta v_m} \vec{J}_{eq}(\vec{r}') \cdot \overleftrightarrow{G}(\vec{r}_{m_i}, \vec{r}')\, dv', \quad i = 1,2,\ldots 8 \tag{7.2}$$

where

$$\vec{J}_{eq}(\vec{r}') = \tau(\vec{r}')\, \vec{E}(\vec{r}') \tag{7.3}$$

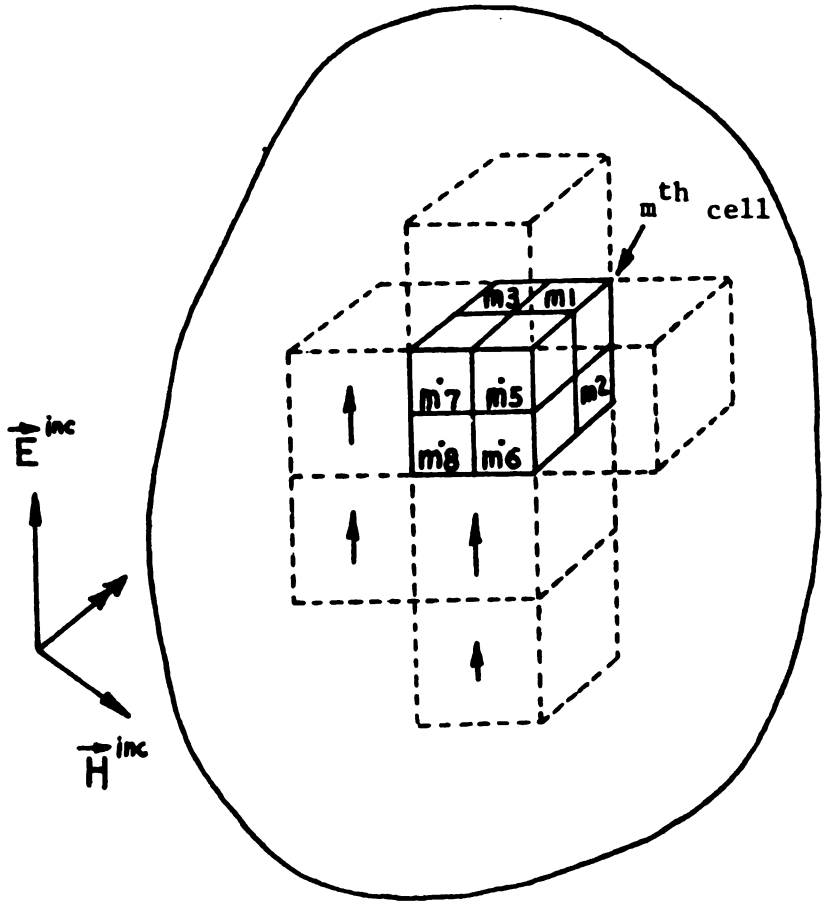

Fig.7.1. An irradiated body is subdivided into N cells, and each of the N cells is then subdivided again into 8 subcells.

$\overleftrightarrow{G}(\vec{r}_{mi}, \vec{r}')$ is the tensor green function. Scattered electric field at $\vec{r}_{m_i}$ can be written as

$$\vec{E}^s(\vec{r}_{mi}) = \int_{V-\Delta Vm} \tau(\vec{r}')\, \vec{E}(\vec{r}') \cdot \overleftrightarrow{G}(\vec{r}_{m_i}, \vec{r}')\, dv' \qquad (7.4)$$

We may represent the inner product $\vec{E}(\vec{r}') \cdot \overleftrightarrow{G}(\vec{r}_{mi}, \vec{r}')$ as

$$\vec{E}(\vec{r}') \cdot \overleftrightarrow{G}(\vec{r}_{m_i}, \vec{r}') = \left[\begin{array}{c|c|c} G_{xx}(\vec{r}_{m_i},\vec{r}') & G_{xy}(\vec{r}_{m_i},\vec{r}') & G_{xz}(\vec{r}_{m_i},\vec{r}') \\ \hline G_{yx}(\vec{r}_{m_i},\vec{r}') & G_{yy}(\vec{r}_{m_i},\vec{r}') & G_{yz}(\vec{r}_{m_i},\vec{r}') \\ \hline G_{zx}(\vec{r}_{mi},\vec{r}') & G_{zy}(\vec{r}_{m_i},\vec{r}') & G_{zz}(\vec{r}_{m_i},\vec{r}') \end{array}\right] \left[\begin{array}{c} E_x(\vec{r}') \\ \hline E_y(\vec{r}') \\ \hline E_z(\vec{r}') \end{array}\right] \qquad (7.5)$$

where $\overleftrightarrow{G}(\vec{r}_{m_i},\vec{r}')$ is the 3Nx3N matrix and $\vec{E}(\vec{r}')$ is a 3N column matrix with zero values for matrix elements corresponding to the m^{th} cell.

Let

$$x_1 = x, \quad x_2 = y, \quad x_3 = z$$

then $G_{x_p x_q}$ is given by

$$G_{x_p x_q}(\vec{r}_{m_i},\vec{r}') = -j\omega\mu_o \left[\delta_{pq} + \frac{1}{k_o^2}\frac{\partial^2}{\partial x_q \partial x_p}\right] \Psi(\vec{r}_{m_i},\vec{r}')$$

$$p,q = 1,2,3 \qquad (7.6)$$

Each scalar component of $\vec{E}^s(\vec{r}_{m_i})$ may be written as

$$\vec{E}^s_{x_p}(\vec{r}_{m_i}) = \int_{V-\Delta Vm} \tau(\vec{r}') \left[\sum_{q=1}^{3} G_{x_p x_q}(\vec{r}_{m_i}, \vec{r}') \, E_{x_q}(\vec{r}') \right] dv'$$

$$p = 1,2,3 \qquad (7.7)$$

We can transform eq. (7.4) into a matrix equation by using the method of moments. The scattered electric field maintained by the first-order induced currents in the N-1 cells (the m^{th} cell excluded) at $\vec{r}_{m_i}$ become

$$\vec{E}^s_{x_p}(\vec{r}_{m_i}) = \sum_{q=1}^{3} \sum_{\substack{n=1 \\ n \neq m}}^{N} \left[\tau(\vec{r}_n) \int_{V_n} G_{x_p x_q}(\vec{r}_{m_i}, \vec{r}') \, dv' \right] E_{x_q}(\vec{r}_n)$$

$$i = 1,2,\ldots,8 \qquad (7.8)$$

Let

$$G^{m_i n}_{x_p x_q} = \tau(r_n) \int_{V_n} G_{x_p x_q}(\vec{r}_{m_i}, \vec{r}') \, dv', \quad m \neq n \qquad (7.9)$$

As a first approximation, we have

$$G^{m_i n}_{x_p x_q} = \tau(r_n) \, G_{x_p x_q}(\vec{r}_{m_i}, \vec{r}_n) \, \Delta V_n \qquad (7.10)$$

$$m \neq n$$

where

$$v_n = \int_{V_n} dv' \tag{7.11}$$

By using eq. (7.6) to evaluate $G_{x_p x_q}(\vec{r}_{m_i}, \vec{r}_n)$ gives

$$G^{m_i n}_{x_p x_q} = -j\omega\mu_o k_o \tau(\vec{r}_n)\, \Delta v_n \exp(-j\alpha_{m_i n}) / 4\pi\alpha^3_{m_i n}$$

$$\cdot \left[(\alpha^2_{m_i n} - 1 - j\alpha_{m_i n})\, \delta_{pq} + \cos\theta^{m_i n}_{x_p} \cos\theta^{m_i n}_{x_q}\right.$$

$$\left. \cdot (3 - \alpha^2_{m_i n} + 3j\alpha_{m_i n})\right] \qquad m \neq n \tag{7.12}$$

where

$$\alpha_{m_i n} = k_o R_{m_i n}, \quad R_{m_i n} = |\vec{r}_{m_i} - \vec{r}_n|$$

$$\cos\theta^{m_i n}_{x_p} = \frac{(x_p^{m_i} - x_p^n)}{R_{m_i n}}, \quad \cos\theta^{m_i n}_{x_q} = \frac{(x_q^{m_i} - x_q^n)}{R_{m_i n}}$$

$$\vec{r}_{m_i} = (x_1^{m_i}, x_2^{m_i}, x_3^{m_i}), \quad \vec{r}_n = (x_1^n, x_2^n, x_3^n)$$

then

$$E^s_{x_p}(\vec{r}_{m_i}) = \sum_{q=1}^{3} \sum_{\substack{n=1 \\ n\neq m}}^{N} G^{m_i n}_{x_p x_q} E_{x_q}(\vec{r}_n) \qquad i = 1,2,\ldots,8 \tag{7.13}$$

After the first-order solution of the induced electric field is obtained in the first step. Then the scattered electric field at $\vec{r}_{m_i}$ can be computed by eq. (7.13). And, equivalent incident electric field at r_{m_i} can be written as

$$\vec{E}^{inc}_{eq}(\vec{r}_{m_i}) = \vec{E}^{inc}(\vec{r}_{m_i}) + \sum_{\substack{n=1 \\ n\neq m}}^{N} \overleftrightarrow{G}^{m_i n}(\vec{r}_{m_i}, \vec{r}_n) \cdot \vec{E}(\vec{r}_n) \qquad (7.14)$$

4. After equivalent incident electric fields at the centers of 8 subcells are calculated based on the first-order solution of the induced current, we can consider the m^{th} cell as an isolated body being irradiated by these equivalent incident electric fields at 8 points inside the m^{th} cell. We have subdivided the m^{th} cell into 8 subcells and the incident electric fields at the centers of these 8 subcells are known, therefore, the induced electric fields in these 8 subcells can now be readily determined based on the tensor integral equation method.

5. After each of the N cells is treated seperately following the above steps, the second-order solutions for the induced electric fields in the body are determined.

6. If more acculate results are needed, each of 8 subcells can be subdivided further into 8 subcells again and the iteration process can be repeated.

The important advantage of this technique is that since the iteration of the induced electric field of each cell is carried out seperately, it does not require the inversion of a large matrix and,

then, computer storage problem is sidestepped.

7.3 Example

An example is given here to show interesting results. Figure 7.2 shows the numerical results on the x-components of the induced electric fields in a muscle layer of 4x2x0.5 cm irradiated by a 1 GHz plane wave.

Due to symmetry, only 1/4 of the body is considered, and it is subdivided into 8 cells, 64 cells or 8 cells with iteration process in the numerical calculation. The incident electric field is 1 V/m (max. value) and the body conductivity and dielectric constant are assumed to be 1.62 S/m and 50, respectively. It is observed in Figure 7.2 that a significant improvement in numerical results is obtained with the 64-cell model or the 8-cell model with iteration process over the 8-cell model. It is also noted that numerical results based on the 64-cell model and 8-cell model with iteration process are quite close. The numerical results based on these three models are graphically compared in Figure 7.3, in which the x-components of the induced electric fields along four lines in the body are shown. From Figure 7.3, it is evident that numerical results based on the 64-cell model and the 8-cell model with iteration process are quite comparable. The most significant difference, however, is in the computation cost: with the 64-cell model the computation cost was $40, but it was only $14 with the 8-cell model with iteration process. It is to be emphasized that saving computation cost is one big advantage with the iteration technique, but the more important point is that with the iteration technique the body can now be divided into many more cells without encountering the computer storage problem.

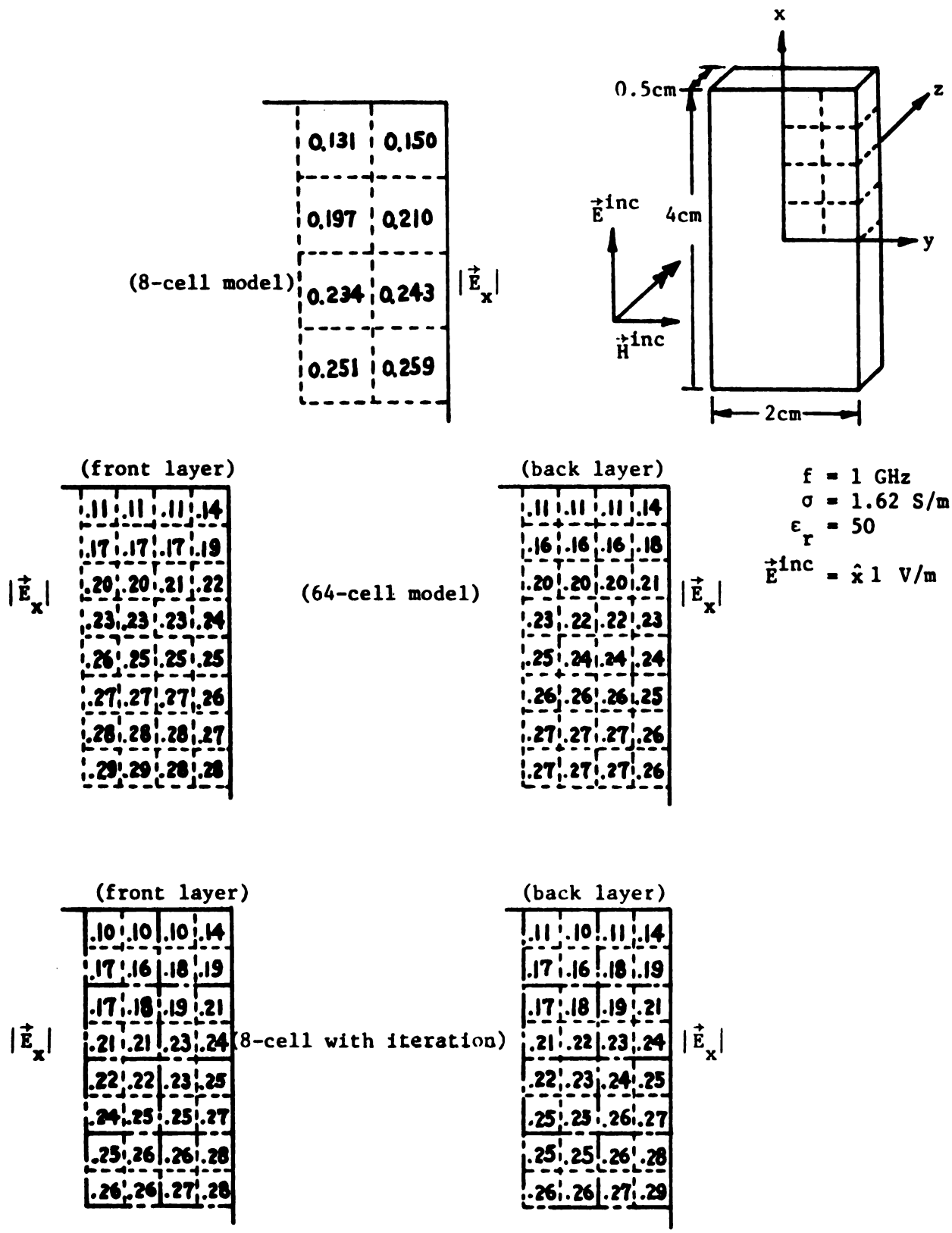

Fig.7.2. X components of induced electric fields inside a muscle layer of 4x2x0.5 cm irradiated by an 1 GHz EM wave, numerically computed when 1/4 of the body is subdivided into 8 cells, 64 cells, and 8 cells with interation process.

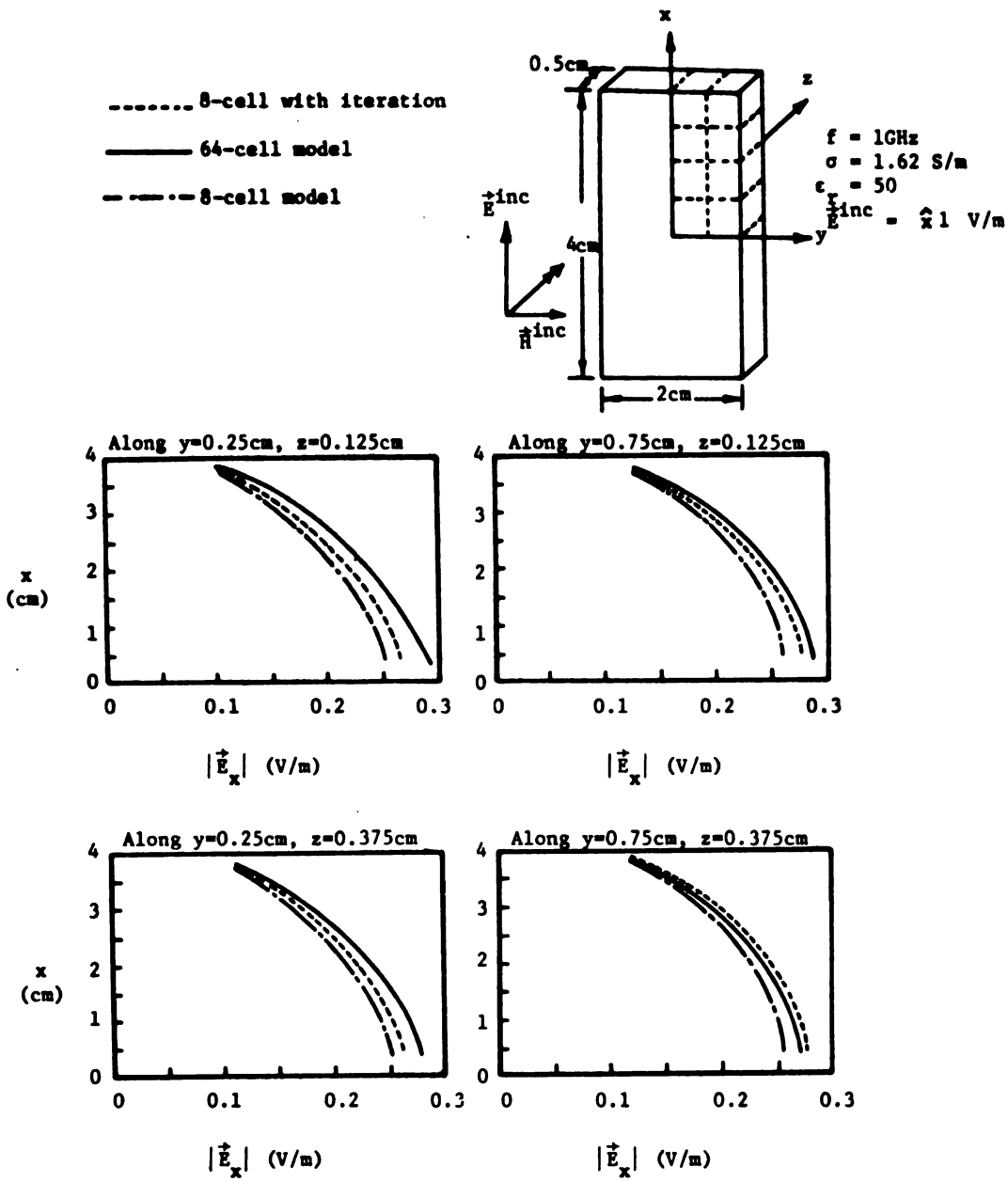

Fig. 7.3. Distributions of the x components of induced electric fields inside a muscle layer of 4x2x0.5 cm irradiated by an 1 GHz EM wave, numerically determined when 1/4 of the body is subdivided into 8 cells, 64 cells and 8 cells with iteration process.

It is noted that the method described in this chapter is particularly useful in the EM local heating of a body where EM energy is concentrated at a local region and detailed distribution of the absorbed power density in that local region is needed. For this problem, only the induced electric fields in that region need to be iterated and, thus, very accurate results can be obtained.

CHAPTER 8

GENERALIZED TENSOR INTEGRAL EQUATION METHOD FOR BODIES WITH ARBITRARY ELECTRICAL PARAMETERS

8.1 Introduction

The existing tensor integral equation was formulated for non-magnetic conducting bodies such as usual biological bodies. In some biological applications, it may be feasible to introduce notoxic magnetic powder into a local region of the body so that when the body is irradiated by an EM field or a magnetic field, the absorbed power density at the local region is enhanced. To analyze such a system the existing tensor integral equation can be generalized to handle a body with an arbitrary permeability in addition to arbitrary conductivity and permittivity. This generalized method will also be useful in the study of the interaction of EM fields with magnetic materials in solid-state electronic area or in other related fields.

8.2 Theoretical development

Consider a finite biological body of arbitrary shape with arbitrary electrical parameters characterized by $\sigma(\vec{r})$, $\varepsilon(\vec{r})$ and $\mu(\vec{r})$, illuminated in a free space by an incident EM wave with an electric field $\vec{E}^i(\vec{r})$ and a magnetic field $\vec{H}^i(\vec{r})$. When a biological body is illuminated by the incident EM field, it creates a distribution of induced charges and currents throughout the body. The induced current in the body includes three types of currents; the conduction current, the polarization current and the magnetization current. These charges and currents

produce a scattered field. The total EM field inside the body is the sum of incident field and the scattered field:

$$\vec{E}(\vec{r}) = \vec{E}^{i}(\vec{r}) + \vec{E}^{s}(\vec{r}) \tag{8.1}$$

$$\vec{H}(\vec{r}) = \vec{H}^{i}(\vec{r}) + \vec{H}^{s}(\vec{r}) \tag{8.2}$$

As developed in Chapter 2, the scattered electric field maintained by the conduction and polarization currents can be determined from the following equation (2,3):

$$\vec{E}^{s}(\vec{r}) = PV \int_{V} \vec{J}_{eq}(\vec{r}') \cdot \overleftrightarrow{G}(\vec{r},\vec{r}')\, dv' - \frac{\vec{J}_{eq}(\vec{r})}{3j\omega\varepsilon_{o}} \tag{8.3}$$

where

$$\vec{J}_{eq}(\vec{r}) = \left[\sigma + j\omega(\varepsilon-\varepsilon_{o})\right] \vec{E}(\vec{r})$$

$$\overleftrightarrow{G}(\vec{r},\vec{r}') = -j\omega\mu_{o}\left[\overleftrightarrow{I} + \frac{1}{k_{o}^{2}} \nabla\nabla\right] \phi(\vec{r},\vec{r}')$$

$$\phi(\vec{r},\vec{r}') = \frac{e^{-jk|\vec{r}-\vec{r}'|}}{4\pi|\vec{r}-\vec{r}'|}$$

Let's introduce new notations for the equivalent current $\vec{J}_{eq}$ and the tensor green function relating to the electric field as:

$$\vec{J}_{e}(\vec{r}) = \left[\sigma+j\omega\ (\varepsilon-\varepsilon_{o})\right] \vec{E}(\vec{r})$$

$$\overleftrightarrow{G}_{e}^{e}(\vec{r},\vec{r}') = -j\omega\mu_{o}\left[\overleftrightarrow{I} + \frac{1}{k_{o}^{2}} \nabla\nabla\right] \phi(\vec{r},\vec{r}')$$

$$\tau_e(\vec{r}) = \{\sigma(\vec{r}) + j\omega[\varepsilon(\vec{r})-\varepsilon_o]\}$$

The scattered electric field $\vec{E}^s(\vec{r})$ in equation 8.3 can then be written as

$$\vec{E}^s(\vec{r}) = PV \int_V \tau_e(\vec{r}') \vec{E}(\vec{r}') \cdot \overleftrightarrow{G}_e^e (\vec{r},\vec{r}') dv' - \frac{\tau_e(\vec{r})\vec{E}(\vec{r})}{3j\omega\varepsilon_o} \quad (8.4)$$

The scattered electric field maintained by the magnetization current can be determined from the magnetic vector potential as

$$\vec{E}^s(\vec{r}) = -\frac{1}{\varepsilon} \nabla \times \vec{A}_m(\vec{r})$$

$$= -\frac{1}{\varepsilon} \int_V \nabla \times \left[\varepsilon \vec{J}_m(\vec{r}') \phi(\vec{r},\vec{r}')\right] dv' \quad (8.5)$$

By using a vector identity $\nabla \times (\psi\vec{A}) = \psi\nabla\times\vec{A} + \nabla\psi\times\vec{A}$ and let $\psi = \phi(\vec{r},\vec{r}')$ and $\vec{A} = \vec{J}_m(\vec{r}')$, equation 8.5 becomes

$$\vec{E}^s(\vec{r}) = -\int_V \left[\phi(\vec{r},\vec{r}') \nabla \times \vec{J}_m(\vec{r}') + \nabla\phi(\vec{r},\vec{r}') \times \vec{J}_m(\vec{r}')\right] dv' \quad (8.6)$$

Since $\nabla \times \vec{J}(\vec{r}') = 0$, equation 8.6 reduces to

$$\vec{E}^s(\vec{r}) = -\int_V \nabla\phi(\vec{r},\vec{r}') \times \vec{J}_m(\vec{r}') dv' \quad (8.7)$$

From a tensor identity $(\overleftrightarrow{I} \times \vec{A}) \cdot \vec{B} = \vec{A} \times \vec{B}$, we let $\vec{A} = \nabla\phi(\vec{r},\vec{r}')$ and

$\vec{B} = \vec{J}_m(\vec{r}')$, equation 8.7 then becomes

$$\vec{E}^s(\vec{r}) = -\int_V \left[\overleftrightarrow{I} \times \nabla\phi(\vec{r},\vec{r}')\right] \cdot \vec{J}_m(\vec{r}')\, dv' \quad (8.8)$$

Defining

$$\overleftrightarrow{G}_m^e(\vec{r},\vec{r}') = -\overleftrightarrow{I} \times \nabla\phi(\vec{r},\vec{r}')$$

$$\vec{J}_m(\vec{r}') = \tau_m(\vec{r}')\, \vec{H}(\vec{r}')$$

where

$$\tau_m(\vec{r}) = j\omega\left[\mu(\vec{r}) - \mu_o\right]$$

Equation 8.8 can be rewritten as

$$\vec{E}^s(\vec{r}) = \int_V \tau_m(\vec{r}')\, \vec{H}(\vec{r}') \cdot \overleftrightarrow{G}_m^e(\vec{r},\vec{r}')\, dv' \quad (8.9)$$

By substituting equations 8.4 and 8.9 in equation 8.1, we obtain an integral equation for the induced electric field as

$$\left[1 + \frac{\tau_e(\vec{r})}{3j\omega\varepsilon_o}\right] \vec{E}(\vec{r}) - PV\int_V \tau_e(\vec{r}')\, \vec{E}(\vec{r}') \cdot \overleftrightarrow{G}_e^e(\vec{r},\vec{r}')\, dv'$$

$$- \int_V \tau_m(\vec{r}')\, \vec{H}(\vec{r}') \cdot \overleftrightarrow{G}_m^e(\vec{r},\vec{r}')\, dv' = \vec{E}^i(\vec{r}) \quad (8.10)$$

By induction, the scattered magnetic field maintained by magnetization current can be obtained as

$$\vec{H}^s(\vec{r}) = PV\int_V \tau_m(\vec{r}')\, \vec{H}(\vec{r}') \cdot \vec{G}_m^m(\vec{r},\vec{r}')\, dv' - \frac{\tau_m(\vec{r})\vec{H}(\vec{r})}{3j\omega\mu_o} \quad (8.11)$$

where

$$\overleftrightarrow{G}_m^m(\vec{r},\vec{r}') = -j\omega\varepsilon_o \left[\overleftrightarrow{I} + \frac{1}{k_o^2}\nabla\nabla\right] \phi(\vec{r},\vec{r}')$$

And the scattered magnetic field maintained by the conduction and polarization currents can be obtained as

$$\vec{H}^s(\vec{r}) = \int_V \tau_e(\vec{r}')\, \vec{E}(\vec{r}') \cdot \overleftrightarrow{G}_e^m(\vec{r},\vec{r}')\, dv' \qquad (8.12)$$

where

$$\overleftrightarrow{G}_e^m(\vec{r},\vec{r}') = \overleftrightarrow{I} \times \nabla\phi(\vec{r},\vec{r}')$$

By substituting equations 8.11 and 8.12 in equation 8.2, we obtain an integral equation for the induced magnetic field as

$$\left[1 + \frac{\tau_m(\vec{r})}{3j\omega\mu_o}\right] \vec{H}(\vec{r}) - PV \int_V \tau_m(\vec{r}')\, \vec{H}(\vec{r}') \cdot \overleftrightarrow{G}_m^m(\vec{r},\vec{r}')\, dv'$$

$$- \int_V \tau_e(\vec{r}')\, \vec{E}(\vec{r}') \cdot \overleftrightarrow{G}_e^m(\vec{r},\vec{r}')\, dv' = \vec{H}^i(\vec{r}) \qquad (8.13)$$

If an incident EM field with an electric field $\vec{E}^i(\vec{r})$ and a magnetic field $\vec{H}^i(\vec{r})$ are defined, the total induced electric field $\vec{E}(\vec{r})$ and the total induced magnetic field $\vec{H}(\vec{r})$ inside the body can be determined from the following two coupled tensor integral equations.

$$\left[1 + \frac{\tau_e(\vec{r})}{3j\omega\varepsilon_o}\right]\vec{E}(\vec{r}) - PV\int_V \tau_e(\vec{r}')\,\vec{E}(\vec{r}')\cdot\overleftrightarrow{G}_e^e(\vec{r},\vec{r}')\,dv'$$

$$- \int_V \tau_m(\vec{r}')\,\vec{H}(\vec{r}')\cdot\overleftrightarrow{G}_m^e(\vec{r},\vec{r}')\,dv' = \vec{E}^i(\vec{r}) \qquad (8.14)$$

$$\left[1 + \frac{\tau_m(\vec{r})}{3j\omega\mu_o}\right]\vec{H}(\vec{r}) - PV\int_V \tau_m(\vec{r}')\,\vec{H}(\vec{r}')\cdot\overleftrightarrow{G}_m^m(\vec{r},\vec{r}')\,dv'$$

$$- \int_V \tau_e(\vec{r}')\,\vec{E}(\vec{r}')\cdot\overleftrightarrow{G}_e^m(\vec{r},\vec{r}')\,dv' = \vec{H}^i(\vec{r}) \qquad (8.15)$$

where

$$\tau_e(\vec{r}) = \sigma(\vec{r}) + j\omega\left[\varepsilon(\vec{r}) - \varepsilon_o\right]$$

$$\tau_m(\vec{r}) = j\omega\left[\mu(\vec{r}) - \mu_o\right]$$

$$\overleftrightarrow{G}_e^e(\vec{r},\vec{r}') = -j\omega\mu_o\left[\vec{I} + \frac{1}{k_o^2}\nabla\nabla\right]\phi(\vec{r},\vec{r}')$$

$$\overleftrightarrow{G}_m^m(\vec{r},\vec{r}') = -j\omega\varepsilon_o\left[\vec{I} + \frac{1}{k_o^2}\nabla\nabla\right]\phi(\vec{r},\vec{r}')$$

$$\overleftrightarrow{G}_e^m(\vec{r},\vec{r}') = \vec{I}\times\nabla\,\phi(\vec{r},\vec{r}')$$

$$\overleftrightarrow{G}_m^e(\vec{r},\vec{r}') = -\vec{I}\times\nabla\,\phi(\vec{r},\vec{r}')$$

$$\phi(r,r') = \frac{e^{-jk_o|\vec{r}-\vec{r}'|}}{4\pi|\vec{r}-\vec{r}'|}$$

$\vec{\bar{I}}$ = identity tensor

$k_o = \omega\sqrt{\mu_o \varepsilon_o}$

PV symbols mean the principle values of the integrals.

These two coupled equations are more complicated than the tensor integral equation treated in the previous chapter. It is evident that they can only be solved numerically for a finite body with an irregular shape. By using the method of moments we can transform these coupled integral equations into a matrix equation. After that the induced electric and induced magnetic fields are obtained by inverting the matrix. Computer program for this problem is explained in part 3 of Chapter 9.

Tranformation to matrix equation

We may represent the inner product of $\vec{E}\cdot\vec{\bar{G}}_e$ in Eq. 8.14 as

$$\vec{E}(\vec{r})\cdot\vec{\bar{G}}_e(\vec{r},\vec{r}') = \begin{bmatrix} G^e_{e_{xx}}(\vec{r},\vec{r}') & G^e_{e_{xy}}(\vec{r},\vec{r}') & G^e_{e_{xz}}(\vec{r},\vec{r}') \\ G^e_{e_{yx}}(\vec{r},\vec{r}') & G^e_{e_{yy}}(\vec{r},\vec{r}') & G^e_{e_{yz}}(\vec{r},\vec{r}') \\ G^e_{e_{zx}}(\vec{r},\vec{r}') & G^e_{e_{zy}}(\vec{r},\vec{r}') & G^e_{e_{zz}}(\vec{r},\vec{r}') \end{bmatrix} \begin{bmatrix} E_x(\vec{r}') \\ E_y(\vec{r}') \\ E_z(\vec{r}') \end{bmatrix} \tag{8.16}$$

Let

$$x_1 = x, \quad x_2 = y, \quad x_3 = z$$

Then $G^e_{e_{x_p x_q}}(\vec{r},\vec{r}')$ is given by

$$G^e_{e_{x_p x_q}}(\vec{r},\vec{r}') = -j\omega\mu_o \left[\delta_{pq} + \frac{1}{k_o^2}\frac{\partial^2}{\partial x_q \partial x_p}\right] \phi(\vec{r},\vec{r}')$$

$$p,q = 1,2,3 \qquad (8.17)$$

We also represent the inner product $\vec{H}\cdot\overleftrightarrow{G}^e_m$ as

$$\vec{H}(\vec{r}')\cdot\overleftrightarrow{G}^e_m(\vec{r},\vec{r}') = \begin{bmatrix} G^e_{m_{xx}}(\vec{r},\vec{r}') & G^e_{m_{xy}}(\vec{r},\vec{r}') & G^e_{m_{xz}}(\vec{r},\vec{r}') \\ G^e_{m_{yx}}(\vec{r},\vec{r}') & G^e_{m_{yy}}(\vec{r},\vec{r}') & G^e_{m_{yz}}(\vec{r},\vec{r}') \\ G^e_{m_{zx}}(\vec{r},\vec{r}') & G^e_{m_{zy}}(\vec{r},\vec{r}') & G^e_{m_{zz}}(\vec{r},\vec{r}') \end{bmatrix} \begin{bmatrix} H_x(\vec{r}') \\ H_y(\vec{r}') \\ H_z(\vec{r}') \end{bmatrix}$$

(8.18)

The scalar components of Eq. 8.14 may be written as

$$\left[1 + \frac{\tau_e(\vec{r})}{3j\omega\varepsilon_o}\right] E_{x_p}(\vec{r}) - PV \int_V \tau_e(\vec{r}') \sum_{q=1}^{3} G^e_{e_{x_p x_q}}(\vec{r},\vec{r}')\, E_{x_q}(\vec{r}')\, dv'$$

$$- \int_V \tau_m(\vec{r}') \sum_{q=1}^{3} G^e_{m_{x_p x_q}}(\vec{r},\vec{r}')\, H_{x_q}(\vec{r}')\, dv' = E^i_{x_p}(\vec{r})$$

$$p = 1,2,3 \qquad (8.19)$$

We can transform eq. 8.14 into a matrix equation by using the method of moments. We partition the body into N subvolumes and assume that $\vec{H}(\vec{r})$, $\vec{E}(\vec{r})$, $\tau_e(\vec{r})$, $\tau_m(\vec{r})$ are constant in each subvolume.

Requiring that eq. 8.19 is satisfied at each $\vec{r}_m$, the center of the m^{th}

subvolume V_m, we have

$$\left[1 + \frac{\tau_e(\vec{r}_m)}{3j\omega\varepsilon_o}\right] E_{x_p}(\vec{r}_m) - \sum_{q=1}^{3}\sum_{n=1}^{N}\left[\tau_e(\vec{r}_n)\ PV \int_{V_n} G^e_{e_{x_p x_q}}(\vec{r}_m,\vec{r}')\ dv'\right]$$

$$\cdot E_{x_q}(\vec{r}_n) - \sum_{q=1}^{3}\sum_{n=1}^{N}\left[\tau_m(\vec{r}_n) \int_{V_n} G^e_{m_{x_p x_q}}(\vec{r}_m,\vec{r}')\ dv'\right]$$

$$\cdot H_{x_q}(\vec{r}_n) = E^i_{x_p}(\vec{r}_m) \qquad (8.20)$$

Defining

$$\bar{G}^{\,e\ mn}_{e_{x_p x_q}} = \tau_e(\vec{r}_n)\ PV \int_{V_n} G^e_{e_{x_p x_q}}(\vec{r}_m,\vec{r}')\ dv' \qquad (8.21)$$

and

$$G^{e\ mn}_{m_{x_p x_q}} = \tau_m(\vec{r}_n) \int_{V_n} G^e_{m_{x_p x_q}}(\vec{r}_m,\vec{r}')\ dv' \qquad (8.22)$$

We can write eq. 8.20 as

$$\sum_{q=1}^{3}\sum_{n=1}^{N}\left\{\left[\bar{G}^{\,e\ mn}_{e_{x_p x_q}} - \delta_{pq}\delta_{mn}\left(1 + \frac{\tau_e(\vec{r}_m)}{3j\omega\varepsilon_o}\right)\right] \cdot E_{x_q}(\vec{r}_n)\right.$$

$$\left. + G^{e\ mn}_{m_{x_p x_q}} \cdot H_{x_q}(\vec{r}_n)\right\} = -E^i_{x_p}(\vec{r}_m)$$

$$n = 1,2,\ldots\ldots N$$

$$p = 1,2,3 \qquad (8.23)$$

Let $G^{e\ mn}_{e_{x_p x_q}}$ be an N x N matrix given by

$$G^{e\ mn}_{e_{x_p x_q}} = \overline{G}^{e\ mn}_{e_{x_p x_q}} - \delta_{pq}\,\delta_{mn}\left[1 + \frac{\tau_e(r_m)}{3j\omega\varepsilon_o}\right] \tag{8.24}$$

Let $\left[E_{x_p}\right]$, $\left[H_{x_p}\right]$, and $\left[E^i_{x_p}\right]$ be N-dimensional vectors. As m and p range over all possible values in eq. 8.23, we obtain a matrix equation approximation for eq. 8.14 as

$$\begin{bmatrix} G^e_{e_{xx}} & G^e_{e_{xy}} & G^e_{e_{xz}} \\ G^e_{e_{yx}} & G^e_{e_{yy}} & G^e_{e_{yz}} \\ G^e_{e_{zx}} & G^e_{e_{zy}} & G^e_{e_{zz}} \end{bmatrix} \begin{bmatrix} E_x \\ E_y \\ E_z \end{bmatrix}$$

$$+ \begin{bmatrix} G^e_{m_{xx}} & G^e_{m_{xy}} & G^e_{m_{xz}} \\ G^e_{m_{yx}} & G^e_{m_{yy}} & G^e_{m_{yz}} \\ G^e_{m_{zx}} & G^e_{m_{zy}} & G^e_{m_{zz}} \end{bmatrix} \begin{bmatrix} H_x \\ H_y \\ H_z \end{bmatrix} = - \begin{bmatrix} E^i_x \\ E^i_y \\ E^i_z \end{bmatrix} \tag{8.25}$$

Symbolically, we can write eq. 8.25 as

$$\left[G_e^e\right]\left[E\right] + \left[G_m^e\right]\left[H\right] = -\left[E^i\right] \tag{8.26}$$

Similarly, for equation 8.15 we may represent the inner products $\vec{H} \cdot \overleftrightarrow{G}_m^m$ and $\vec{E} \cdot \overleftrightarrow{G}_e^m$ as

$$\vec{H}(\vec{r}') \cdot \overleftrightarrow{G}_m^m(\vec{r},\vec{r}') = \begin{bmatrix} G^m_{m_{xx}}(\vec{r},\vec{r}') & G^m_{m_{xy}}(\vec{r},\vec{r}') & G^m_{m_{xz}}(\vec{r},\vec{r}') \\ G^m_{m_{yx}}(\vec{r},\vec{r}') & G^m_{m_{yy}}(\vec{r},\vec{r}') & G^m_{m_{yz}}(\vec{r},\vec{r}') \\ G^m_{m_{zx}}(\vec{r},\vec{r}') & G^m_{m_{zy}}(\vec{r},\vec{r}') & G^m_{m_{zz}}(\vec{r},\vec{r}') \end{bmatrix} \begin{bmatrix} H_x(\vec{r}') \\ H_y(\vec{r}') \\ H_z(\vec{r}') \end{bmatrix} \tag{8.27}$$

and

$$\vec{E}(\vec{r}') \cdot \overleftrightarrow{G}_e^m(\vec{r},\vec{r}') = \begin{bmatrix} G^m_{e_{xx}}(\vec{r},\vec{r}') & G^m_{e_{xy}}(\vec{r},\vec{r}') & G^m_{e_{xz}}(\vec{r},\vec{r}') \\ G^m_{e_{yx}}(\vec{r},\vec{r}') & G^m_{e_{yy}}(\vec{r},\vec{r}') & G^m_{e_{yz}}(\vec{r},\vec{r}') \\ G^m_{e_{zx}}(\vec{r},\vec{r}') & G^m_{e_{zy}}(\vec{r},\vec{r}') & G^m_{e_{zz}}(\vec{r},\vec{r}') \end{bmatrix} \begin{bmatrix} E_x(\vec{r}') \\ E_y(\vec{r}') \\ E_z(\vec{r}') \end{bmatrix} \tag{8.28}$$

The scalar components of equation 8.15 may be written as

$$\left[1 + \frac{\tau_m(\vec{r})}{3j\omega\mu_o}\right] H_{x_p}(\vec{r}) - PV \int_V \tau_m(\vec{r}') \sum_{q=1}^{3} G^m_{m_{x_p x_q}}(\vec{r},\vec{r}') H_{x_q}(\vec{r}')\, dv'$$

$$- \int_V \tau_e(\vec{r}') \sum_{q=1}^{3} G^m_{e_{x_p x_q}}(\vec{r},\vec{r}') E_{x_q}(\vec{r}')\, dv' = H^i_{x_p}(\vec{r})$$

$$p = 1,2,3 \qquad (8.29)$$

By using the method of moments, we partition the body into N subvolumes and $\vec{E}(\vec{r})$, $\tau_e(\vec{r})$, $\vec{H}(\vec{r})$, $\tau_m(\vec{r})$ are assumed to be constant in each subvolume. Requiring that equation 8.29 is satisfied at each $\vec{r}_m$, we have

$$\left[1 + \frac{\tau_m(\vec{r}_m)}{3j\omega\mu_o}\right] H_{x_p}(\vec{r}_m) - \sum_{q=1}^{3}\sum_{n=1}^{N}\left[\tau_m(\vec{r}_n)\, PV \int_{V_n} G^m_{m_{x_p x_q}}(\vec{r}_m,\vec{r}')\, dv'\right]$$

$$\cdot H_{x_q}(\vec{r}_n) - \sum_{q=1}^{3}\sum_{n=1}^{N}\left[\tau_e(\vec{r}_n) \int_{V_n} G^m_{e_{x_p x_q}}(\vec{r}_m,\vec{r}')\, dv'\right] E_{x_q}(\vec{r}_n)$$

$$= H^i_{x_p}(\vec{r}_m)$$

$$p = 1,2,3 \qquad (8.30)$$

Defining

$$\bar{G}^{mmn}_{m_{x_p x_q}} = \tau_m(\vec{r}_n)\, PV \int_{V_n} G^m_{m_{x_p x_q}}(\vec{r}_m,\vec{r}')\, dv' \qquad (8.31)$$

and

$$G^{mn}_{e_{x_p x_q}} = \tau_e(\vec{r}_n) \int_{V_n} G^m_{e_{x_p x_q}}(\vec{r}_m,\vec{r}')\, dv' \qquad (8.32)$$

We can write equation 8.30 as

$$\sum_{q=1}^{3}\sum_{n=1}^{N}\left\{\left[\bar{G}^{m\,mn}_{m\,x_p x_q} - \delta_{pq}\delta_{mn}\left(1+\frac{\tau_m(\vec{r}_m)}{3j\omega\mu_o}\right)\right]\cdot H_{x_q}(\vec{r}_n) + G^{m\,mn}_{e\,x_p x_q}\cdot E_{x_q}(\vec{r}_n)\right\} = -H^{i}_{x_p}(\vec{r}_m) \qquad (8.33)$$

$$m = 1,2,.....N$$

$$p = 1,2,3$$

Let $G^{m\,mn}_{m\,x_p x_q}$ be an N x N matrix given by

$$G^{m\,mn}_{m\,x_p x_q} = \bar{G}^{m\,mn}_{m\,x_p x_q} - \delta_{pq}\delta_{mn}\left(1+\frac{\tau_m(r_m)}{3j\omega\mu_o}\right) \qquad (8.34)$$

As m and p range over all possible values in equation 8.33 we obtain another matrix equation.

$$\begin{bmatrix} G^m_{m_{xx}} & G^m_{m_{xy}} & G^m_{m_{xz}} \\ G^m_{m_{yx}} & G^m_{m_{yy}} & G^m_{m_{yz}} \\ G^m_{m_{zx}} & G^m_{m_{zy}} & G^m_{m_{zz}} \end{bmatrix} \begin{bmatrix} H_x \\ H_y \\ H_z \end{bmatrix}$$

$$+ \begin{bmatrix} G^m_{e_{xx}} & G^m_{e_{xy}} & G^m_{e_{xz}} \\ G^m_{e_{yx}} & G^m_{e_{yy}} & G^m_{e_{yz}} \\ G^m_{e_{zx}} & G^m_{e_{zy}} & G^m_{e_{zz}} \end{bmatrix} \begin{bmatrix} E_x \\ E_y \\ E_z \end{bmatrix} = - \begin{bmatrix} H^i_x \\ H^i_y \\ H^i_z \end{bmatrix} \qquad (8.35)$$

Symbolically equation 8.35 can be represented as

$$\left[G^m_m\right]\left[H\right] + \left[G^m_e\right]\left[E\right] = -\left[H^i\right] \qquad (8.36)$$

and combining equations 8.25, 8.26, 8.35, 8.36, we have

$$\left[G^e_e\right]\left[E\right] + \left[G^e_m\right]\left[H\right] = -\left[E^i\right]$$

$$\left[G^m_e\right]\left[E\right] + \left[G^m_m\right]\left[H\right] = -\left[H^i\right]$$

Where $\left[G^e_e\right]$, $\left[G^e_m\right]$, $\left[G^m_m\right]$, $\left[G^m_e\right]$ are 3N x 3N matrices and $\left[E\right]$, $\left[H\right]$, $\left[E^i\right]$, $\left[H^i\right]$ are 3N dimensional vectors. Finally we can write

$$\begin{bmatrix} G_e^e & G_m^e \\ G_e^m & G_m^m \end{bmatrix} \begin{bmatrix} E \\ H \end{bmatrix} = - \begin{bmatrix} E^i \\ H^i \end{bmatrix} \tag{8.37}$$

This matrix equation represents 6N simultaneous equations for 6N unknowns. If the incident electric field $\vec{E}^i(\vec{r})$ and the incident magnetic field $\vec{H}^i(\vec{r})$ are specified, the total induced electric field $\vec{E}(\vec{r})$ and the total induced magnetic field $\vec{H}(\vec{r})$ inside the body can be determined from equation 8.37 by inverting the $[\,G\,]$ matrix.

8.3 Example

Two examples are given here to show theoretical results of the magnetic heating inside biological systems which are injected with magnetic materials and when they are irradiated by a uniform magnetic field. Figure 8.1 shows the theoretical model of a muscle layer of 12x2x12 cm with a magnetized central part (shaded region) where the magnetic property was modified to possess an arbitrary permeability. The body is divided into 36 cells and the incident field is assumed to be a 30 MHz uniform magnetic field in y-direction.

First example is the case of a muscle layer of 8x2x8 cm irradiated by a 30 MHz uniform magnetic field. The body is divided into 16 of 2 cm-cubic cells and the permeability of the magnetized, central 4 cells has been modified by a magnetic powder injection. Figure 8.2 shows the absorbed power density in cell A located at x = 3, y = 1, z = 3 cm as a function of relative permeability of the magnetized part. At this frequency the conductivity and dielectric constant are assumed to be 0.62 S/m and 150, respectively, and the relative permeability of the

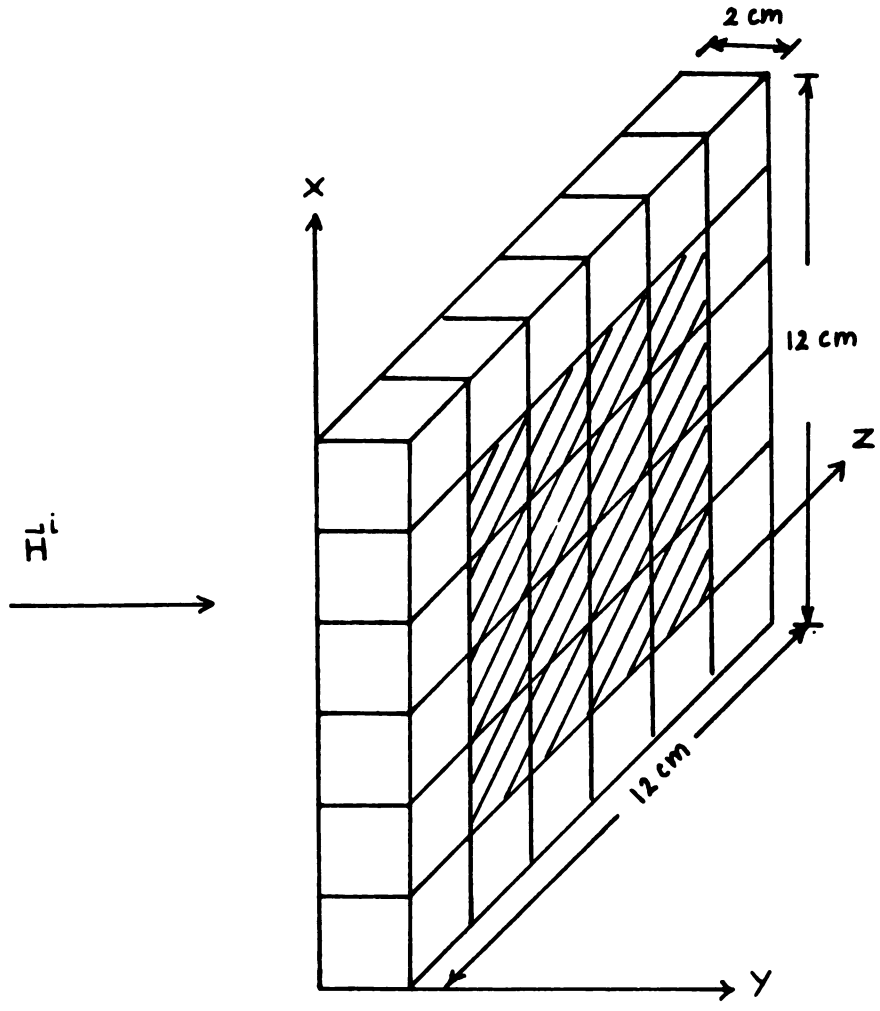

Figure 8.1 A simulated muscle layer (12x2x12 cm) with a magnetized central part irradiated by a uniform field ($\vec{H}^i$) of 1 A/m (max. value) at 30 MHz in y-direction. The body is divided into 36 of 2 cm-cubic cells.

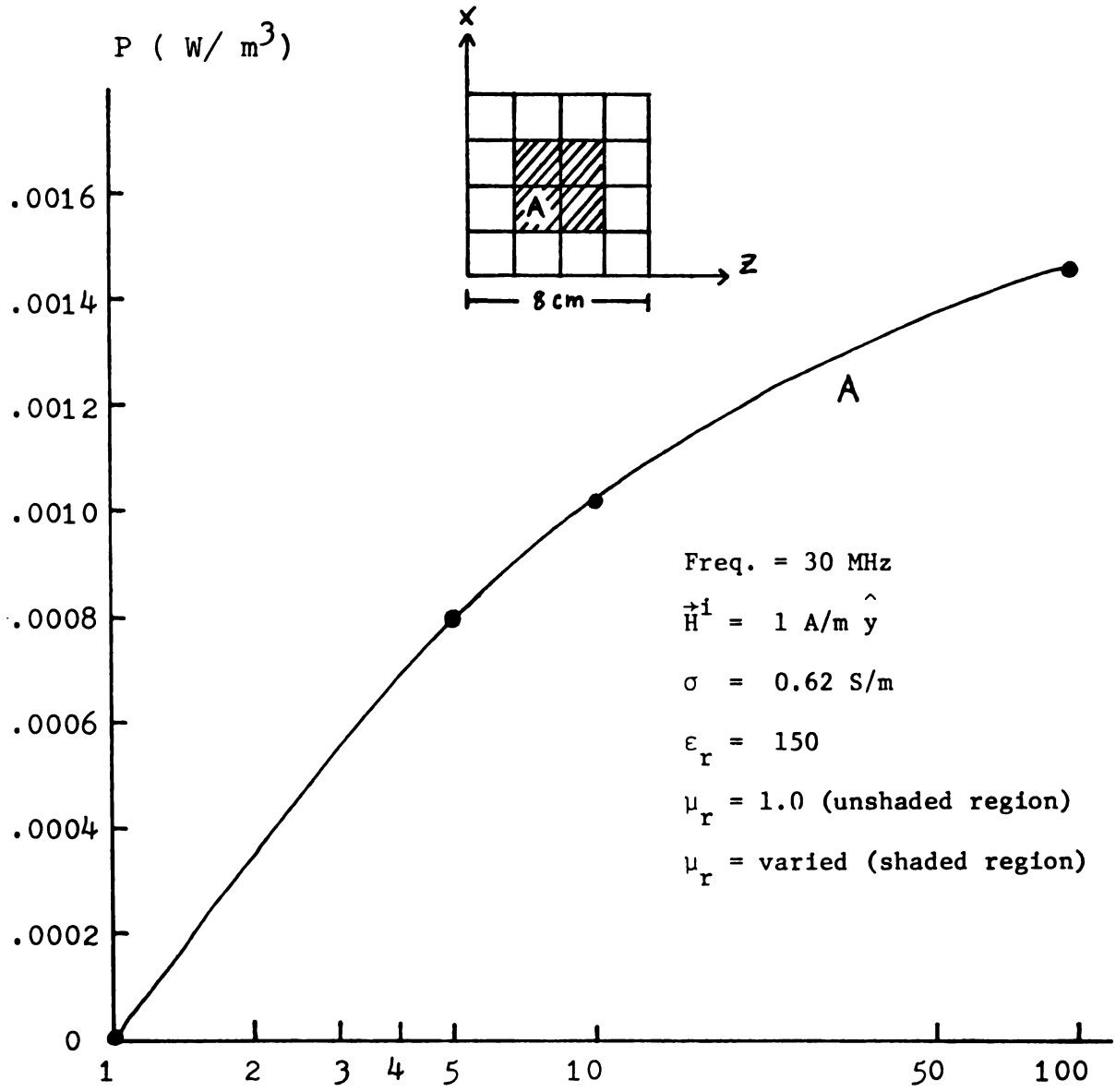

Figure 8.2 The absorbed power density in cell A varying as a function of relative permeability of the magnetized region inside a muscle layer (8x2x8 cm) for the case of frequency = 30 MHz, $\vec{H}^i$ = 1 A/m$\hat{y}$, σ = 0.62 S/m and ε_r = 150.

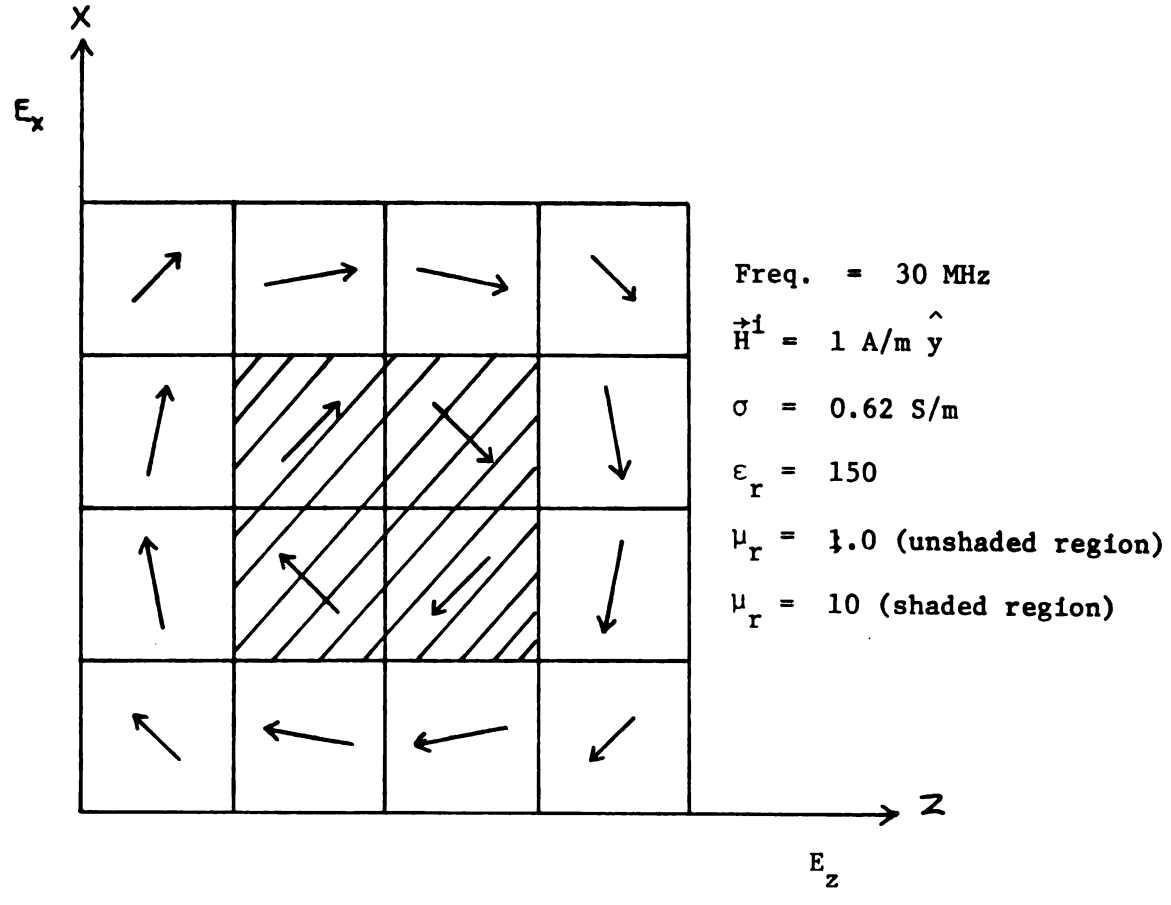

Figure 8.3 Distribution of induced electric fields (or currents) inside a muscle layer (8x2x8 cm) with a magnetized region (shaded region, $\mu_r = 10$) when frequency = 30 MHz, $\vec{H}^i = 1$ A/m $\hat{y}$, $\sigma = 0.62$ S/m and $\varepsilon_r = 150$.

unshaded region (unmagnetized region) is assumed to be unity. It is found that the absorbed power is rapidly increased when $1 < \mu_r < 10$ and slowly increased when $10 < \mu_r < 100$, where μ_r is the relative permeability of the magnetized region.

These results imply the effectiveness of magnetic heating induced by a uniform magnetic field in a magnetized body. The distribution of induced currents inside the body is shown in Figure 8.3. The relative permeability of the magnetized region is assumed to be $\mu_r = 10$. As expected the induced currents are circulatory on xz-plane around the direction of the incident magnetic field.

Another example is the case of a muscle layer of 12x2x12 cm with a magnetized region, excited by a 30 MHz uniform magnetic field as depicted in Figure 8.1. The body is divided into 36 2 cm-cubic cells with 16 cells consisting of the magnetized region (shaded region). Figure 8.4 shows the absorbed power densities in cells A and B located at x = 5, y = 1, z = 3 cm and x = 5, y = 1, z = 5 cm, respectively, as functions of the relative permeability μ_r of the magnetized region. This result shows that the absorbed power density increases rapidly when $1 < \mu_r < 10$ and then start to saturate after $\mu_r > 50$. Figure 8.5 shows the current distribution induced inside the muscle layer of Figure 8.4 when $\mu_r = 10$. It is clearly shown in this figure that circulartory currents are induced inside the body with their magnitudes increasing with the distance from the center of the body.

A study on this generalized TIEM at this point is not complete. Further studies on the numerical convergence and the accuracy test are needed in the future. One may be able to find new distribution

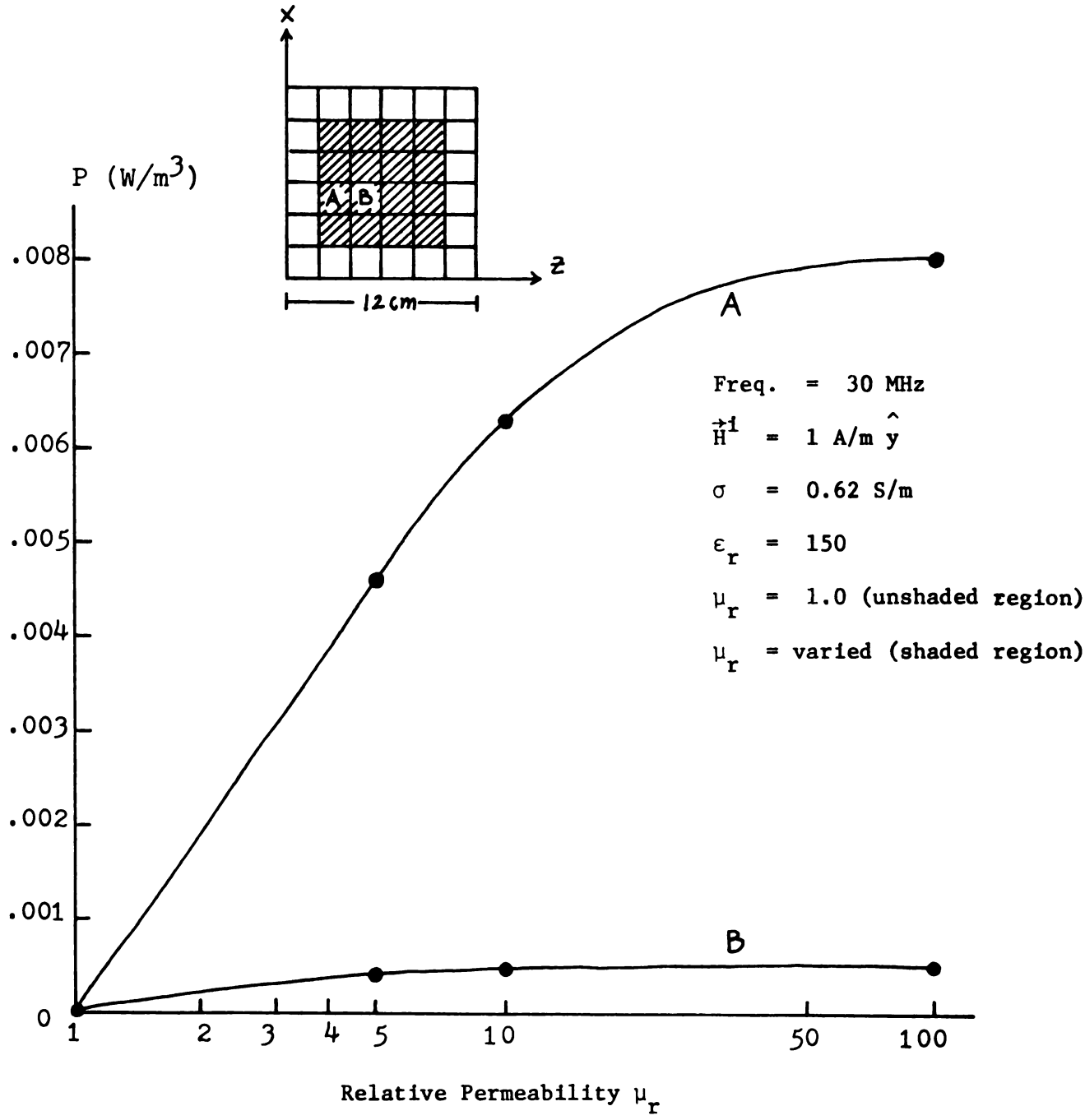

Figure 8.4 The absorbed power densities in cells A and B varying as functions of the relative permeability of magnetized region (shaded region) inside a muscle layer (12x2x12 cm) for the case of frequency = 30 MHz, $\vec{H}^i$ = 1 A/m $\hat{y}$, σ = 6.2 S/m, and ε_r = 150.

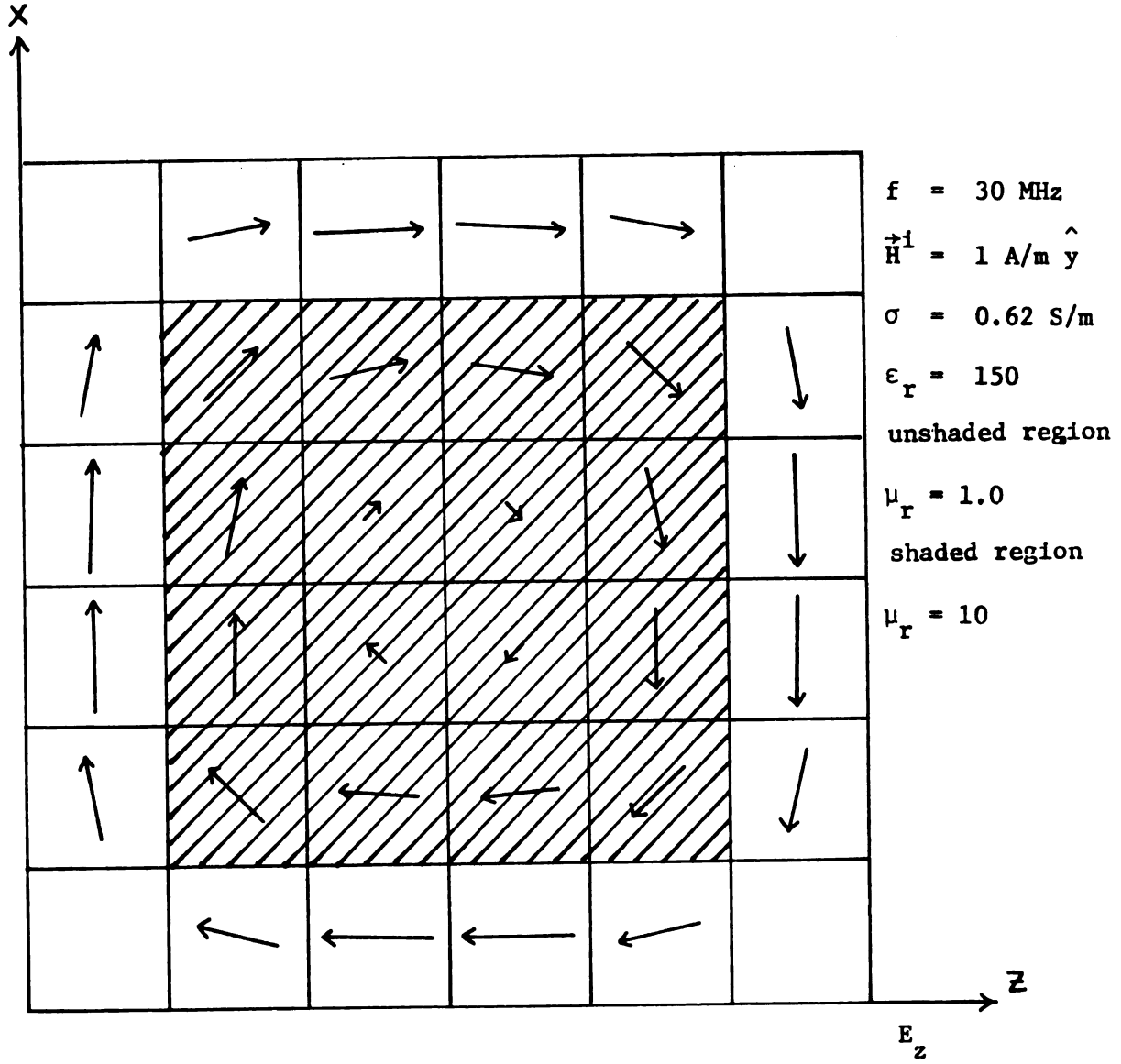

Figure 8.5 Distribution of induced electric fields (or currents) inside a muscle layer (12x2x12 cm) with magnetized region (shaded region, μ_r = 10) when frequency = 30 MHz, $\vec{H}^1$ = 1 A/m $\hat{y}$, σ = 0.62 S/m and ε_r = 150.

functions beside the pulse functions that when combined with the moment method, will lead to a more efficient solution to these coupled tensor integral equations.

CHAPTER 9

A USER'S GUIDE TO COMPUTER PROGRAM FOR INDUCED ELECTRIC FIELD INSIDE AN ARBITRARLLY SHAPED, FINITELY CONDUCTING BIOLOGICAL BODY

This chapter explains the computer programs used to obtain the numerical results on the induced EM fields in an irradiated biological body, based on the tensor integral equation method. There are 3 computer programs used.

First, program "FIELDS" is used to quantify the induced electric field at various locations of the biological system.

Second, program "ITERATE" is used to quantify the induced electric fields at the centers of 8 subcells in each cell of the biological system based on the first-order solutions of induced electric fields from program "FIELDS".

Third, program "EMFIELD" is used to quantify both induced electric field and induced magnetic field at various locations of a biological system with arbitrary permittivity, permeability and conductivity.

A listing of the program deck and instructions for their useage are also provided.

PART I PROGRAM FIELDS

9.1 Description of the program

This program is the modification of the program "FIELDS" developed

by Guru (23). The program is exactly the same mathematically but was modified to conform with a standard FORTRAN IV . The reason for this modification is to increase the "capacity" of the program to be able to handle a larger number of cells. By using the "MERIT" network, this program can handle the maximum size of the matrix up to 300 x 300 (100 cells).

The "MERIT" network (MTS) is the computing facility which combines the three host computing facilities located at Michigan State University, University of Michigan and Wayne State University. The IBM G&H compilers, waterloo Fortran and interactive FORTRAN (IF) are available under MTS at the University of Michigan. At Wayne State University the IBM FORTRAN G&H extended compilers, waterloo Fortran and IF are available under MTS. CDC FORTRAN extended version 4(FTN4) and Minnesota FORTRAN are available under scope/Hustler at Michigan State University.

With this computing facility CPU is ten times faster than CDC 6500 with 250 K 32 bit word real memory and unlimited virtual storage.

A biological system is divided into N small cubic cells with the side of each cubic cell not exceeding $\lambda/4$ where λ is the wavelength inside the body. The body is illuminated by an electromagnetic plane wave. Only normal incidence will be considered and the incident field is given by

$$\vec{E}^{i}(\vec{r}) = \hat{x}\, e^{-jk_o z}$$

Program "FIELDS" will calculate the induced electric field and power density at the center of each cell inside the body.

9.2 Data Structure and Input Variables

The data file for program FIELDS, showing the input variables, their FORMAT specifications, and their locations within the file, is outlined in Table 9.1. A detailed description of the variables is given in the next section.

A sample partitioning scheme for an arbitrary biological system is shown in Fig. 9.1. The biological body is divided into 4 quadrants and the center of the body is assumed to be the reference point. The body has two layers in z-direction. The quadrants are numbered in the clockwise order. In this example we assume that all the cells have the same physical dimension and electrical parameters. Under the symmetrical conditions, it is always intended to solve for the induced field in first quadrant and then interpret the result in other quadrant.

It is noted that the body can also be divided into 8 quadrants if the symmetry conditions for the body and the incident electric field exist for this division. For example, a plane EM wave in exponential form, $e^{-jk_o z}$, can be divided into cos $k_o z$ and -j sin $k_o z$.

The induced electric fields in the body due to cos $k_o z$ and -j sin $k_o z$ can be determined separately using 8 quadrants symmetry. The total induced electric fields in the body are then the sum of these two modes.

9.3 Description of the Input Variables

In this section we describe the function of each input variable and explain how it is used in PROGRAM FIELDS.

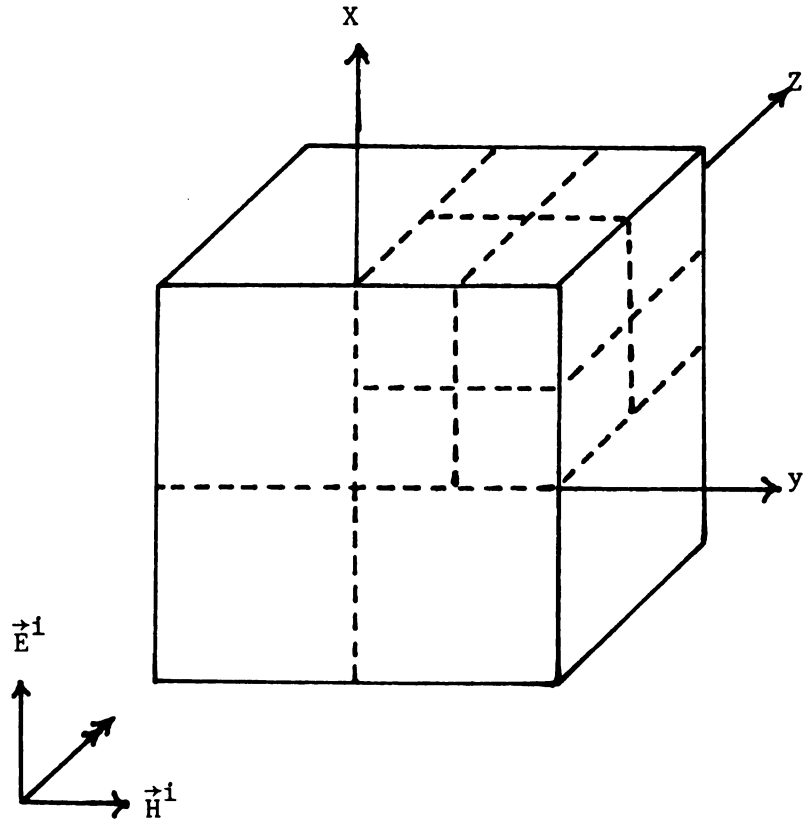

Figure 9.1. A two-layer biological body illuminated by an EM wave at normal incidence is shown divided into 4 quadrants under symmetry conditions.

File No.	Card No.	Symbolic name	Columns	Format
1	1	NDIV	1	I1
2	1	COMP	1-3	A3
		Q(J), J = 1,8	11-18	8I1
		FMEG	21-31	F10.0
		SCAT	41-45	A5
3	1	NX	1-2	I2
		NY	6-7	I2
		NZ	11-12	I2
4	1	N	1-3	I3
5	1-N	AMX	1-10	F10.3
		AMY	11-20	F10.3
		AMZ	21-30	F10.3
		RLEP1	31-40	F10.3
		SIG1	41-50	F10.3
		DXCM	51-60	F10.3
		DYCM	61-70	F10.3
		DZCM	71-80	F10.3

Table 9.1 The symbolic names of input variables and corresponding specifications for the data files used in the data structure for the program "FIELDS".

First data file

NDIV — This variable allows the user to control the accuracy with which the elements of $[G]$ are evaluated.

Second data file

COMP — being the code name for the component of the induced electric field which may have any one of the following forms

"XXX" x-component only

"XAY" x- and y-components

"XYZ" all three components

Q(J), J=1,8 — is the symbolic name for the quadrants. Quadrant 1-8 corresponding to column 11-18. If any one of the quadrants used then punch the quadrant number in corresponding column otherwise is "0" (zero).

FMEG — read frequency of incident wave in Mega Hz.

SCAT — being a code name for the incident wave.

EXPKZ,COSKZ,SINKZ --- for the exponential, cosine, sine variation of the incident electric field.

Third data file

NX,NY,NZ — defines the maximum number of cells in x-, y- and z-directions.

Fourth data file

N — Total number of cells being considered.

Fifth data file

There are as many as "N" data cards which help to

simulate the biological body. Each card contains

AMX,AMY,AMZ maximum boundaries of a cell in x-, y- and z-directions in cm.

RLEP1,SIG1 are the codes for relative dielectric constant and conductivity (S/m).

DXCM,DYCM,DZCM are the dimensions of the cell in x-, y- and z-directions in cm.

9.4 How to Use the Program

We will construct the data file for the example shown in Fig. 9.1. Let us assume that the incident field is of exponential form, the frequency of the incident wave is 2.45 GHz, and the electric parameters are $\varepsilon = 50\ \varepsilon_o$, $\sigma = 2.21$ S/m with a cell volume of 1x1x1 cm. The sequential order of the data files is as follows.

File No.	Information on the File							
1	2							
2	XYZ 12340000 2450.0 EXPKZ							
3	02 02 02							
4	008							
5.1	1.0	1.0	1.0	50.0	2.21	1.0	1.0	1.0
5.2	1.0	2.0	1.0	50.0	2.21	1.0	1.0	1.0
5.3	2.0	1.0	1.0	50.0	2.21	1.0	1.0	1.0
5.4	2.0	2.0	1.0	50.0	2.21	1.0	1.0	1.0
5.5	1.0	1.0	2.0	50.0	2.21	1.0	1.0	1.0
5.6	1.0	2.0	2.0	50.0	2.21	1.0	1.0	1.0
5.7	2.0	1.0	2.0	50.0	2.21	1.0	1.0	1.0
5.8	2.0	2.0	2.0	50.0	2.21	1.0	1.0	1.0

The list of the control cards needed for execution of the program in MERIT network is as follows:

Card No.	It's purpose	Information on the card
1	Authorization to use the computer	PNC
2	Job card (MSU)	B,CM30000,T100,RG1,JC100.
3	Pass word	PW=SUTUS
4	Input to MERIT network	DISPOSE,INPUT,IN=UM.
5		7/8/9
6		7/8/9
7	Job card (UM)	$SIG XS2Q T=160 PRIO=D P=300
8	Pass work (UM)	FIELDS
9		$RUN *FTN PAR=FORMAT=IBM

The deck card structure is as follows:

Control cards

Program

:

:

$ENDFILE

$SET DEBUG=ON

$SDS SET ERRORDUMP=ON

$RUN - LOAD SPUNCH=*PUNCH*

data cards

:

:

:

$ENDFILE

$SIGNOFF

6/7/8/9

```
C
C
C     PROGRAM FIELDS DETERMINES THE INDUCED ELECTRIC FIELDS INSIDE A
C     BIOLOGICAL BODY OF FINITE SHAPE, AND FINITE CONDUCTIVITY WHEN
C     EXPOSED TO INCIDENT PLANE WAVE OF UNIT MAGNETUDE POLARIZED
C     IN X - DIRECTION.
C
C     THE PROGRAM FIELDS MAKES USE OF THE FOLLOWING SUBPROGRAMS
C
C     ANGLES  ..... TO FIND PHASE ANGLES OF THE INDUCED FIELDS
C
C     CMATP  .....  SOLVES  N BY N  MATRIX BY BACK SUBSTITUTION
C
C     GMAT  .....  DEFINES ELEMENTS OF G MATRIX
C
C     REN  .....  FINDS DISTANCE R FROM ONE CELL TO ANOTHER
C
C     THE PROGRAM PUNCH OUT ON COMPUTER CARDS THE RESULT
C     INDUCED ELECTRIC FIELDS
C
C
      COMPLEX G,GMAT,DET
      REAL MU
      INTEGER*4 Q1,Q2,Q3,Q4,Q5,Q6,Q7,Q8
      COMMON VOL(270,7),XC,YC,ZC,K4
      COMMON/FIELD/SIZE(3),K1,K2,PI,EPS,MU,WVN,OMEG
      COMMON/BLKGMT/NDIV,GRID,PART,START1,START2,START3,
     1 ADD1,ADD2,ADD3,DENOM,REX1
      COMMON/FIELD1/G(270,271)
      REAL*8 SCAT,EXPKZ,COSKZ,SINKZ
      DATA EXPKZ/5HEXPKZ/,COSKZ/5HCOSKZ/,SINKZ/5HSINKZ/
      DATA XYZ/3HXYZ/,AXX/3HXXX/,XAY/3HXAY/
C
C
      PI = 3.141592653E
      EPS = 8.854E-12
      MU = 1.257E-6
C
C     ******************************************************************
C     READ FIRST DATA CARD FOR NDIV.
C     ******************************************************************
C
      READ 105, NDIV
      GRID = FLOAT(NDIV)
      PART = GRID**3
      DENOM = 4.* PI* PART
      GFACT = 0.5 * (( 1.0/ GRID ) - 1.0 )
```

```
C
C     ******************************************************************
C     READ 2ND CARD FOR COMPONENTS, QUADRANTS, FREQUENCY
C         AND TYPE OF INCIDENT ELECTRIC FIELD.
C     ******************************************************************
      READ 100,COMP,Q1,Q2,Q3,Q4,Q5,Q6,Q7,Q8,FMEG,SCAT
      IF ( COMP.EQ.XYZ )              GO TO 501
      IF ( COMP.EQ.XXX )              GO TO 500
      IF ( COMP.EQ.XAY )              GO TO 499
      PRINT 150,COMP
      GO TO 999
  499 KRON = 2
      GO TO 502
  500 KRON = 1
      GO TO 502
  501 KRON = 3
C
C     ******************************************************************
C     READ 3RD CARD FOR NUMBER OF CELLS IN X, Y, Z-DIRECTIONS RESP.
C     ******************************************************************
C
  502 READ 101, NX, NY, NZ
      OMEG = 2.* PI* FMEG * 1.0E6
      WVN = OMEG * SQRT (MU*EPS)
C
C     ******************************************************************
C     READ 4TH CARD FOR THE TOTAL NUMBER OF CELLS OF THE BODY
C     ******************************************************************
C
      READ 102, N
      MA = KRON * N
      MAP1 = MA + 1
      DO 300 I = 1,MA,1
      DO 300 J = 1,MAP1,1
  300 G(I,J) = CMPLX( 0.0,0.0 )
      REX1 = OMEG * MU * WVN
      PRINT 151
      PRINT 171
C
C     ******************************************************************
C     READ 5TH CARD AS MANY TIMES AS THERE ARE NUMBER OF CELLS OF
C     THE BIOLOGICAL BODY. THIS CARD DEFINES THE LOCATION OF THE
C     CELL, ITS ELECTRIC PARAMETERS AND ITS PHYSICAL DIMENSIONS
C     ******************************************************************
C
      DO 303 M = 1,N
      READ 104,AMX,AMY,AMZ,RLEP1,SIG1,DXCM,DYCM,DZCM
      VOL(M,1) = (AMX - (0.5 * DXCM))/ 100.0
      VOL(M,2) = (AMY - (0.5 * DYCM))/ 100.0
      VOL(M,3) = (AMZ - (0.5 * DZCM))/ 100.0
```

```
      DELTAX = DXCM / 100.0
      DELTAY = DYCM / 100.0
      DELTAZ = DZCM / 100.0
      VOL(M,4) = DELTAX*DELTAY*DELTAZ
      VOL(M,5) = RLEP1
      VOL(M,6) = SIG1
      VOL(M,7) = DELTAX
      Z = VOL(M,3)
      IF(SCAT.EQ.COSKZ)       G(M,MAP1) = CMPLX( -COS(WVN*Z),0.0 )
      IF(SCAT.EQ.SINKZ)       G(M,MAP1) = CMPLX( 0.0, SIN(WVN*Z ))
      IF(SCAT.EQ.EXPKZ)       G(M,MAP1) = -1.0*CEXP(CMPLX(0.,-WVN*Z))
303   PRINT 172,M,AMX,AMY,AMZ,DXCM,DYCM,DZCM
      PRINT 153
      DO 304 J = 1,N
304   PRINT 172,J,( VOL(J,L),L=1,6)
C
C     ****************************************************************
C     PRINT THE INCIDENT FIELD VALUES AT THE CENTRAL LOCATION
C           OF EACH CELL
C     ****************************************************************
C
      PRINT 163
      IF ( KRON - 2 ) 524,525,526
524   DO 309 I = 1,N
309   PRINT 165, I, G(I,MAP1)
      GO TO 527
525   DO 310 J = 1,N
      JPN = J + N
310   PRINT 165, J, G(J,MAP1), G(JPN,MAP1)
      GO TO 527
526   DO 311 K = 1,N
      KPN = K + N
      KNN = KPN + N
311   PRINT 165, K, G(K,MAP1) , G(KPN,MAP1) , G(KNN,MAP1)
527   PRINT 166,SCAT
C
C     ****************************************************************
C     CHECK FOR THE TYPE OF INCIDENT FIELD FOR THE CALCULATIONS
C     OF THE ELEMENTS OF THE G MATRIX
C     ****************************************************************
C
505   IF(SCAT.EQ.SINKZ)       GO TO 528
      DO 306 I = 1,KRON
      DO 306 J = 1,KRON
      DO 306 M1 = 1,N
      K = (I - 1) * N + M1
      XO = VOL(M1,1)
      YO = VOL(M1,2)
      ZO = VOL(M1,3)
```

```
      DO 306 M2 = 1,N
      DELTAX = VOL(M2,7)
      DELTAY = VOL(M2,7)
      DELTAZ = VOL(M2,7)
      SIZE(1) = DELTAX
      SIZE(2) = DELTAX
      SIZE(3) = DELTAX
      START1 = GFACT * SIZE(1)
      START2 = GFACT * SIZE(2)
      START3 = GFACT * SIZE(3)
      ADD1 = DELTAX / GRID
      ADD2 = DELTAY / GRID
      ADD3 = DELTAZ / GRID
      L = ( J - 1 )* N + M2
      K1 = I
      K2 = J
      K4 = M2
      IF( J.EQ.1 )          GO TO 513
      IF( J.EQ.2 )          GO TO 514
      G(K,L) = GMAT(Q1) - GMAT(Q2) - GMAT(Q3) + GMAT(Q4)
     1       - GMAT(Q5) + GMAT(Q6) + GMAT(Q7) - GMAT(Q8)
      GO TO 306
C
513   G(K,L) = GMAT(Q1) + GMAT(Q2) + GMAT(Q3) + GMAT(Q4)
     1       + GMAT(Q5) + GMAT(Q6) + GMAT(Q7) + GMAT(Q8)
      GO TO 306
C
514   G(K,L) = GMAT(Q1) - GMAT(Q2) + GMAT(Q3) - GMAT(Q4)
     1       + GMAT(Q5) - GMAT(Q6) + GMAT(Q7) - GMAT(Q8)
C
306   CONTINUE
      GO TO 510
C
528   DO 312 I = 1,KRON
      DO 312 J = 1,KRON
      DO 312 M1 = 1,N
      K = ( I - 1 )* N + M1
      XO = VOL(M1,1)
      YO = VOL(M1,2)
      ZO = VOL(M1,3)
      DO 312 M2 = 1,N
      L = ( J - 1 )* N + M2
      K1 = I
      K2 = J
      K4 = M2
      DELTAX = VOL(M2,7)
      DELTAY = VOL(M2,7)
      DELTAZ = VOL(M2,7)
      SIZE(1) = DELTAX
      SIZE(2) = DELTAX
      SIZE(3) = DELTAX
```

```
      START1 = GFACT * SIZE(1)
      START2 = GFACT * SIZE(2)
      START3 = GFACT * SIZE(3)
      ADD1 = SIZE(1) / GRID
      ADD2 = SIZE(2) / GRID
      ADD3 = SIZE(3) / GRID
      IF( J.EQ.1 )          GO TO 529
      IF( J.EQ.2 )          GO TO 530
      G(K,L) = GMAT(Q1) - GMAT(Q2) - GMAT(Q3) + GMAT(Q4)
     1       + GMAT(Q5) - GMAT(Q6) - GMAT(Q7) + GMAT(Q8)
      GO TO 312
C
529   G(K,L) = GMAT(Q1) + GMAT(Q2) + GMAT(Q3) + GMAT(Q4)
     1       - GMAT(Q5) - GMAT(Q6) - GMAT(Q7) - GMAT(Q8)
      GO TO 312
C
530   G(K,L) = GMAT(Q1) - GMAT(Q2) + GMAT(Q3) - GMAT(Q4)
     1       - GMAT(Q5) + GMAT(Q6) - GMAT(Q7) + GMAT(Q8)
C
312   CONTINUE
C
C     ***********************************************************************
C     PRINT FREQUENCY, MAXIMUM DIMENSIONS OF THE BODY, TYPE OF
C     COMPONENTS AND THE NUMBER OF QUADRANTS USED FOR SYMMETRY.
C     ***********************************************************************
C
510   PRINT 155,FMEG,NX,NY,NZ,COMP,Q1,Q2,Q3,Q4,Q5,Q6,Q7,Q8
      PRINT 159, NDIV
      PRINT 156
C
C     ***********************************************************************
C     CALCULATE THE INDUCED FIELDS IN EACH CELL
C     ***********************************************************************
C
      CALL CMATP(G,MA,1,DET,1.0E-50)
      PTOT = 0.0
      DO 307 M = 1,N
      EF1 = CABS( G(M,MAP1))
      IF( KRON.EQ.1 )       GO TO 516
      J = M + N
      EF2 = CABS( G(J,MAP1))
      IF( KRON.EQ.2 )       GO TO 488
      K = J + N
      EF3 = CABS( G(K,MAP1))
      GO TO 517
516   EF2 = 0.0
488   EF3 = 0.0
517   PWR = 0.5* VOL(M,6) * ( EF1*EF1 + EF2*EF2 + EF3*EF3 )
      PTOT = PTOT + PER *VOL(M,4)
307   PRINT 157,M,EF1,EF2,EF3,PWR
```

```
      PRINT 152, PTOT
      PRINT 161
C
C     ******************************************************************
C     PRINT REAL ,IMAGINARY,ABS. VALUE AND PHASE ANGLE OF
C     INCIDENT FIELD
C     ******************************************************************
C
      F = 57.2957795131
      DO 320 M= 1,N
      J = M + N
      K = J + N
      EFA = 0.0
      EFB = 0.0
      EFC = 0.0
      EF1 = 0.0
      EF2 = 0.0
      EF3 = 0.0
      IF( KRON-2 ) 555,554,553
  553 EFC = CABS( G(K,MAP1))
      CALL ANGLES(G,K,EF3,F,MAP1)
  554 EFB = CABS( G(J,MAP1))
      CALL ANGLES(G,J,EF2,F,MAP1)
  555 EFA = CABS( G(M,MAP1))
      CALL ANGLES(G,M,EF1,F,MAP1)
      IF ( KRON.EQ.1 )     GO TO 315
      IF ( KRON.EQ.2 )     GO TO 314
      PRINT 173,M,G(M,MAP1),EFA,EF1,G(J,MAP1),EFB,EF2,
     1 G(K,MAP1) ,EFC,EF3
      GO TO 320
  314 PRINT 173,M,G(M,MAP1),EFA,EF1,G(J,MAP1),EFB,EF2
      GO TO 320
  315 PRINT 173,M,G(M,MAP1),EFA,EF1
  320 CONTINUE
      DO 330 M=1,N,1
      MPN = M + N
      MP2N = 2 * N + M
      PUNCH 328 , G(M,MAP1), G(MPN,MAP1), G(MP2N,MAP1)
  328 FORMAT(2E12.5,4X,2E12.5,4X,2E12.5)
  330 CONTINUE
C
C
C     ******************************************************************
C     READ FORMATS
C     ******************************************************************
C
   10 FORMAT(2E12.5)
  100 FORMAT(A3,7X,8I1,2X,F10.0,10X,A5)
  101 FORMAT(3(I2,3X))
  102 FORMAT(I3)
```

```
104       FORMAT(8F10.3)
105       FORMAT(I1)
C
C         ******************************************************************
C         FORMATS TO GENERATE THE PRINT OUT
C         ******************************************************************
C
150       FORMAT(1H0,1H(,A6,38H) ERROR IN COLS 1-6 OF FIRST DATA CARD)
151       FORMAT(1H1,//,15X,38HTHE PARAMETERS OF EACH CELL AS READ IN,
     1    1X,23HARE GIVEN BELOW IN CMS.,//)
152       FORMAT(1H0,//,19X,35HTOTAL POWER ABSORBED BY THE BODY = ,
     1          1PE14.4,5X,5HWATTS,//)
153       FORMAT(1H1,//,15X,36HX,Y,Z CORRESPOND TO CENTRAL LOCATION,
     1          1X,22HOF EACH CELL IN METERS,//,7X,1HN,9X,1HX,13X,1HY,
     2          13X,1HZ,10X,6HVOLUME,10X,3HEPS,8X,10HSIG(MHO/M),//)
155       FORMAT(1H1,//,25X,41H( INDUCED ELECTRIC FIELDS IN QUADRANT 1 ),
     1          //,18X,12HFREQUENCY = ,F12.6,5H MHZ.,5X,7H( NX = ,I2,
     2          5X,5HNY = ,I2,5X,5HNZ = ,I2,3H ) ,
     3          //,18X,20H FIELD COMPONENTS = ,A6,5X,
     4          17HQUADRANTS USED = ,I1,7(1X,I1))
156       FORMAT(1H0,//,16X,1HN,8X,7HEX(V/M),11X,7HEY(V/M),11X,7HEZ(V/M),
     1          13X,3HPWR,//)
157       FORMAT(1H0,13X,I3,3X,4(E16.8,2X))
159       FORMAT(1H0,//,18X,30H NUMBER OF PARTITIONS PER EDGE,
     1          1X,17HIN INTEGRATION = ,I1,/)
161       FORMAT(1H1,//,3X,1HN,5X,6HEXREAL,6X,6HEXIMAG,6X,6HEX-ABS,2X,
     1          7HTHETA-X,2X,6HEYREAL,6X,6HEYIMAG,6X,6HEY-ABS,2X,
     2          7HTHETA-Y,2X,6HEZREAL,6X,6HEZIMAG,6X,6HEZ-ABS,2X,
     3          7HTHETA-Z,//)
163       FORMAT(1H1,//,15X,41HINCIDENT ELECTRIC FIELD HAS THE FOLLOWING,
     1          1X,10HCOMPONENTS,//,12X,23HE INCIDENT  X-DIRECTION,4X,
     2          23HE INCIDENT  Y-DIRECTION,4X,23HE INCIDENT  Z-DIRECTION
     3,//,6X,1HN,9X,4HREAL,10X,4HIMAG,10X,4HREAL,10X,4HIMAG,
     4          10X,4HREAL,10X,4HIMAG,//)
165       FORMAT(1H0,5X,I3,2X,1P6E14.4)
166       FORMAT(1H0,//,10X,35H THE INCIDENT FIELD IS OF THE FORM ,A5)
171       FORMAT(1H0,//,7X,1HN,8X,3HAMX,11X,3HAMY,11X,3HAMZ,10X,4HDXCM,
     1          10X,4HDYCM,10X,4HDZCM,//)
172       FORMAT(1H0,4X,I3,1X,1P6E14.4)
173       FORMAT(1H0,I3,3(3E12.4,F6.1))
999       CONTINUE
          END
C
C
          COMPLEX FUNCTION GMAT(QD)
C
          REAL MU
          INTEGER*4 QD
          DIMENSION U(3)
          COMPLEX TAUM2,FCTR1,FCRT2,EXPO,FUNC,TOTAL
```

```
C
      COMMON VOL(270,7),XO,YO,ZO,M2
      COMMON/FIELD/SIZE(3),I,J,PI,EPS,MU,WVN,OMEG
      COMMON/GMTRF/UO(3),RO
      COMMON/BLKGMT/NDIV,GRID,PART,START1,START2,START3,
     1              ADD1,ADD2,ADD3,DENOM,REX1
C
      DVM2 = VOL(M2,4)
      RLEP = VOL(M2,5) - 1.0
      SIG = VOL(M2,6)
      TAUM2 = CMPLX(SIG,OMEG*EPS*RLEP)
      IF( QD.EQ.0 ) GO TO 55
      CALL RFN(QD)
      IF( RO.EQ.0. )       GO TO 54
      TOTAL = CMPLX ( 0.,0. )
      U1MIN = UO(1) + START1
      U2MIN = UO(2) + START2
      U3MIN = UO(3) + START3
      U(3) = U3MIN
      DO 32 IZ = 1,NDIV
      U(1) = U1MIN
      DO 31 IX = 1,NDIV
      U(2) = U2MIN
      DO 30 IY = 1,NDIV
      R = SQRT( U(1)*U(1) + U(2)*U(2) + U(3)*U(3) )
      ALPHA = WVN * R
      FCTR2 = U(I)*U(J)*CMPLX( 3.0 - ALPHA*ALPHA, 3.0*ALPHA)/R**2
      FCTR1 = CEXP((0.,-1.)*ALPHA)/(ALPHA*ALPHA*ALPHA)
      IF( I.EQ.J )         GO TO 52
      FUNC = FCTR1 * FCTR2
      GO TO 53
52    FUNC = FCTR1*(FCTR2 + CMPLX(-1. + ALPHA*ALPHA, -ALPHA))
53    TOTAL = TOTAL + FUNC
30    U(2) = U(2) + ADD2
31    U(1) = U(1) + ADD1
32    U(3) = U(3) + ADD3
      GMAT = (0.,-1.)*REX1*TAUM2*DVM2*TOTAL/DENOM
      GO TO 99
54    IF( I.EQ.J )         GO TO 56
55    GMAT = CMPLX(0.,0. )
      GO TO 99
56    A = ((3.*DVM2)/(4.*PI))**(1./3.)
      FCTR1 = (0.,-1.)*2.*OMEG*MU*TAUM2/(3.*WVN*WVN)
      EXPO = CEXP((0.,-1.)*WVN*A)
      FCTR2 = EXPO* CMPLX(1. , WVN*A) - (1.,0.)
      GMAT = (FCTR1*FCTR2) - (1.,0.) - (TAUM2/((0.,3.)*OMEG*EPS))
99    CONTINUE
      RETURN
      END
```

```
C
C
      SUBROUTINE RFN(QD)
C
      INTEGER*4 QD
      COMMON VOL(270,7),XO,YO,ZO,IN
      COMMON/GMTRF/U(3),R
C
      IF( QD.EQ.1 )        GO TO 1
      IF( QD.EQ.2 )        GO TO 2
      IF( QD.EQ.3 )        GO TO 3
      IF( QD.EQ.4 )        GO TO 4
      IF( QD.EQ.5 )        GO TO 5
      IF( QD.EQ.6 )        GO TO 6
      IF( QD.EQ.7 )        GO TO 7
      IF( QD.EQ.8 )        GO TO 8
      GO TO 51
C
1     U(1) = XO - VOL(IN,1)
      U(2) = YO - VOL(IN,2)
      U(3) = ZO - VOL(IN,3)
      GO TO 50
C
2     U(1) = XO + VOL(IN,1)
      U(2) = YO - VOL(IN,2)
      U(3) = ZO - VOL(IN,3)
      GO TO 50
C
3     U(1) = XO + VOL(IN,1)
      U(2) = YO + VOL(IN,2)
      U(3) = ZO - VOL(IN,3)
      GO TO 50
C
4     U(1) = XO - VOL(IN,1)
      U(2) = YO + VOL(IN,2)
      U(3) = ZO - VOL(IN,3)
      GO TO 50
C
5     U(1) = XO - VOL(IN,1)
      U(2) = YO -VOL(IN,2)
      U(3) = ZO + VOL(IN,3)
      GO TO 50
C
6     U(1) = XO + VOL(IN,1)
      U(2) = YO - VOL(IN,2)
      U(3) = ZO + VOL(IN,3)
      GO TO 50
```

```
C
7       U(1) = XO + VOL(IN,1)
        U(2) = YO + VOL(IN,2)
        U(3) = ZO + VOL(IN,3)
        GO TO 50
C
8       U(1) = XO - VOL(IN,1)
        U(2) = YO + VOL(IN,2)
        U(3) = ZO + VOL(IN,3)
C
50      R = SQRT( U(1)*U(1) + U(2)*U(2) + U(3)*U(3) )
        GO TO 99
51      PRINT 15,QD
C
15      FORMAT(1H0,I1,32H IS AN IMPROPER QUADRANT NUMBER.,/)
C
99      CONTINUE
        RETURN
        END
C
C
C
        SUBROUTINE CMATP(A,N,M,DET,EP)
C
        COMPLEX A,B,DET,CONST,S
        DIMENSION A(270,271)
        DET = CMPLX(1.0 , 0.0)
        NP1 = N + 1
        NPM = N + M
        NM1 = N - 1
2       DO 4 J = 1,NM1
        C = CABS(A(J,J))
        JP1 = J + 1
        DO 5 I = JP1,N
        D = CABS(A(I,J))
        IF( C-D ) 6,5,5
6       DET = -DET
        DO 7 K = J,NPM
        B = A(I,K)
        A(I,K) = A(J,K)
7       A(J,K) = B
        C = D
5       CONTINUE
        IF(CABS(A(J,J))-EP)  14,15,15
15      DO 4 I = JP1,N
        CONST = A(I,J)/A(J,J)
        DO 4 K = JP1,NPM
4       A(I,K) = A(I,K) - CONST*A(J,K)
```

```
      IF( CABS(A(N,N))-EP ) 14,18,18
14    DET = CMPLX(0. , 0.)
      PRINT 30
      RETURN
18    CONTINUE
      DO 12 I = 1,N
      K = N - I + 1
      KP1 = K + 1
      DO 12 L = NP1,NPM
      S = CMPLX(0. , 0.)
      IF( N - KP1) 12,19,19
19    DO 13 J= KP1,N
13    S = S + A(K,J) * A(J,L)
12    A(K,L) = (A(K,L) - S)/A(K,K)
30    FORMAT(1X,42HTHE DETERMINANT OF THE SYSTEM EQUALS ZERO./
     1       1X,36HTHE PROGRAM CANNOT HANDLE THIS CASE.//)
      RETURN
      END
C
C
      SUBROUTINE ANGLES(G,K,EF,F,M)
C
      COMPLEX G(270,271)
C
      IF(AIMAG(G(K,M))) 10,20,30
10    IF(REAL(G(K,M)))  40,50,40
40    EF = F*ATAN2(AIMAG(G(K,M)) , REAL(G(K,M)))
      GO TO 100
C
50    EF = -90.0
      GO TO 100
C
20    IF( REAL(G(K,M))) 60,65,65
C
60    EF = - 180.0
      GO TO 100
C
65    EF = 0.0
      GO TO 100
C
30    IF( REAL(G(K,M))) 40,75,40
C
75    EF = 90.0
100   CONTINUE
      RETURN
      END
```

PART 2 PROGRAM ITERATE

9.5 Formulation of the Problem

The numerical method of program "FIELDS" sometimes encounters difficulties in the numerical convergence when the body is electrically large. It is evident that in order to generate accurate results and a good numerical convergence the cell size has to be electrically small, thus, a large number of cells is needed. This, in turn, leads to an unmanageably large number of unknowns in the numerical calculation. The program "ITERATE" is designed to overcome this difficulty.

Program "ITERATE" needs the first-order solutions on the induced electric fields from program "FIELDS". Starting with a biological body with N cells (this N-cells model gives reasonably good results and a reasonable computer cost), the induced electric fields in these N cells are obtained based on the tensor integral equation method.

In the next step, program "ITERATE" considers any one of N cells in the body (e.g. m^{th} cell) and divide this cell into 8 subcells. It then calculates the equivalent incident electric field at the center of each of the 8 subcells, which is equal to the incident electric field of the incident plane wave plus the scattered electric field maintained by the induced currents and charges in the rest of the cells in the body.

Finally, program "ITERATE" solves the induced electric fields at the centers of 8 subcells. After repeating each of these N cells, we determine the induced electric fields in the biological body with 8 N cells.

9.6 Description of Computer Program

The computer program is coded in standard FORTRAN IV and can be compiled on any FTN compiler. The main program is symbolically named as "ITERATE". Program "ITERATE" uses the following complex functions and subroutines for the numerical evaluation of induced electric fields inside a biological system.

"GMAT" is a complex function which calculates the elements of G matrix.

"CMATP" is a subprogram which calculates the induced electric field in each cell by solving a 24x24 matrix.

"ANGLES" This subprogram determines the phase angle between real and imaginary parts of the induced electric field in each cell.

A listing for the main program "ITERATE", the complex function "GMAT", and subprograms "CMATP" and "ANGLES" is given at the end of this part.

9.7 Structure of the Data File

The data file for program "ITERATE" showing the input variables, their FORMAT specifications and their locations within the file, is outlined in Table 9.2. A detailed description of the variables is given in this section.

A sample partitioning scheme for a biological body is shown in Fig. 9.2 and we will use this sample to run the program. The body is a cube of size 4x4x4 cm and it is divided into 8 subcells with the size of 2x2x2 cm. The body has two layers in the z-direction and these

2 layers touch each other. The reference point is shown in the figure which is located at the lower left corner of the body. The location of each cell is read with respect to the reference point.

After defining the location and electrical properties of each cell, we find the induced electric field at the center of each cell by using program "FIELDS" with an incident field of $\vec{E}^{i}(\vec{r}) = \hat{x}\, e^{-jk_o z}$. These results will be considered as the first-order solutions and input variables for program "ITERATE".

It is important to identify the order of these 8 subcells and their number system. These subcells are numbered in the clockwise order beginning with the back layer. In the program "ITERATE", the center location of each subcell is calculated based on this number system.

Next, the information in each data file is explained below.

First data file

This data file has only one data card which defines a symbolic name "NDIV" under I-format and "FMEG" under F-format.

NDIV	This variable allows the user to control the accuracy with which the elements of $\left[G \right]$ are evaluated.
FMEG	read frequency of the incident electromagnetic wave in MHz under F-format.

Second data file

This data file has only one data card which defines a symbolic name "NT" under I-format in the first three columns of the data card.

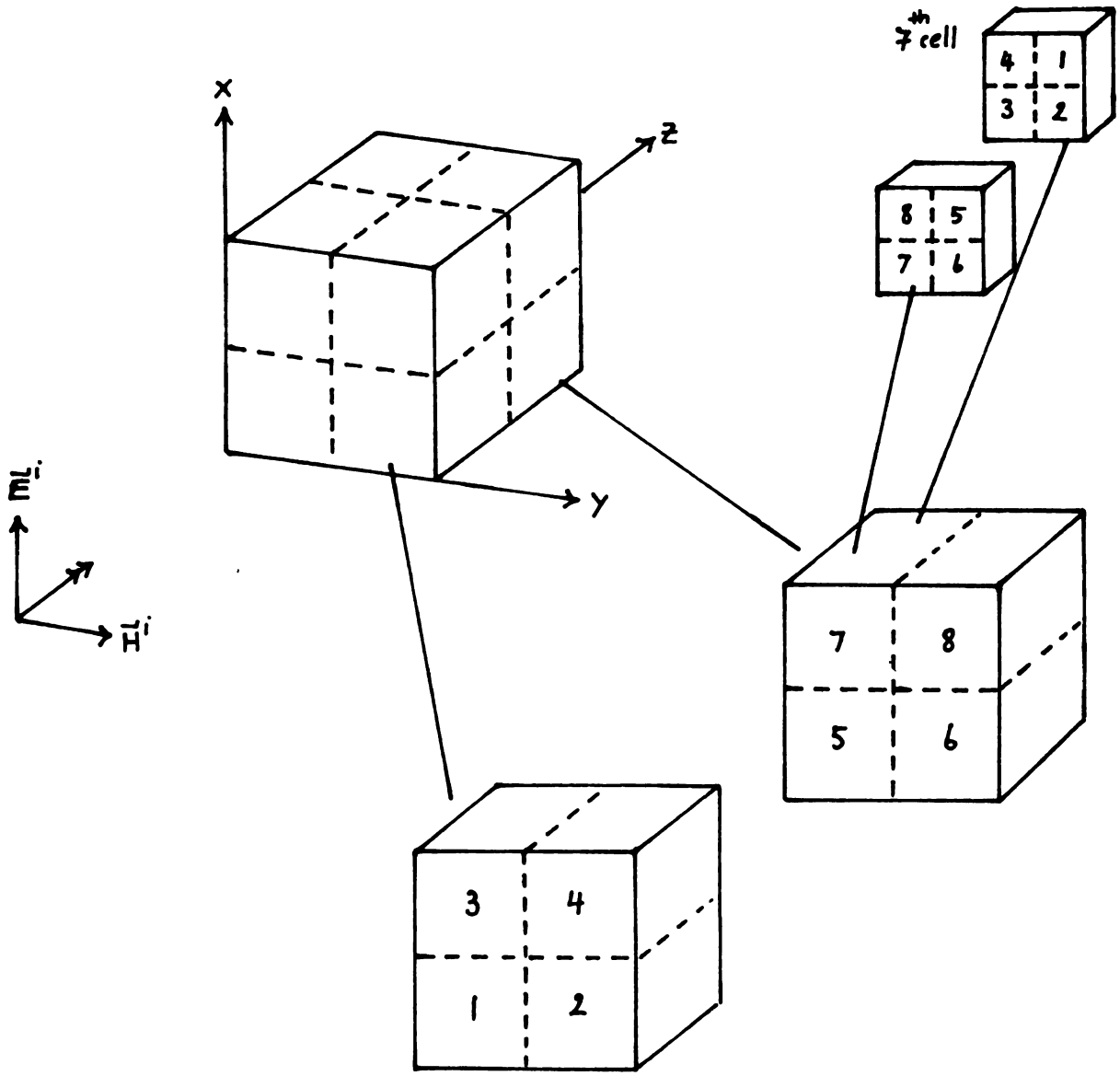

Fig. 9.2 A two-layer biological body illuminated by an EM wave at normal incident is shown divided into 8 cells in the 1st quadrant.

Table 9.2 The symbolic names of input variables and corresponding specifications for the data files used in the data structure for the program "ITERATE".

File No.	Card No.	Symbolic Name	Columns	Format
1	1	NDIV	1	I1
		FMEG	2-11	F10.0
2	1	NT	1-3	I3
3	1-NT	AMX	1-10	F10.3
		AMY	11-20	F10.3
		AMZ	21-30	F10.3
		RLEP1	31-40	F10.3
		SIG1	41-50	F10.3
		DXCM	51-60	F10.3
		DYCM	61-70	F10.3
		DZCM	71-80	F10.3
4	1-NT	E(K),K=1,NT	1-24	2E12.5
		E(KPN),KPN=NT,2NT	29-52	2E12.5
		E(KNN),KNN=2NT, 3NT	57-80	2E12.5
5	1	NQ	1-2	I2

It tells the computer about the total number of cells being considered. "NT" is also the total number of cell in the body.

Third data file

This data file has as many as NT data cards. This set of data cards helps simulate the biological system and each card contains the following information.

AMX,AMY,AMZ These codes correspond to the maximum boundaries of a cell in the x-, y- and z-directions in cm.

RLEP1,SIG1 are the codes for relative dielectric constant and conductivity of the cell.

DXCM,DYCM,DZCM are the symbolic names for the dimensions of the cell in x-, y- and z-directions in cm.

Fourth data file

This data file has NT data cards and this set of data defines the induced electric field at the center of each cell (first-order solution). Each card contains the x-, y- and z- components of the induced electric field.

Fifth data file

This data file has only one card which defines a symbolic name "NQ" under I-format in the first two columns of data card. It tells the computer how many quadrants have been used. If more than one quadrant are used only the cells in the 1st quadrant are considered.

To get better understanding of how these variables are used,an example is worked out in the next section for induced electric fields in a biological body as shown in Fig. 9.2.

9.8 An example to use the program

We will construct the data files for a sample problem in this section, to illustrate how the input variables are used. Also we will discuss some of the important features of the printed output.

A sample problem is a biological body as shown in Fig. 9.2. The body has 8 cells with a cell volume of 2x2x2 cm. Let's assume that the frequency of the incident wave is 1.0 GHz and the electrical parameters of the biological body are $\varepsilon = 50\ \varepsilon_o$, and $\sigma = 1.62$ S/m. The first-order solutions of the induced electric fields at the centers of 8 cells are punched on the computer cards as

Card no.	E_x		E_y		E_z	
1	6.318E-2	2.488E-2	8.373E-3	9.604E-4	8.185E-3	-1.055E-2
2	6.318E-2	2.488E-2	-8.373E-3	-9.604E-4	8.185E-3	-1.055E-2
3	6.318E-2	2.488E-2	-8.373E-3	-9.604E-4	-8.185E-3	1.055E-2
4	6.318E-2	2.488E-2	8.373E-3	9.604E-4	-8.185E-3	1.055E-2
5	6.513E-2	-2.870E-2	8.505E-3	-1.819E-3	-8.693E-3	-9.694E-3
6	6.513E-2	-2.870E-2	-8.505E-3	1.819E-3	-8.693E-3	-9.694E-3
7	6.513E-2	-2.870E-2	-8.505E-3	1.819E-3	8.693E-3	9.694E-3
8	6.513E-2	-2.870E-2	8.505E-3	-1.819E-3	8.603E-3	9.694E-3

After knowing all these induced fields, we can start setting the data files with the aid of Section 9.7 and Table 9.2. The sequential order of the data files is as follows:

File no.	Information on the file							
1	2	1000.0						
2	008							
3.1	2.0	2.0	2.0	50.0	1.62	2.0	2.0	2.0
3.2	2.0	4.0	2.0	50.0	1.62	2.0	2.0	2.0
3.3	4.0	2.0	2.0	50.0	1.62	2.0	2.0	2.0
3.4	4.0	4.0	2.0	50.0	1.62	2.0	2.0	2.0
3.5	2.0	2.0	4.0	50.0	1.62	2.0	2.0	2.0
3.6	2.0	4.0	4.0	50.0	1.62	2.0	2.0	2.0
3.7	4.0	2.0	4.0	50.0	1.62	2.0	2.0	2.0
3.8	4.0	4.0	4.0	50.0	1.62	2.0	2.0	2.0
4	First-order solution (see the previous page)							
5	01							

The list of the control cards needed for the execution of the program is as follows:

Card no.	Its purpose	Information on the card
1	Authorization to use the computer	PNC
2	job card	B,CM60000,T300,RG1,JC2000.
3		AUTORFL,PART.
4	Pass word	PW=SUTUS
5	Identification name	HAL,BANNER,SR.
6	Compile the program	FTN(R=3)
7	Execute the program	LGO.
8	End of control card	7/8/9

9.9 Printed Output

Although most of the items in the output are self-explaintory, a few of them need to be explained. The printed output consist of 4 output files. First, second and third output files are the data from the input files in order to check on the data used for the input variables and for further future references.

First output file consists of the maximum boundaries limited of each cell as read in through the symbolic code names "AMX', "AMY" and "AMZ' and the dimensions of each cell "DXCM", "DYCM" and "DZCM" in centimeters in x-, y- and z-direction, respectively.

Second output file, the internally calculated coordinates in the x-, y- and z-directions for the central location of each call, its volume and its permittivity and conductivity.

Third output file, the components of the induced electric field in each cell (the first-order solution).

Fourth output file consists of as many sets as the number of cells considered. Each set contains:

1. The coordinates in the x-, y- and z-directions for the central location of each subcell, its volume, permittivity and conductivity.
2. The equivalent incident electric field at the center of each subcell.
3. The most needed results for the induced electric field and the power density in each subcell in addition to the frequency

of incident wave and total power absorbed by the cell.

4. The real and imaginary parts of each component of the induced electric field in each subcell along with absolute magnetude and phase angle.

Listing of the program

A Fortran listing of the PROGRAM ITERATE and its subprogram begins on the next page. The subprogram is listed in order of their first appearance in the main program. The program required approximately 24600 octal words of storage.

```
      PROGRAM ITERATE (INPUT,OUTPUT)
C
C     PROGRAM ITERATE DETERMINES THE INDUCED ELECTRIC FIELDS IN
C     EACH ONE OF 8 SUBCELLS OF A CELL INSIDE A BIOLOGICAL BODY
C     OF FINITE SHAPE, AND FINITE CONDUCTIVITY WHEN EXPOSED TO
C     INCIDENT PLANE WAVE OF UNIT MAGNETUDE POLARIZED IN
C     X - DIRECTION
C     THE PROGRAM ITERATE MAKES USE OF THE FOLLOWING SUBPROGRAMS
C
C     CMATP  .....  SOLVES 24 X 24 MATRIX BY BACK SUBSTITUTION
C
C     GMAT   .....  DEFINES ELEMENTS OF G MATRIX-
C
C     ANGLES .....  TO FIND PHASE ANGLES OF THE INDUCED FIELDS
C
      COMPLEX G,GMAT,DET,E(324),S,TOTAL,ES(24)
      REAL MU
      COMMON VOL(110,7),XO,YO,ZO,K4
      COMMON/FIELD/K1,K2,PI,EPS,MU,WVN,OMEG
      COMMON/BLKGMT/NDIV,GRID,PART,START1,START2,START3,
     1 ADD1,ADD2,ADD3,DENOM,REX1
      COMMON/FIELD1/G(24,25)
      DIMENSION XMI(8),YMI(8),ZMI(8),BOD(110,7)
C
C
      PI = 3.1415926536
      EPS = 8.854E-12
      MU = 1.257E-6
C
C     ****************************************************************
C     READ 1ST DATA NDIV AND FREQUENCY IN MHZ.
C     ****************************************************************
C
      READ 100,NDIV,FMEG
      GRID = FLOAT(NDIV)
      PART = GRID**3
      DENOM = 4.0*PI*PART
      GFACT = 0.5*((1.0/GRID)-1.0)
      KRON = 3
      OMEG = 2.0*PI*FMEG*1.0E6
      WVN = OMEG*SQRT(MU*EPS)
C
C     ****************************************************************
C     READ 2ND DATA TOTAL NUMBER OF CELLS IN THE WHOLE BODY
C     ****************************************************************
C
      READ 102,NT
      MT = KRON*NT
      MTP1 = MT+1
      REX1 = OMEG*MU*WVN
```

```
      PRINT 103
      PRINT 104
C
C     ****************************************************************
C     READ 3RD DATA AS MANY TIMES AS THERE ARE NUMBER OF CELL OF
C     THE BIOLOGICAL BODY, THIS CARD DEFINES THE LOCATION OF THE
C     THE CELL, ITS ELECTRICAL PARAMETERS AND ITS PHYSICAL DIMENSIONS
C     ****************************************************************
C
      DO 202 M=1,NT
      READ 105,AMX,AMY,AMZ,RLEP1,SIG1,DXCM,DYCM,DZCM
      BOD(M,1) = (AMX-(0.5*DXCM))/100.0
      BOD(M,2) = (AMY-(0.5*DYCM))/100.0
      BOD(M,3) = (AMZ-(0.5*DZCM))/100.0
      DELTAX = DXCM/100.0
      DELTAY = DYCM/100.0
      DELTAZ = DZCM/100.0
      BOD(M,4) =  DELTAX*DELTAY*DELTAZ
      BOD(M,5) = RLEP1
      BOD(M,6) = SIG1
      BOD(M,7) = DELTAX
  202 PRINT 106,M,AMX,AMY,AMZ,DXCM,DYCM,DZCM
      PRINT 107
      DO 203 J=1,NT
  203 PRINT 108,J,(BOD(J,L),L=1,6)
C
C     ****************************************************************
C     READ 4TH DATA THE INDUCED ELECTRIC FIELDS VALUES AT THE
C     CENTRAL LOCATION OF EACH CELL AND PRINT OUT
C     ****************************************************************
C
C
      PRINT 108
      DO 204 K=1,NT
      KPN = K+NT
      KNN = KPN+NT
      READ 109,E(K),E(KPN),E(KNN)
  204 PRINT 110,K,E(K),E(KPN),E(KNN)
C
C     ****************************************************************
C     READ 5TH DATA NUMBER OF QUADRANTS USED AND CALCULATE
C     NUMBER OF CELLS WILL BE CONSUDERED
C     ****************************************************************
C
      READ 112,NQ
      NCL = NT/NQ
      DO 340 MCL=1,NCL
      MCPN = MCL + NT
      MCNN = MCPN + NT
```

```
      DO 206 I=1,7,1
      DO 206 M=1,NT,1
  206 VOL(M,I) = BOD(M,I)
C
C     CALCULATE CENTRAL LOCATION OF EACH SUBCELL
C
      X = VOL(MCL,1)
      Y = VOL(MCL,2)
      Z = VOL(MCL,3)
      DX = VOL(MCL,7)/4.0
      DY = VOL(MCL,7)/4.0
      DZ = VOL(MCL,7)/4.0
      XMI(1) = X + DX
      YMI(1) = Y + DY
      ZMI(1) = Z + DZ
      XMI(2) = X - DX
      YMI(2) = Y + DY
      ZMI(2) = Z + DZ
      XMI(3) = X- DX
      YMI(3) = Y - DY
      ZMI(3) = Z+ DZ
      XMI(4) = X + DX
      YMI(4) = Y -DY
      ZMI(4) = Z + DZ
      XMI(5) = X + DX
      YMI(5) = Y + DY
      ZMI (5) = Z - DZ
      XMI(6) = X -DX
      YMI(6) = Y + DY
      ZMI(6) = Z -DZ
      XMI(7) = X - DX
      YMI(7) = Y -DY
      ZMI(7) = Z -DZ
      XMI(8) = X + DX
      YMI(8) = Y -DY
      ZMI(8) = Z -DZ
C
C     CALCULATE SCATTERING ELECTRIC FIELD AT THE CENTER
C     OF EACH SUBCELL
C
  210 DO 221 I=1,KRON
      DO 221 M1=1,8
      TOTAL = CMPLX(0.0,0.0)
      K = (I-1)*8  + M1
      XO = XMI(M1)
      YO = YMI(M1)
      ZO = ZMI(M1)
      DO 220 J=1,KRON
      DO 220 M2=1,NT
     -DELTAX = VOL(M2,7)
```

```
      DELTAY = VOL(M2,7)
      DELTAZ = VOL(M2,7)
      START1 = GFACT*DELTAX
      START2 = GFACT*DELTAY
      START3 = GFACT*DELTAZ
      ADD1 = DELTAX/GRID
      ADD2 = DELTAY/GRID
      ADD3 = DELTAZ/GRID
      L = (J-1)*NT + M2
      IF(L.EQ.MCL) GO TO 220
      IF(L.EQ.MCPN) GO TO 220
      IF(L.EQ.MCNN) GO TO 220
      K1 = I
      K2 = J
      K4 = M2
      S = GMAT(1)*E(L)
      TOTAL = S + TOTAL
  220 CONTINUE
      ES(K) = TOTAL
  221 CONTINUE
C
C     CALCULATE 2ND INCIDENT ELECTRIC FIELD AT THE CENTER OF
C     EACH SUBCELL WHICH EQUAL TO PLANE WAVE + SCATTERING ELECTRIC
C     FIELDS
C
      N = 8
      MA = 24
      MAP1 = 25
      DO 300 I=1,MA,1
      DO 300 J=1,MAP1,1
  300 G(I,J) = CMPLX(0.0,0.0)
      DELTA = VOL(MCL,7)/2.0
      SIG = VOL(MCL,6)
      RLEP = VOL(MCL,5)
      DO 303 M=1,8
      MPN = M+N
      MNN = MPN+N
      VOL(M,1) = XMI(M)
      VOL(M,2) = YMI(M)
      VOL(M,3) = ZMI(M)
      VOL(M,4) = DELTA*DELTA*DELTA
      VOL(M,5) = RLEP
      VOL(M,6) = SIG
      VOL(M,7) = DELTA
      Z = VOL(M,3)
      G(M,MAP1) = -1.0*CEXP(CMPLX(0.0,-WVN*Z))-ES(M)
      G(MPN,MAP1) = -ES(MPN)
      G(MNN,MAP1) = -ES(MNN)
  303 CONTINUE
      PRINT 107
```

```
      DO 304 J=1,8
304   PRINT 106,J,(VOL(J,L),L=1,6)
      PRINT 118,MCL
      DO 311 K=1,N
      KPN = K+N
      KNN = KPN+N
311   PRINT 110,K,G(K,MAP1),G(KPN,MAP1),G(KNN,MAP1)
      DO 320 I=1,KRON
      DO 320 J=1,KRON
      DO 320 M1=1,N
      K=(I-1)*N + M1
      X0 = VOL(M1,1)
      Y0 = VOL(M1,2)
      Z0 = VOL(M1,3)
      DO 320 M2=1,N
      DELTAX = VOL(M2,7)
      DELTAY = VOL(M2,7)
      DELTAZ = VOL(M2,7)
      START1 = GFACT*DELTAX
      START2 = GFACT*DELTAY
      START3 = GFACT*DELTAZ
      ADD1 = DELTAX/GRID
      ADD2 = DELTAY/GRID
      ADD3 = DELTAZ/GRID
      L=(J-1)*N + M2
      K1 = I
      K2 = J
      K3 = M2
      G(K,L) = GMAT(1)
320   CONTINUE
C
CC
C     PRINT NUMBER OF THE CELLS THAT IS CONSIDERING AND FREQUENCY
C     OF INCIDENT WAVE
C
      PRINT 120,MCL,FMEG
      PRINT 122,NDIV
      PRINT 124
C
CC    CALCULATE THE INDUCED ELECTRIC FIELDS IN EACH SUBCELL
C
      CALL CMATP(G,MA,1,DET,1.0E-50)
      PTOT = 0.0
      DO 330 M=1,N
      EF1 = CABS(G(M,MAP1))
      J=M+N
      EF2 = CABS(G(J,MAP1))
      K=J+N
      EF3 = CABS(G(K,MAP1))
      PWR = 0.5*VOL(M,6)*(EF1*EF1 + EF2*EF2 + EF3*EF3)
```

```
      PTOT = PTOT + PWR*VOL(M,4)
  330 PRINT 130,M,EF1,EF2,EF3,PWR
      PRINT 132,PTOT
      PRINT 133
C
CC    ***************************************************************
C     PRINT REAL, IMAGINARY, ABSOLUTE VALUE AND PHASE ANGLES OF
C     INDUCED ELECTRIC FUELDS
CC    ***************************************************************
C
      F = 57.2957795131
      DO 340 M=1,N
      J = M+N
      K = J+N
      EFA = 0.0
      EFB = 0.0
      EFC = 0.0
      EF1 = 0.0
      EF2 = 0.0
      EF3 = 0.0
      EFC =  CABS(G(K,MAP1))
      CALL ANGLES(G,K,EF3,F,MAP1)
      EFB = CABS(G(J,MAP1))
      CALL ANGLES(G,J,EF2,F,MAP1)
      EFA = CABS(G(M,MAP1))
      CALL ANGLES(G,M,EF1,F,MAP1)
      PRINT 140,M,G(M,MAP1),EFA,EF1,G(J,MAP1),EFB,EF2,
     1 G(K,MAP1),EFC,EF3
  340 CONTINUE
C
CC    ***************************************************************
C
C     READ AND PRINT FORMAT
CC    ***************************************************************
C
  100 FORMAT(I1,F10.0)
  102 FORMAT(I3)
  105 FORMAT(8F10.3)
  109 FORMAT(2E12.5,4X,2E12.5,4X,2E12.5)
  110 FORMAT(1H0,5X,I3,2X,1P6E14.4)
  112 FORMAT(I2)
  103 FORMAT(1H1,//,15X,38HTHE PARAMETERS OF EACH CELL AS READ IN,
     1 1X,23HARE GIVEN BELOW IN CMS.,//)
  104 FORMAT(1H0,//,7X,1HN,8X,3HAMX,11X,3HAMY,11X,3HAMZ,10X,4HDXCM,
     1          10X,4HDYCM,10X,4HDZCM,//)
  106 FORMAT(1H0,4X,I3,1X,1P6E14.4)
  107 FORMAT(1H1,//,15X,36HX,Y,Z CORRESPOND TO CENTRAL LOCATION,
     1          1X,22HOF EACH CELL IN METERS,//,7X,1HN,9X,1HN,13X,1HY,
     2          13X,1HZ,10X,6HVOLUME,10X,3HEPS,8X,10HSIG(MHO/M),//)
```

```
 116      FORMAT(1H1,//,15X,40HINDUCED ELECTRIC FIELD HAS THE FOLLOWING,
     1           1X,10HCOMPONENTS,//,12X,22HE INDUCED  X-DIRECTION,4X,
     2           22HE INDUCED  Y-DIRECTION,4X,22HE INDUCED  Z-DIRECTION,
     3           //,6X,1HN,9X,4HREAL,10X,4HIMAG,10X,4HREAL,10X,4HIMAG,
     4           10X,4HREAL,10X,4HIMAG,//)
 118      FORMAT(1H0,//,5X,69H2ND INCIDENT ELECTRIC FIELD AT THE CENTER O
     1F EACH SUBCELL OF CELL NO ,I2,//,12X,23HE INCIDENT  X-DIRECTION,
     2   4X,23HE INCIDENT  Y-DIRECTION,4X,23HE INCIDENT  Z-DURECTION,
     3   //,6X,1HN,9X,4HREAL,10X,4HIMAG,10X,4HREAL,10X,4HIMAG,
     4   10X,4HREAL,10X,4HIMAG,//)
 120      FORMAT(1H1,//,25X,66H INDUCED ELECTRIC FIELDS AT THE CENTER OF
     1EACH SUBCELL OF CELL NO ,I2,//,18X,12HFREQUENCY = ,F12.6,5H MHZ.,
     2   //,18X,23HFIELD COMPONENTS = XYZ.)
 122      FORMAT(1H0,//,18X,30H NUMBER OF PARTITIONS PER EDGE,
     1           1X,17HIN INTEGRATION = ,I1,/)
 124      FORMAT(1H0,//,16X,1HN,8X,7HEX(V/M),11X,7HEY(V/M),11X,7HEZ(V/M),
     1           13X,3HPWR,//)
 130      FORMAT(1H0,13X,I3,3X,4(E16.8,2X))
 132      FORMAT(1H0,//,19X,35HTOTAL POWER ABSORBED BY THE BODY = ,
     1           1PE14.4,5X,5HWATTS,//)
 133      FORMAT(1H0,//,3X,1HN,5X,6HEXREAL,6X,6HEXIMAG,6X,6HEX-ABS,2X,
     1           7HTHETA-X,2X,6HEYREAL,6X,6HEYIMAG,6X,6HEY-ABS,2X,
     2           7HTHETA-Y,2X,6HEZREAL,6X,6HEZIMAG,6X,6HEZ-ABS,2X,
     3           7HTHETA-Z,//)
 140      FORMAT(1H0,I3,3(3E12.4,F6.1))
 599      CONTINUE
          END
C
 C
C
C         ***************************************************************
C         SUBPROGRAM GMAT BEGIN HERE
C         ***************************************************************
C
          COMPLEX FUNCTION GMAT(IQ)
          REAL MU
          DIMENSION U(3),UO(3)
          COMPLEX TAUM2,FCTR1,FCTR2,EXPO,FUNC,TOTAL
          COMMON VOL(110,7),XO,YO,ZO,M2
          COMMON/FIELD/I,J,PI,EPS,MU,WVN,OMEG
          COMMON/BLKGMT/NDIV,GRID,PART,START1,START2,START3,
     1           ADD1,ADD2,ADD3,DENOM,REX1

          DVM2 = VOL(M2,4)
          RLEP = VOL(M2,5) - 1.0
          SIG = VOL(M2,6)
          TAUM2 = CMPLX(SIG,OMEG*EPS*RLEP)
          IF(IQ.EQ.0) GO TO 55
```

```
      UO(1) = XO - VOL(M2,1)
      UO(2) = YO - VOL(M2,2)
      UO(3) = ZO - VOL(M2,3)
      RO = SQRT(UO(1)*UO(1) + UO(2)*UO(2) + UO(3)*UO(3))
      IF(RO.EQ.0.) GO TO 54
      TOTAL = CMPLX(0.0,0.0)
      U1MIN = UO(1) + START1
      U2MIN = UO(2) + START2
      U3MIN = UO(3) + START3
      U(3) = U3MIN
      DO 32 IZ = 1,NDIV
      U(1) = U1MIN
      DO 31 IX = 1,NDIV
      U(2) = U2MIN
      DO 30 IY = 1,NDIV
      R = SQRT( U(1)*U(1) + U(2)*U(2) + U(3)*U(3))
      ALPHA = WVN*R
      FCTR2 = U(I)*U(J)*CMPLX( 3.0 - ALPHA*ALPHA,3.0*ALPHA)/R**2
      FCTR1 = CEXP((0.,-1.)*ALPHA)/(ALPHA*ALPHA*ALPHA)
      IF(I.EQ.J) GO TO 52
      FUNC = FCTR1*FCTR2
      GO TO 53
52    FUNC = FCTR1*(FCTR2 + CMPLX(-1. + ALPHA*ALPHA, -ALPHA))
53    TOTAL = TOTAL + FUNC
30    U(2) = U(2) + ADD2
31    U(1) = U(1) + ADD1
32    U(3) = U(3) + ADD3
      GMAT = (0.,-1.)*REX1*TAU**2*DVM2*TOTAL/DENOM
      GO TO 99
54    IF(I.EQ.J) GO TO 56
55    GMAT = CMPLX(0.,0.)
      GO TO 99
56    A = ((3.*DVM2)/(4.*PI))**(1./3.)
      FCTR1 = (0.,-1.)*2.*OMEG*MU*TAUM2/(3.*DVN*WVN)
      EXPO = CEXP((0.,-1.)*WVN*A)
      FCTR2 = EXPO*CMPLX(1.,WVN*A) - (1.,0.)
      GMAT = (FCTR1*FCTR2) - (1.,0.) - (TAUM2/((0.,3.)*OMEG*EPS))
99    CONTINUE
      RETURN
      END

      SUBROUTINE CMATP(A,N,M,DET,EP)
      COMPLEX A,B,DET,CONST,S
      DIMENSION A(24,25)
C
      DET = CMPLX(1.0,0.0)
      NP1 = N + 1
      NPM = N + M
      NM1 = N - 1
```

```
      DO 4 J = 1,NM1
      C = CABS(A(J,J))
      JP1 = J + 1
      DO 5 I = JP1,N
      D = CABS(A(I,J))
      IF( C-D )6,5,5
    6 DET = -DET
      DO 7 K= J,NPN
      B = A(I,K)
      A(I,K) = A(J,K)
    7 A(J,K) = B
      C = D
    5 CONTINUE
      IF(CABS(A(J,J))-EP)14,15,15
   15 DO 4 I= JP1,N
      CONST = A(I,J)/A(J,J)
      DO 4 K= JP1,NPM
    4 A(I,K) = A(I,K) - CONST*A(J,K)
      IF(CABS(A(N,N))-EP)14,18,18
   14 DET = CMPLX(0.0,0.0)
      PRINT 38
      RETURN
   18 CONTINUE
      DO 12 I=1,N
      K = N - I + 1
      KP1 = K + 1
      DO 12 L = KP1,NPM
      S = CMPLX(0.0,0.0)
      IF( L - KP1) 12,19,19
   19 DO 13 J= KP1,N
   13 S = S + A(K,J)*A(J,L)
   12 A(K,L) = (A(K,L) - S)/A(K,K)
   38 FORMAT(1X,42HTHE DETERMINANT OF THE SYSTEM EQUALS ZERO..
     1       1X,36HTHE PROGRAM CANNOT HANDLE THIS CASE.,//)
      RETURN
      END
      SUBROUTINE ANGLES(G,K,EF,F,M)
      COMPLEX G(24,25)
      IF(AIMAG(G(K,M)))10,20,30
   10 IF(REAL(G(K,M)))40,50,40
   40 EF = F*ATAN2(AIMAG(G(K,M)) , REAL(G(K,M)))
      GO TO 100
   50 EF = -90.0
      GO TO 100
   20 IF(REAL(G(K,M)))60,65,65
   60 EF = -180.0
      GO TO 100
   65 EF = 0.0
      GO TO 100
   30 IF(REAL(G(K,M)))40,75,40
   75 EF = 90.0
  100 CONTINUE
      RETURN
      END
```

PART 3 PROGRAM EMFIELD

9.10 Formulation of the Problem

In this computer program, we consider the biological body with arbitrary permeability, permittivity and conductivity. When such a body is irradiated by an EM wave, both the induced electric field and the induced magnetic fields need to be determined. Furthermore these induced electric fields and magnetic fields are coupled together.

We now have to solve the system with 6 unknowns, three components each for the induced electric and magnetic fields, in each cell. Thus, the size of $[G]$ matrix increases twice to 6Nx6N, where N is the number of cells in the body. The formulas used to compute the elements of $[G]$ matrix become more complicated because of the coupling term between the electric and magnetic fields.

In this program, the incident electromagnetic wave is assumed to be a simple plane wave with an electric field polarized in the x-direction and a magnetic field polarized in the y-direction. The arbitrarily shaped biological body is divided into N small cubic cells with the side of the cube not exceeding $\lambda/4$.

After defining the incident electric and magnetic fields, electrical parameters and physical dimensions, program EMFIELD then calculates the induced electric and magnetic fields, and the power density at the center of each cell in the body.

9.11 Description of the Computer Program

The computer program is coded in standard FORTRAN IV. The main program is symbolically named as "EMFIELD". Program EMFIELD uses the

following complex functions and subroutines for the numerical evaluation of induced electric fields and induced magnetic fields inside the biological body.

GMAT1 and GMAT2	are 2 complex functions which calculate the elements of G matrix.
GMATP	is a subprogram which calculates the induced electric and magnetic fields in each cell.
RFN	is a subprogram which calculates the distance between one cell and another.
ANGLES	This subprogram determines the phase angle between real and imaginary parts of the induced electric and magnetic fields.

A listing for the main program "EMFIELD", the complex function GMAT1 and GMAT2, subprogram CMATP, RFN and ANGLES is given at the end of this part.

9.12 Structure of the Data File and Input Variables

The sequential structure of the data files, the format specifications and the symbolic names of the variables appearing in each file are outlined in Table 9.3.

Figure 9.3 shows a sample biological body with one layer which consists of 4 cells in the 1st quadrant (there is no symmetry condition which exists in general). The body is a block of size 20x20x10 cm with each cell size of 10x10x10 cm. The reference point is located at the lower left corner of the body. We will show how to construct the data file in the next section. The information in each data file

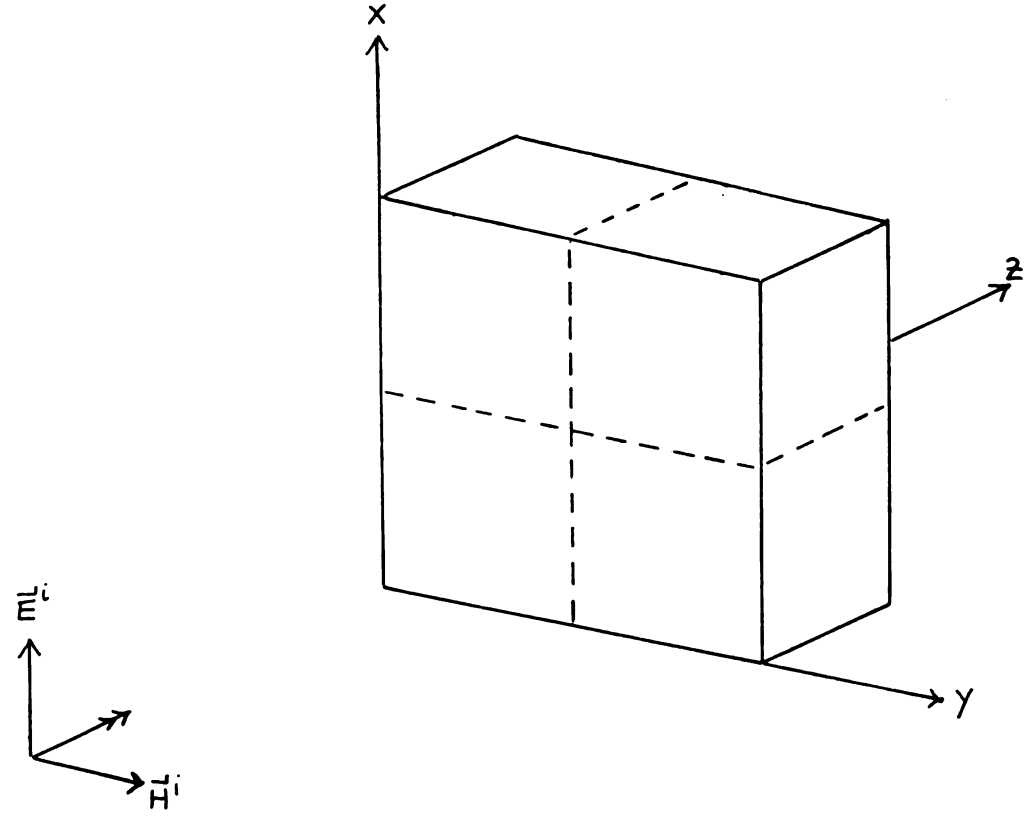

Figure 9.3 A layer of biological body illuminated by Electromagnetic wave at normal incidence is shown divided into 4 cells.

Table 9.3 The symbolic names of input variables and corresponding specifications for the data files used in the data structure for the program EMFIELD.

File No.	Card No.	Symbolic Name	Columns	Format
1	1	NDIV	1	I1
2	1	COMP	1-3	A3
		Q1	11	I1
		FMEG	21-30	F10.0
		SCAT	41-45	A5
3	1	NX	1-2	I2
		NY	6-7	I2
		NZ	11-12	I2
4	1	N	1-3	I3
5	1-N	AMX	1-10	F10.3
		AMY	11-20	F10.3
		AMZ	21-30	F10.3
		RLMU1	31-36	F6.3
		RLEP1	37-42	F6.3
		SIG1	43-50	F8.3
		DXCM	51-60	F10.3
		DYCM	61-70	F10.3
		DZCM	71-80	F10.3

is as follows:

First data file This data file has one card which defines a symbolic name NDIV. This variable allows the user to control the accuracy with which the elements of $[G]$ are evaluated.

Second data file consists of one data card which defines the components of induced electric and magnetic fields, quadrant, frequency of the incident wave and type of the incident field.

Third data file consists of one data card which defines the maximum number of cells in the x-, y- and z-direction. The symbolic names for these numbers are NX, NY, and NZ, respectively.

Fourth data file has only one data card which defines a symbolic name "N" under I-format in the first three columns of the data card. "N" is the total number of cells being considered.

Fifth data file This data file has as many as "N" data cards. This set of data cards helps simulate the biological system and each card contains the following information.

AMX,AMY,AMZ — These codes correspond to the maximum boundaries of a cell in the x-, y- and z- direction in cm.

RLMU1,RLEP1,SIG1 are the codes for permeability, dielectric constant and conductivity of the cell.

DXCM,DYCM,DZCM are the symbolic names for the dimension of the cell in x-, y- and z-directions in cm.

9.13 An Example to Use the Program

Let us now try to determine the electric and magnetic fields induced inside a biological system as shown in Fig. 9.3 by an incident EM wave. Let's assume that the frequency of the incident wave is 500 MHz and the electrical parameters of the biological body are $\mu = 1.2\mu_o$, $\varepsilon = 53\varepsilon_o$ and $\sigma = 1.45$ S/m with the cell volume of 10x10x10 cm. We use "EXPKZ", an exponential variation for the incident EM wave. From section 12 and Table 9.3, the sequential order of the data files is as follows.

File No.	Information on the File								
1	2								
2	XYZ 1			500.0	EXPKZ				
3	02 02 01								
4	004								
5.1	10.0	10.0	10.0	1.2	53.0	1.45	10.0	10.0	10.0
5.2	10.0	20.0	10.0	1.2	53.0	1.45	10.0	10.0	10.0
5.3	20.0	10.0	10.0	1.2	53.0	1.45	10.0	10.0	10.0
5.4	20.0	20.0	10.0	1.2	53.0	1.45	10.0	10.0	10.0

9.14 Printed output

The printed output consists of 2 parts. First part is the echo of the data from the input files in order to check on the data needed for the input variables and for further references. Second part is the required output. The information on each output file can be explained as follows.

First output file consists of the maximum boundary limits of each cell as read in through the symbolic code names AMX, AMY and AMZ and the dimensions of each cell DXCM, DYCM and DZCM in cm.

Second output file consists of the central location of each cell in the x-, y- and z-directions, its permeability, dielectric constant and conductivity.

Third output file The components of the incident electric and magnetic fields in each cell and the type of its variation.

Fourth output file The results for the induced electric field and the power density in each cell in addition to the frequency of the incident field and the total power absorbed in the biological system. Following these results are the real and imaginary parts of each component of the induced electric field in each cell along with its absolute magnetude and phase angle.

Fifth output file The results for the induced magnetic fields in each cell in addition to the frequency of the incident wave in the body. Also the real and imaginary parts of each component of the induced magnetic field along with its absolute magnetude and phase angle.

Listing of the program

A Fortran listing of the program EMFIELD and its subprogram starts on the next page. The program requires approximately 12000 octal words of storage.

```
C
C       PROGRAM EMFIELD DETERMINE THE INDUCED ELECTRIC FIELDS AND
C       INDUCED MAGNETIC FIELDS INSIDE A BIOLOGICAL BODY OF FINITE
C       CONDUCTIVITY WITH BOTH ELECTRIC AND MAGNETIC PROPERTIES
C       (RELATIVE PERMEABILITY AND PERMITTIVITY CAN BE GREATER OR
C       EQUAL TO ONE)  THE BODY IS EXPOSED TO INCIDENT PLANE WAVE
C       OF UNIT AMPLITUDE ELECTRIC FIELD POLARIZED IN X-DIRECTION
C       AND MAGNETIC FIELD POLARIZED IN Y-DIRECTION
C       THIS PROGRAM MAKES USE OF THE FOLLOWING SUBPROGRAMS
C
C       GMAT1  .....  COMPUTE ELEMENTS OF G MATRIX
C
C       GMAT2  .....  COMPUTE ELEMENTS OF G MATRIX
C
C       CMATP  .....  SOLVES N X N MATRIX
C
C       REN  .....  CALCULATE DISTANCE  BETWEEN EACH CELL
C
C       ANGLES  .....  CALCULATE PHASE ANGLE OF THE INDUCED FIELDS
        COMPLEX G,GMAT1,GMAT2,DET,G1,G2,DIA,TAUF,TAUM,DIV
        DIMENSION G1(100,50),G2(100,50),DIA(50)
        REAL MU
        INTEGER*4 G1
        COMMON VOL(100,7),XO,YO,ZO,K4
        COMMON/FIELD/K1,K2,PI,EPS,MU,WVN,OMEG
        COMMON/GIC/ DIVR,DIVI
        COMMON/BLKCMT/NDIV,GRID,PART,START1,START2,START3,ADD1,ADD2,
     1  ADD3,DENOM,REX1
        COMMON/FIELD1/G(100,101)
        REAL*8 SCAT,EXPKZ,COSKZ,SINKZ
        DATA EXPKZ/5HEXPKZ/,COSKZ/5HCOSKZ/,SINKZ/5HSINKZ/
        DATA XYZ/3HXYZ/
C
C
C
        PI = 3.1415926536
        EPS = 8.854E-12
        MU = 1.257E-6
C
        ************************************************************************
C
        READ FIRST DATA CARD FOR NDIV
C
        ************************************************************************
C
        READ 105,NDIV
        GRID = FLOAT(NDIV)
```

```
      PART = GRID ** 3
      DENOM = 4.0*PI*PART
      GFACT = 0.5 * (( 1.0/ GRID ) - 1.0 )
C
CC    ******************************************************************
C
C     READ 2ND CARD FOR COMPONENTS, QUADRANTS, FREQUENCY AND
C     TYPE OF INCIDENT ELECTRIC AND MAGNETIC FIELD.
C
CC    ******************************************************************
C
      READ 100,COMP,Q1,FMEG,SCAT
      IF ( COMP.EQ.XYZ )              GO TO 202
      PRINT 150,COMP
      GO TO 999
  202 KRON = 3
C
CC    ******************************************************************
C
C     READ 3RD CARD FOR NUMBER OF CELLS IN X, Y, Z-DIRECTIONS
C
CC    ******************************************************************
C
  210 READ 101, NX,NY,NZ
      OMEG = 2.0 * PI * FMEG * 1.0E6
      WVN = OMEG * SQRT(MU * EPS )
C
CC    ******************************************************************
C
C     READ 4TH CARD FOR THE TOTAL NUMBER OF CELLS IN THE BODY
C
CC    ******************************************************************
C
      READ 102, N
      MA = KRON * N * 2
      MAP1 = MA + 1
      DO 220 I = 1,MA ,1
      DO 220 J = 1,MAP1 ,1
  220 G(I,J) = CMPLX(0.0,0.0)
      REX1 = OMEG * MU * WVN
      PRINT 151
      PRINT 171
C
CC    ******************************************************************
C
C     READ 5TH CARD AS MANY TIMES AS THERE ARE NUMBER OF CELLS OF
C     THE BIOLOGICAL BODY. THIS CARD DEFINES THE LOCATION OF THE
C     CELL, ITS ELECTRIC AND MAGNETIC PARAMETERS AND ITS PHYSICAL
C     DIMENSIONS.
```

```
C
      DO 230 M = 1,N
      READ 104, AMX,AMY,AMZ,RLMU1,RLEP1,SIG1,DXCM,DYCM,DZCM
      VOL(M,1) = (AMX - (0.5 * DXCM))/ 100.0
      VOL(M,2) = (AMY - (0.5 * DYCM))/ 100.0
      VOL(M,3) = (AMZ - (0.5 * DZCM))/ 100.0
      DELTAX = DXCM / 100.0
      DELTAY = DYCM / 100.0
      DELTAZ = DZCM / 100.0
      RLMU1 = 1.001
      VOL(M,4) = RLMU1
      VOL(M,5) = RLEP1
      VOL(M,6) = SIG1
      VOL(M,7) = DELTAX
      Z = VOL(M,3)
      N4= 4.0*N + M
      IF(SCAT.EQ.EXPKZ)  G(M,MAP1) = -1.0*CEXP(CMPLX(0.0,-WVN*Z))
      IF(SCAT.EQ.COSKZ)  G(M,MAP1) = CMPLX( -COS(WVN*Z),0.0)
      IF(SCAT.EQ.SINKZ)  G(M,MAP1) = CMPLX(0.0, SIN(WVN*Z))
      G(N4,MAP1) =  CMPLX(-1.0,0.0)
230   PRINT 172,M,AMX,AMY,AMZ,DXCM,DYCM,DZCM
      VOL(6,4) = 100.0
      VOL(7,4) = 100.0
      VOL(10,4) = 100.0
      VOL(11,4) = 100.0
      PRINT 163
      DO 232 J =1,N
232   PRINT 172,J,(VOL(J,L),L=1,6)
C
CC    **********************************************************************
C
C     PRINT THE INCIDENT FIELD S VALUES AT THE CENTRAL LOCATION
C     OF EACH SMALL SUB- VOLUME
C
CC    **********************************************************************
C
      PRINT 163
26    DO 242 K=1,N
      KPN = K+N
      KNN = KPN+N
242   PRINT 165,K,G(K,MAP1),G(KPN,MAP1), G(KNN,MAP1)
27    PRINT 166,SCAT
      PRINT 164
30    DO 248 I=1,N
      IPN = I + N*3
      JPN = IPN+N
      KPN = JPN+N
248   PRINT 165,I,G(IPN,MAP1),G(JPN,MAP1),G(KPN,MAP1)
31    PRINT 166,SCAT
```

```
C
C     ******************************************************************
C
C     CALCULATE ELEMENTS OF G MATRIX
C
C     ******************************************************************
C
      DO 260 I=1,KRON
      DO 260 J=1,KRON
      DO 260 M1=1,N
      XO = VOL(M1,1)
      YO = VOL(M1,2)
      ZO = VOL(M1,3)
      K = (I -1)*N + M1
      DO 260 M2=1,N
      DELTAX = VOL(M2,7)
      DELTAY = VOL(M2,7)
      DELTAZ = VOL(M2,7)
      START1 = GFACT * DELTAX
      START2 = GFACT * DELTAY
      START3 = GFACT * DELTAZ
      ADD1 = DELTAX / GRID
      ADD2 = DELTAY / GRID
      ADD3 = DELTAZ / GRID
      L = (J-1)*N + M2
      K1 = I
      K2 = J
      K4 = M2
      G1(K,L) = GMAT1(G1)
      G2(K,L) = GMAT2(G1)
      DIV = CMPLX(DIVR,DIVI)
      IF( K.EQ.L ) DIA(K) = DIV
  256 IF( NERR.EQ. 1 ) GO TO 999
  260 CONTINUE
C
C     ******************************************************************
C     CONSTRUCT G MATRIX
C     ******************************************************************
C
      DO 280 I=1,KRON
      DO 280 J=1,KRON
      DO 280 M1=1 ,N
      K = (I-1)*N + M1
      DO 280 M2=1,N
      RLEP = VOL(M2,5) - 1.0
      SIG = VOL(M2,6)
      RLMU = VOL(M2 ,4) - 1.0
      TAUE = CMPLX(SIG,OMEG*EPS*RLEP)
      TAUM = CMPLX(0.0 ,OMEG*MU*RLMU)
      L = (J-1)*N + M2
```

```
      KP3N = K + N*3
      LP3N = L + N *3
      G(K,LP3N) = TAUM*G2(K,L)
      G(KP3N,L) = -1.0*TAUE*G2(K,L)
      G(KP3N,LP3N) = TAUM * G1(K,L)*EPS
      IF( K.EQ.L ) G1(K,L) = DIA(K)
  280 G(K,L) = TAUE * G1(K,L)*MU
C
CCCCC ********************************************************************
C
C     PRINT FREQUENCY,MAXIMUN DIMENSIONS OF THE BODY, TYPE OF
C     COMPONENTS
C
CCCCC ********************************************************************
C
  271 PRINT 155,FREQ,NX,NY,NZ,COMP,Q1
      PRINT 159,NDIV
      PRINT 156
C
CCCCC ********************************************************************
C
C     CALCULATE THE INDUCED FIELDS ON EACH SUB - VOLUME
C
CCCCC ********************************************************************
C
      CALL CMATP(G,MA,1,DET,1,1E-50)
      PTOT = 0.0
      DO 290 M=1,N
      EF1 = CABS(G(M,MAP1))
      J = M + N
      EF2 = CABS(G(J,MAP1))
      K = J + N
      EF3 = CABS(G(K,MAP1))
  286 PWR = 0.5 * VOL(M,6)*(EF1*EF1 + EF2*EF2 + EF3*EF3 )
      PTOT = PTOT + PWR*VOL(M,7)*VOL(M,7)*VOL(M,7)
  290 PRINT 157,M,EF1,EF2,EF3,PWR
      PRINT 152,PTOT
      PRINT 161
C
CCCCC ********************************************************************
C
C     PRINT REAL ,IMAGINARY,ABS. VALUE AND PHASE ANGLE OF INDUCED
C     ELECTRIC FIELD
C
CCCCC ********************************************************************
C
      F = 57.2957795131
      DO 300 M =1,N
      J = M + N
      K = J + N
```

```
      EFA = 0.0
      EFB = 0.0
      EFC = 0.0
      EF1 = 0.0
      EF2 = 0.0
      EF3 = 0.0
  251 EFC = CABS(G(K,MAP1))
      CALL ANGLES(G,K,EF3,F,MAP1)
  292 EFB = CABS(G(J,MAP1))
      CALL ANGLES(G,J,EF2,F,MAP1)
  293 EFA = CABS(G(M,MAP1))
      CALL ANGLES(G,M,EF1,F,MAP1)
      PRINT 173,M,G(M,MAP1),EFA,EF1,G(J,MAP1),EFB,EF2,
     1 G(K,MAP1),EFC,EF3
  300 CONTINUE
C
CCCCC ********************************************************************
CCCCC
CCCCC PRINT INDUCED MAGNETIC FIELDS IN EACH CELL
CCCCC
CCCCC ********************************************************************
C
      PRINT 154,FMFC,NX,NY,NZ,COMP,G1
      PRINT 159,NDIV
      PRINT 160
      DO 310 M=1,N
      M1 = M + N*3
      EF1 = CABS(G(M1,MAP1))
      J = M1 + N
      EF2 = CABS(G(J,MAP1))
      K = J + N
      EF3 = CABS(G(K,MAP1))
  306 CONTINUE
  310 PRINT 158,M,EF1,EF2,EF3
      PRINT 162
C
CCCCC ********************************************************************
CCCCC
CCCCC PRINT REAL , IMAGINARY,ABS. VALUE AND PHASE ANGLE OF INDUCED
CCCCC MAGNETIC FIELDS
CCCCC
CCCCC ********************************************************************
C
      DO 320 M =1,N
      M1 = M + N*3
      J = M1 + N
      K = J + N
      EFA = 0.0
      EFB = 0.0
```

```
      EFC = 0.0
      EF1 = 0.0
      EF2 = 0.0
      EF3 = 0.0
  311 EFC = CABS(G(K,MAP1))
      CALL ANGLES(G,K,EF3,F,MAP1)
  312 EFB = CABS(G(J,MAP1))
      CALL ANGLES(G,J,EF2,F,MAP1)
  313 EFA = CABS(G(M1,MAP1))
      CALL ANGLES(G,M1,EF1,F,MAP1)
      PRINT 173,M,G(M1,MAP1),EFA,EF1,G(J,MAP1),EFB,EF2,
     1 G(K,MAP1),EFC,EF3
  320 CONTINUE
C
CCCCC ******************************************************************
CCCCC
CCCCC READ FORMATS
CCCCC
CCCCC ******************************************************************
C
   10 FORMAT(2E12.5)
  100 FORMAT(A3,7X,I1,19X,F10.2,A5)
  101 FORMAT(3(I2,3X))
  102 FORMAT(I3)
  104 FORMAT(3F10.3,2F6.3,F8.3,3F10.3)
  105 FORMAT(I1)
C
CCCCC ******************************************************************
CCCCC
CCCCC FORMAT S TO GENERATE THE PRINT OUT
CCCCC
CCCCC ******************************************************************
C
  150 FORMAT(1H0,1H(,A6,38H) ERROR IN COLS 1-6 OF FIRST DATA CARD)
  151 FORMAT(1H1,//,15X,38HTHE PARAMETERS OF EACH CELL AS READ IN,
     1 1X,23HARE GIVEN BELOW IN CMS.,//)
  152 FORMAT(1H0,//,19X,35HTOTAL POWER ABSORBED BY THE BODY = ,
     1 1PE14.4,5X,5HWATTS,//)
  153 FORMAT(1H1,//,15X,36HX,Y,Z CORROSPOND TO CENTRAL LOCATION,
     1 1X,22HOF EACH CELL IN METERS,//,7X,1HN,9X,1HX,13X,1HY,
     2 13X,1HZ,10X,6H  MU  ,10X,3HEPS,8X,10HSIG(MHO/M),//)
  154 FORMAT(1H1,//,25X,41H( INDUCED MAGNETIC FIELDS IN QUADRANT 1 ),
     1 //,18X,12HFREQUENCY = ,F12.6,5H MHZ.,5X,7H( NX = ,I2,
     2 5X,5HNY = ,I2,5X,5HNZ = ,I2,3H ) ,
     3 //,18X,20H FIELD COMPONENTS = ,A6,5X,
     4 17HQUADRANT  USED = ,I1)
  155 FORMAT(1H1,//,25X,41H( INDUCED ELECTRIC FIELDS IN QUADRANT 1 ),
     1 //,18X,12HFREQUENCY = ,F12.6,5H MHZ.,5X,7H( NX = ,I2,
     2 5X,5HNY = ,I2,5X,5HNZ = ,I2,3H ) ,
     3 //,18X,20H FIELD COMPONENTS = ,A6,5X,
     4 17HQUADRANT  USED = ,I1)
```

```
 156      FORMAT(1H0,//,16X,1HN,8X,7HEX(V/M),11X,7HEY(V/M),11X,7HEZ(V/M),
     1    13X,3HFWR,//)
 157      FORMAT(1H0,13X,I3,3X,4(E16.8,2X))
 158      FORMAT(1H0,13X,I3,3X,3(E16.8,2X))
 159      FORMAT(1H0,//,18X,30H NUMBER OF PARTITIONS PER EDGE,
     1    1X,17HIN INTEGRATION = ,I1,/)
 160      FORMAT(1H0,//,16X,1HN,8X,7HHX(A/M),11X,7HHY(A/M),11X,7HHZ(A/M),
     1    13X,//)
 161      FORMAT(1H1,//,3X,1HN,5X,6HEXREAL,6X,6HEXIMAG,6X,6HEX-ABS,2X,
     1    7HTHETA-X,2X,6HEYREAL,6X,6HEYIMAG,6X,6HEY-ABS,2X,
     2    7HTHETA-Y,2X,6HEZREAL,6X,6HEZIMAG,6X,6HEZ-ABS,2X,
     3    7HTHETA-Z,//)
 162      FORMAT(1H1,//,3X,1HN,5X,6HHXREAL,6X,6HHXIMAG ,6X,6HHX-ABS,2X,
     1    7HTHETA-X,2X,6HHYREAL,6X,6HHYIMAG,6X,6HHY-ABS,2X,
     2    7HTHETA-Y ,2X,6HHZREAL,6X,6HHZIMAG ,6X,6HHZ-ABS,2X,
     3    7HTHETA-Z,//)
 163      FORMAT(1H1,//,15X,41HINCIDENT ELECTRIC FIELD HAS THE FOLLOWING,
     1    1X,10HCOMPONENTS,//,12X,23HE INCIDENT  X-DIRECTION,4X,
     2    23HE INCIDENT  Y-DIRECTION,4X,23HE INCIDENT  Z-DIRECTION,
     4    //,6X,1HN,9X,4HREAL,10X,4HIMAG,10X,4HREAL,10X,4HIMAG,
     5    10X,4HREAL,10X,4HIMAG,//)
 164      FORMAT(1H1,//,15X,41HINCIDENT MAGNETIC FIELD HAS THE FOLLOWING,
     1    1X,10HCOMPONENTS,//,12X,23HH INCIDENT  X-DIRECTION,4X,
     2    23HH INCIDENT  Y-DIRECTION,4X,23HH INCIDENT  Z-DIRECTION.//,
     3    6X,1HN,9X,4HREAL,10X,4HIMAG,10X,4HREAL,10X,4HIMAG,
     4    10X,4HREAL,10X,4HIMAG,//)
 165      FORMAT(1H0,5X,I3,2X,1P6E14.4)
 166      FORMAT(1H0,//,10X,35H THE INCIDENT FIELD IS OF THE FORM ,A5)
 171      FORMAT(1H0,//,7X,1HN,8X,3HAMX,11X,3HAMY,11X,3HAMZ,10X,4HDXCM,
     1    10X,4HDYCM,10X,4HDZCM,//)
 172      FORMAT(1H0,4X,I3,1X,1P6E14.4)
 173      FORMAT(1H0,I3,3(3E12.4,F6.1))
 999      CONTINUE
          END
C
C         ******************************************************************
C         COMPLEX FUNCTION GMAT1 BEGIN HERE
C         ******************************************************************
C
          COMPLEX FUNCTION GMAT1(QD)
C
C
          REAL MU
          INTEGER*4 QD
          DIMENSION U(3)
          COMPLEX TAUE,TAUH,FCTR1,FCTR2,EXPO,FUNC,TOTAL,DIV
          COMPLEX FCTR1E,FCTR1M
          COMMON VOL(100,7),X0,Y0,Z0,M2
          COMMON/FIELD/I,J,PI,EPS,MU,WVN,OMEG
          COMMON/GID/ DIVR,DIVI
```

```
      COMMON/GMTRF/UC(3),RO
      COMMON/BLKGMT/NDIV,GRID,PART,START1,START2,START3,
     1 ADD1,ADD2,ADD3,DENOM,REX1
C
C
      DVM2 = VOL(M2,7)*VOL(M2,7)*VOL(M2,7)
      RLEP = VOL(M2,5) - 1.0
      SIG = VOL(M2,6)
      TAUE  = CMPLX(SIG,OMEG*EPS*RLEP)
      RLMU = VOL(M2,4) - 1.0
      TAUM = CMPLX(0.0,OMEG*MU*RLMU)
      IF( GD.EQ.0) GO TO 55
      CALL RFN(GD)
      IF( RO.EQ.0.)GO TO 54
      TOTAL = CMPLX(0.,0.)
      U1MIN = UC(1) + START1
      U2MIN = UC(2) + START2
      U3MIN = UC(3) + START3
      U(3) = U3MIN
      DO 32 IZ = 1,NDIV
      U(1) = U1MIN
      DO 31 IX=1,NDIV
      U(2) = U2MIN
      DO 30 IY =1,NDIV
      R = SQRT( U(1)*U(1) + U(2)*U(2) + U(3) *U(3) )
      ALPHA = WVN * R
      FCTR2 = U(I)*U(J)*CMPLX( 3.0 - ALPHA*ALPHA, 3.0*ALPHA)/R**2
      FCTR1 = CEXP((0.,-1.)*ALPHA)/(ALPHA*ALPHA*ALPHA)
      IF(I.EQ.J) GO TO 52
      FUNC = FCTR1 * FCTR2
      GO TO 53
52    FUNC = FCTR1*(FCTR2 + CMPLX(-1. + ALPHA*ALPHA, -ALPHA))
53    TOTAL = TOTAL + FUNC
30    U(2) = U(2) + ADD2
31    U(1) = U(1) + ADD1
32    U(3) = U(3) + ADD3
      GMAT1 = (0.,-1.)*OMEG*WVN*DVM2*TOTAL/DENOM
      GO TO 99
54    IF(I.EQ.J) GO TO 56
55    GMAT1 = CMPLX(0.,0.)
      GO TO 99
56    A = ((3.*DVM2)/(4.*PI))**(1./3.)
      FCTR1E = (0.,-1.)*2.*OMEG*MU*TAUE/(3.*WVN*WVN)
      FCTR1M = (0.,-1.)*2.*OMEG*EPS*TAUM/(3.*WVN*WVN)
      EXPO = CEXP((0.,-1.)*WVN*A)
      FCTR2 = EXPO* CMPLX(1. ,WVN*A) - (1.,0.)
      DIV = ((FCTR1E*FCTR2)-(1.,0.)-(TAUE/((0.,3.)*OMEG*EPS)))/
     1 (MU*TAUE)
      DIVR = REAL(DIV)
      DIVI = AIMAG(DIV)
```

```
      GMAT1 = ((FCTR1M*FCTR2)-(1.,0.)-(TAUM/((0.,3.)*OMEG*MU)))/
     1  (EPS*TAUM)
 99   CONTINUE
      RETURN
      END
C
C     ****************************************************************
C     SUBPROGRAM GMAT2 BEGIN HERE
C     ****************************************************************
C
      COMPLEX FUNCTION GMAT2(QD)
C
      INTEGER*4 QD
      DIMENSION U(3)
      COMPLEX FCTR1,FCTR2,FUNC,TOTAL
     COMMON VOL(100,7),XO,YO,ZO,M2
      COMMON/FIELD/I,J,PI,EPS,MU,WVN,OMEG
      COMMON/SMTRF/UO(3),RO
      COMMON/BLKGMT/NDIV,GRID,PART,START1,START2,START3,
     1  ADD1,ADD2,ADD3,DENOM,REX1
C
C
      DVM2 = VOL(M2,7)*VOL(M2,7)*VOL(M2,7)
      IF( QD.EQ.0) GO TO 55
      CALL REM(QD)
      IF(RO.EQ.0.) GO TO 55
      IF(I.EQ.J) GO TO 55
      TOTAL = CMPLX(0.,0.)
      K1 = I+J
     AMUL = -1.0
      IF(K1.EQ.4)AMUL = 1.0
      IF(I.GT.J) AMUL = -1.0*AMUL
      K = K1
      IF(K1.GT.3) K =6 - I - J
      U1MIN = UO(1) + START1
      U2MIN = UO(2) + START2
      U3MIN = UO(3) + START3
      U(3) = U3MIN
      DO 32 IZ=1,NDIV
      U(1) = U1MIN
      DO 31 IX=1,NDIV
      U(2) = U2MIN
      DO 30 IY=1,NDIV
      R = SQRT( U(1)*U(1) + U(2)*U(2) + U(3)*U(3) )
      ALPHA = WVN*R
      FCTR2 = U(K)*CMPLX(1.,ALPHA)
      FCTR1 = CEXP((0.,-1.)*ALPHA)/R**3
      FUNC = FCTR1*FCTR2
      TOTAL = TOTAL + FUNC
 30   U(2) = U(2) + ADD2
 31   U(1) = U(1) + ADD1
 32   U(3) = U(3) + ADD3
```

```
      GMAT2 =AMUL*DUM2*TOTAL/DENOM
      GO TO 99
   55 GMAT2 = CMPLX(0.,0.)
   99 RETURN
      END
C
CC    ***************************************************************
CC    SUBPROGRAM CMATP BEGIN HERE
CC    ***************************************************************
C
      SUBROUTINE CMATP(A,N,M,DET,EP)
      COMPLEX A,B,DET ,CONST,S
      DIMENSION A(100,101)
C
C
      DET = CMPLX(1.0 , 0.0)
      NP1 = N + 1
      NPM = N + M
      NM1 = N - 1
    2 DO 4 J=1,NM1
      C = CABS(A(J,J))
      JP1 = J + 1
      DO 5 I=JP1,N
      D = CABS(A(I,J))
      IF( C-D )6,5,5
    6 DET = -DET
      DO 7 K=J,NPM
      B = A(I,K)
      A(I,K) = A(J,K)
    7 A(J,K) = B
      C = D
    5 CONTINUE
      IF(CABS(A(J,J))-EP)14,15,15
   15 DO 4 I=JP1,N
      CONST = A(I,J)/A(J,J)
      DO 4 K=JP1,NPM
    4 A(I,K) = A(I,K) - CONST*A(J,K)
      IF(CABS(A(N,N))-EP)14,18,18
   14 DET = CMPLX(0.,0.)
      PRINT 33
      RETURN
   18 CONTINUE
      DO 12 I=1,N
      K = N - I + 1
      KP1 = K+1
      DO 12 L = NP1,NPM
      S = CMPLX(0.,0.)
      IF( N-KP1 )12,19,19
   19 DO 13 J =KP1,N
   13 S = S + A(K,J)*A(J,L)
   12 A(K,L) = (A(K,L) - S)/A(K,K)
   33 FORMAT(1X,42HTHE DETERMINANT OF THE SYSTEM EQUALS ZERO./
     1 1X,36HTHE PROGRAM CANNOT HANDLE THIS CASE.//)
```

```
      RETURN
      END
C
C     ******************************************************************
C     SUBPROGRAM RFN START HERE
C     ******************************************************************
C
      SUBROUTINE RFN(QD)
C
C
      INTEGER*4 QD
      COMMON VOL(100,7),XO,YO,ZO,IN
      COMMON/GMTRF/U(3),R
C
      IF(QD.EQ.1) GO TO 1
      GO TO 51
C
    1 U(1) = XO - VOL(IN,1)
      U(2) = YO - VOL(IN,2)
      U(3) = ZO - VOL(IN,3)
C
   50 R = SQRT( U(1)*U(1) + U(2)*U(2) + U(3)*U(3) )
      GO TO 99
   51 PRINT 15,QD
   15 FORMAT(1HO,I1,32H IS AN IMPROPER QUADRANT NUMBER.,/)
   99 CONTINUE
      RETURN
      END
C
C     ******************************************************************
C     SUBPROGRAM ANGLES START HERE
C     ******************************************************************
C
      SUBROUTINE ANGLES(G ,K,EF,F,M)
C
      COMPLEX G(100,101)
      IF(AIMAG(G(K,M)))10 ,20,30
   10 IF(REAL(G(K,M)))40,50,40
   40 EF = F*ATAN2(AIMAG(G(K,M)),REAL(G(K,M)))
      GO TO 100
   50 EF = -90.0
      GO TO 100
   20 IF(REAL(G(K,M)))60,65,65
   60 EF = -180.0
      GO TO 100
   65 EF = 0.0
      GO TO 100
   30 IF(REAL(G(K,M)))40,75,40
   75 EF = 90.0
  100 CONTINUE
      RETURN
      END
```

BIBLIOGRAPHY

BIBLIOGRAPHY

1. Livesay, D.E., and K.M. Chen, "Electromagnetic fields induced inside arbitrarily shaped biological bodies." IEEE Trans. Micro. Th. and Tech. MTT-22, pp. 1273-1280, 1974.

2. Van Bladel, J., "Some remarks on Green's dyadic for infinite space." IRE Trans. Antennas Propag., vol. AP-9, pp. 563-566, Nov. 1961.

3. Chen, K.M., "A Simple Physical Picture of Tensor Green's Function in Source Region," Proceedings of IEEE, pp. 1202-1204, August 1977.

4. Johnson, C., and A.W. Guy, "Non-ionizing EM effects in biological materials and systems," Proc. IEEE, vol 60, June 1972, p. 692.

5. Stratton, J.A., Electromagnetic Theory, McGraw-Hill Co., New York, 1941, pp. 563-567.

6. Schwan, H., "Survey of microwave absorption characteristics of body tissues," Proc. 2nd Tri-serv. Conf. on Biol. Effects of Microwave Energy, 1958, pp. 126-145.

7. Kritikos, H. and H. Schwan, "Hot spots generated in conducting spheres by EM wave and biological implications," IEEE BME-19, Jan. 1972, pp. 53-58.

8. Shapiro, A.R., et al., "Induced fields and heating within the cranial structure irradiated by an EM plane wave," IEEE MTT-19, Feb. 1971, p. 187.

9. Kritikos, H. and H. Schwan, "Formation of hot spots in multilayer spheres," IEEE-BME-23, March 1976, pp. 168-172.

10. Chen, K.M., and B.S. Guru (1977a), "Induced EM fields inside human bodies irradiated by EM waves of up to 500 MHz," Journal of Microwave power, 12(2), 173-183.

11. Chen, K.M. and B.S. Guru (1977b), "Internal EM field and absorbed power density in human torsos induced by 1 - 500 MHz EM waves," IEEE Trans on Microwave Theory and Techniques, MTT-25,9, 746-756.

12. Gandhi, O.P., K. Sedigh, G.S. Beck and E.L. Hunt (1975), "Distribution of EM energy deposition in models of man with frequencies near resonance," Selected papers of USNC/URSI Annual Meeting, Boulder, Colorado, HEW publication (FDA) 77-8010, 44-67.

13. Gandhi, O.P., M.J. Hagmann, and J.A. D'Andrea (1977), "Some recent results on deposition of EM energy in animals and models of man," presented at 1977 International Symposium on the Biological Effects of EM waves, Arlie, Virginia, Oct. 30- Nov. 4.

14. Guy, A.W., M. Webb and C.C. Sorensen (1976), "Determination of power absorption in man exposed to high frequency EM fields by thermographic measurements on scale models," IEEE Trans. on Biomedical Engr., BME-23, 5, 361-371.

15. Overgaad, J., "Combined adriamycin and hyperthermia treatment of a murine mammary carcinoma in vivo," Cancer Research 36, 3077-3081, 1976.

16. Suit, H.D. and M. Shwayder, Cancer 34, 1, 122-129, (1974).

17. Robinson, J.E., M.J. Wizenberg and W.A. McCready, Radiology 113, 1, 195-198, (1974).

18. Burdette, E.C., J. Seals, J.C. Toler, F.L. Cain and R.L. Magin, "Proceedings of 1977 International Microwave Symposium, 344-347, (1977).

19. Marmor, J.B., N. Hahn and G.M. Hahn, "Tumor cure and cell survival after localized radiofrequency heating," Cancer Research 37, 879-883, March 1977.

20. Leveen, H.H., S. Wapnick, V. Piccone, G. Falk and N. Ahmed, "Tumor eradication by radiofrequency therapy," JAMA, 230, 29, 2198-2200, May 17, 1976.

21. Cheung, A.Y., D. McCulloch, J.E. Robinson and G.M. Samaras, "A bolusing technique for batch microwave irradiation of tumors in the far field," Proc. of 1977 International Microwave Symposium, 357-359, June 21-23, 1977.

22. Baker, R.J., V. Smith, T.L. Phillips, L. Kobe and L. Kane, "A system for developing microwave induced hyperthermia in small animals," Proceedings of 1977 International Microwave Symposium, 360-363, June 21-23, 1977.

23. Guru, B.S., "An experimental and theoretical study of the interaction of EM fields with arbitrarily shaped biological bodies," Ph.D. Dissertation, Michigan State University, 1976.